

https://dspace.org/

Gas atomized versus water atomized nickel powder for the development of WC-Ni cold spray wear resistant coatings

Chingosho, Tatenda

2019

https://hdl.handle.net/10539/29074

Chingosho, Tatenda (2019) Gas Atomised versus Water Atomised Nickel powder for development of WC-Ni cold spray wear resistant coatings, University of the Witwatersrand, https://hdl.handle.net/10539/29074

Downloaded from a DSpace repository. https://dspace.org/

Gas Atomized versus Water Atomized Nickel powder for the development of WC-Ni cold spray wear resistant coatings

TATENDA CHINGOSHO

A dissertation presented in partial fulfillment of the requirements for the degree Master of Science in Engineering at the University of the Witwatersrand.

March 2019

DECLARATION

I declare that this is my own unaided work. It is being submitted for the degree of Master of Science in Engineering to the University of the Witwatersrand, Johannesburg. It has not been submitted before for any degree or examination to any other university.

…….

Tatenda Chingosho

….Day of…….Year……

ABSTRACT

A research study was done to compare cold sprayed cermet coatings produced from two nickel (Ni) powders manufactured by the gas atomization and water atomization processes respectively. The aim of the research was to investigate if the Ni powders could be used to fabricate cold sprayed cermet coatings having good slurry abrasion resistance properties. The Ni powder was blended with tungsten carbide (WC) powder and deposited onto mild steel substrates using a low pressure cold spray machine to produce WC-5wt%Ni coatings. A Design of Experiments matrix was used to determine the near-optimal deposition parameters. The resulting coatings were relatively thin which exhibited mostly rebounding of feedstock powder rather than deposition. An annealing stage was introduced so as to make the Nickel powders more favourable for deposition on the mild steel substrate. The annealing caused softening of the Ni powder which led to better deformation properties upon impingement with the mild steel surface. Several materials characterization tests were conducted on the coatings to determine the microstructural and mechanical properties. Three body slurry abrasion tests were done to investigate the wear properties. Both Ni powders produced WC-5wt%Ni coatings without new phases, decarburization or oxidation. The coatings based on the annealed gas atomized Ni powder showed improved deposition, better adherence to the substrate, thicker and dense coatings whereas the coatings based on the annealed water atomized Ni powder showed little deposition improvement, the powder particles bounced off the substrate more than they adhered to the substrate. The coatings based on the annealed gas atomized Ni powder had a thickness of 255 ± 33.5 µm, a hardness of 361 ± 38 $HV_{0.3}$, WC retention of 42.9 ± 0.7 % and a percentage porosity of 0.7 ± 0.3 % whereas the coatings based on the annealed water atomized Ni powder had a thickness of 28.5 ± 1.1 µm, a hardness of 426 ± 12 $HV_{0.3}$, WC retention of 49.5 ± 2.5 % and a percentage porosity of 1.3 ± 0.8 %. The gas atomized Ni powder provided coatings with the best slurry abrasion properties.

DEDICATION

I would like to dedicate this to my beloved mother, Angela, my wonderful sisters, Lucia, Rudo and Rutendo who through God, have encouraged me and blessed me with prayers and constant support. Thank you for always believing in me.

ACKNOWLEDGEMENTS

My deepest gratitude goes to the Lord our creator, for blessing me with the gift of life and blessing everyone who was involved in the success of this work.

- **Professor N. Sacks,** for recognizing me as a potential student and for bringing me to South Africa to pursue my studies. Unwavering, constant guidance and assistance with very professional supervision and guidance. I truly appreciate your ever presence.
- **Professor I. Botef,** for constant guidance and technical training, I truly appreciate all your help.
- **Pilot Tools (Pty) SA,** assistance with milling facilities.
- **Microscopy & Microanalysis Unit (MMU), University of the Witwatersrand,** for the use of the microscopy facilities.
- **School of Chemical and Metallurgical Engineering, University of the Witwatersrand,** Staff Mr. B. Mothibedi (Lab manager), Mr. S. Moqabolane (sample preparation training) and Mr. B. Nelwalani (FESEM)
- **School of Mechanical, Industrial and Aeronautical Engineering, University of the Witwatersrand, Staff** Mr. S. Riekert (Lab manager) and Mr. Dean van Aswegen (Hardness Lab)
- **The Department of Science and Technology (DST) and the National Research Foundation (NRF), South Africa, for supporting the DST/NRF Centre of Excellence in Strong Materials,** for granting me the opportunity to carry out my studies at an internationally acclaimed institution and for supporting my research and welfare. I am truly honored and grateful.

TABLE OF CONTENTS

DECLARATION i

ABSTRACT ii

DEDICATION iii

ACKNOWLEDGEMENTS iv

LIST OF FIGURES x

LIST OF TABLES xv

Chapter 1 1

Introduction 1

1.1 Research background and motivation 1

1.2 Research Aim and Objectives 2

1.3 Contribution to knowledge 3

1.4 Layout of research 3

Chapter 2 5

Literature Review 5

2.1 Cold gas dynamic spraying 5

2.2 Tungsten carbide-based cold spray coatings 7

2.3 Abrasive Wear 15

2.3.1 Slurry abrasion wear 16

2.4 Abrasion of WC-based coatings 19

2.4.1 Abrasion of high temperature cemented tungsten carbide coatings 19

2.4.2 Abrasion of cold sprayed cemented tungsten carbide coatings 24

2.5 Annealing of WC and Ni-based coatings 27
2.6 Summary 34
Chapter 3 35
Experimental Procedures 35
3.1 Powders 35
3.2 Steel substrate 36
3.3 Deposition Parameter Optimization 36
3.4 Coating Deposition 39
3.5 Coating Characterization 41
3.5.1 Sample preparation 41
3.5.2 Thickness 42
3.5.3 Hardness 42
3.5.4 Phase analyses 42
3.5.5 Microstructure 43
3.5.6 Crack density 43
3.5.7 Fracture toughness 44
3.5.8 Elastic Modulus 44
3.5.9 Plasticity Index 45
3.5.10 Atomic Force Microscopy (AFM) 45
3.6 Annealing of Nickel powders 46
3.6.1 Raman Spectroscopy 46
3.6.2 Electron Probe Micro-analyzer 46
3.7 Slurry Abrasion Testing 47
Chapter 4 50

Results 50
4.1 Powder Characterization and Hardness 50
4.1.1 Morphology of nickel powders 50
4.1.2 Particle size distribution of nickel powders 51
4.1.3 Morphology of WC and WC-5wt%Ni powder blends 53
4.1.4 Particle size distribution of WC and WC-5wt%Ni powder blends 53
4.2 Design of Experiments Optimization 56
4.3 Characterization of Ni-only coatings 58
4.3.1 Nickel-only coating characterization 58
4.4 Characterization of WC-5wt%Ni coatings based on un-annealed Ni powders 60
4.4.1 Coating microstructures 61
4.4.2 Phase analyses 63
4.4.3 Properties of WC-5wt%Ni coatings based on un-annealed Ni 64
4.5 Annealing of nickel powder 67
4.5.1 Morphologies of Ni powders 67
4.5.2 Phase analyses 69
4.6 Characterization of WC-5wt%Ni coatings based on annealed Ni powders 71
4.6.1 Coating microstructures 71
4.6.2 Phase analyses 72
4.6.3 Topographical analyses (AFM) 74
4.6.4 Properties of WC-5wt%Ni coatings based on annealed Ni powder 76
4.7 Slurry Abrasion Tests 78
4.7.1 Mass loss plots 79
4.7.2 Worn surfaces 80

4.7.3 Wear rates 82
Chapter 5 83
Discussion 83
5.1 Gas Atomized versus Water Atomized Nickel Powders 83
5.1.1 Powder property comparison 83
5.1.2 Coating deposition and material properties 85
5.1.3 Slurry abrasion comparison 86
5.2 Effect of Annealing Nickel Powder prior to coating Deposition 87
5.2.1 Powder property comparison 88
5.2.2 Coating deposition and material properties 89
5.2.3 Slurry abrasion comparison 93
Chapter 6 96
Conclusions 96
Chapter 7 98
Future work 98
References 99
APPENDIX A 107
CROSS-SECTIONAL VIEWS FOR WEAR SURFACES 107
APPENDIX B 108
SLURRY ABRASION TESTS RAW DATA 108
APPENDIX C 109
PORE ANALYSIS IMAGES 109
APPENDIX D 111
PROBABILITY AND CUMULATIVE CURVES 111

APPENDIX E 112
PARTICLE SIZE DISTRIBUTION OF ANNEALED NI POWDERS 112
APPENDIX F 113
ANNEALED NI POWDERS EDS RAW DATA 113
APPENDIX G 114
PRESENTATIONS AND CONFERENCES 114

LIST OF FIGURES

Figure 2.1 Low pressure cold spray system [21]. 6
Figure 2. 2: Microstructures of (a) WC + 50wt.%Ni and (b) WC + 4wt. %Ni coatings [12]. The white regions are the WC phase, while the Ni binder is the grey region. ..8
Figure 2. 3: Curves of reinforcing carbide particle content in the coating versus carbide particle contents in the powder (weight percentage) [29]. 11
Figure 2. 4: Relationship between porosity and reinforcing carbide particle content in the coating [29]. 11
Figure 2. 5: Coating formation with different feedstock PM-17 (a, b) and nanostructured IN-17 or BN-17 (c, d) [6]. 14
Figure 2. 6: Schematics showing (a) two-body abrasion and (b) three-body abrasion [38]. 16
Figure 2. 7: Schematic illustration of four common methods used to measure abrasive wear rates of materials: (a) pin on abrasive disc; (b) pin on abrasive plate; (c) pin on abrasive drum; (d) rubber wheel abrasion test [36]. 17
Figure 2. 8: Slip line fields for the deformation of a perfectly plastic material caused by the sliding of a rigid two-dimensional wedge from right to left. Three distinct modes can be identified, (a) cutting; (b) wedge formation; (c) ploughing. The angle ϴ is termed the ‘attack angle’[36].....18
Figure 2. 9 Wear rates of WC-Co coatings under (A) high-stress, and (B) low-stress conditions [25]. 20
Figure 2. 10: Mass loss curves in wet abrasion. (i) Cumulative mass loss curves, (ii) Mass loss per unit time curves [1].....22
Figure 2. 11: Micrographs of multimodal and conventional WC-12Co powder at different magnification (a and b) multimodal powder and (c and d) conventional powder [26]. 23
Figure 2. 12 Influence of binder mean free path on wear rate [8]. 25

Figure 2. 13: Abrasive wear rate Vs heat treatment temperature of WC-12Co [47].28
Figure 2. 14: Abrasive wear rate Vs heat treatment temperature of Cr_3C_2-25NiCr [47]. 28
Figure 2. 15: Abrasive wear rate of WC-12Co and Cr_3C_2-25NiCr vs. severity contact of SoC [47]. 30
Figure 2. 16: Vickers hardness as a function of temperature and (b) mass loss of as-sprayed and heat treated coatings [49]. 31
Figure 2. 17: The effects of heat treatment on the hardness of as-sprayed and heat-treated coatings. 32
Figure 2. 18: BSE images of the microstructure of HVOF-sprayed CoNiCrAlY bond-coating after heat treatment in stationary atmospheric conditions at (a) 900 °C and (b) 1100 °C. 33

Figure 3. 1: (a) Cold spray machine and (b) gravitational powder feeder. 39
Figure 3. 2: WC spray nozzle 40

Figure 4. 1:Scanning electron images of different nickel powders showing different morphologies a) Centerline nickel powder, b) gas atomized nickel powder and c) water atomized nickel powder 51
Figure 4. 2: Particle size distribution a) Centerline nickel powder, b) gas atomized nickel powder and c) water atomized nickel powder 52
Figure 4. 3: Scanning electron images of different nickel powders showing different morphologies a) WC powder, WC-5wt%Ni based on b) gas atomized Ni powder and c) water atomized Ni powder. 53
Figure 4. 4: Particle Size distribution a) WC powder, WC-5wt%Ni powder blends based on b)gas atomized Ni powder and c) water atomized Ni powder 54
Figure 4. 5: Powder and silica sand Vickers hardness 55
Figure 4. 6: Centerline Ni coating cross-sectional view. 58

Figure 4. 7: Centerline Ni coating microstructure. 59
Figure 4. 8: EDS mapping for Centerline Ni coating showing (a) Ni powder, (b) elemental spectrum, (c) elemental mapping of Ni and (d) Fe. 59
Figure 4. 9: Coating microstructures for Ni coatings deposited at (a-b) 2 passes and (c-d) 8 passes. 60
Figure 4. 10: Coating microstructures WC-5wt%Ni coatings based on gas atomized Ni powder (a & c) and water atomized powder Ni (b & d). 61
Figure 4. 11: High magnification image of WC-5wt%Ni based on gas atomized Ni powder. 62
Figure 4. 12: High magnification image of WC-5wt%Ni based on water atomized Ni powder. 62
Figure 4. 13: XRD patterns for coating (black) and powder (red) for coatings based on un-annealed gas atomized Ni powder. 63
Figure 4. 14: XRD patterns for coating (black) and powder (red) in descending order for coatings based on un-annealed water atomized Ni powder 63
Figure 4. 15: EDS mapping for a WC-5wt%Ni coating based on gas atomized Ni powder, (a) Ni, (b) W, (c) Fe and (d) elemental spectrum. 66
Figure 4. 16: EDS mapping for a WC-5wt%Ni coating based on water atomized Ni powder, (a) Ni, (b) W, (c) Fe and (d) elemental spectrum. 67
Figure 4. 17: Annealed gas atomized Nickel powder morphology. 68
Figure 4. 18: Annealed water atomized Nickel powder morphology. 68
Figure 4. 19: XRD patterns of un-annealed and annealed powders based on (a) gas atomized Ni powder and (b) water atomized Ni powder. 69
Figure 4. 20: Raman spectra for un-annealed and annealed powder based on (a) gas atomized Ni powder and (b) water atomized Ni powder. 70
Figure 4. 21: Microstructures of WC-5wt%Ni coatings based on annealed water atomized Ni powder. 72
Figure 4. 22: Microstructures of WC-5wt%Ni coatings based on annealed gas atomized Ni powder. 72

Figure 4. 23: XRD patterns for WC-5wt%Ni coating (black) and powder (red) based on gas atomized Ni powder. 73
Figure 4. 24: XRD patterns for WC-5wt%Ni coating (black) and powder (red) based on water atomized Ni powder. 73
Figure 4. 25: (a) SEM and (b) EDS for gas atomized based WC-5wt%Ni. 74
Figure 4. 26: (a) SEM and (b) EDS for water atomized based WC-5wt%Ni. 74
Figure 4. 27: AFM image showing alumina grit (white arrow) embedded in the substrate surface. 75
Figure 4. 28: 3D AFM image of alumina grit in the substrate surface. 75
Figure 4. 29: 3D AFM topographies of coatings based on un-annealed and annealed (a & b) gas atomized Ni powder and (c & d) water atomized Ni powder. 76
Figure 4. 30: Particle size distribution of silica sand. 78
Figure 4. 31: Mass loss curve WC-5wt%Ni coatings based on gas atomized Ni powder. 80
Figure 4. 32: Mass loss curve WC-5wt%Ni coatings based on water atomized Ni powder. 80

Figure 5. 1: Powder hardness relative to annealing 95

Figure A 1: Cross-sectional views showing the severity of the slurry abrasive medium (a & b) 5 ° tilted views and (c & d) level views. 107

Figure C 1: Pore analysis for coatings based on water atomized Ni (a) pore identification & (b) pore count. 109
Figure C 2: Pore analysis for coatings based on gas atomized Ni (a) pore identification & (b) pore count. 110

Figure D 1: Probability and cumulative curves for the CS coatings (a & b) for the carbide grain size and (c & d) for the particle area size of the carbide grains. Red = WC-Niwa and blue = WC-Niga coating. 111

Figure E 1: Particle size of annealed gas atomized Ni powder 112
Figure E 2: Particle size of annealed water atomized Ni powder 112

LIST OF TABLES

Table 2. 1: Nominal composition of respective powders. 13
Table 2. 2: WC-Co coatings hardness values [25]. 20

Table 3.1: Centerline Ni recommended spray parameters [18]. 37
Table 3. 2: Design of Experiments matrix. 38
Table 3. 3: Grinding and polishing procedure 41

Table 4. 1: Experimental matrix for coatings based on gas atomized Ni powder. 56
Table 4. 2: Experimental matrix for coatings based on water atomized Ni powder. 57
Table 4. 3: Properties of coatings based on un-annealed Ni powders. 65
Table 4. 4: Nickel powder hardness. 71
Table 4. 5: Properties of coatings based on annealed Ni powders. 78

Table B 1: Slurry Abrasion Tests Raw Data (in descending order) for WC-5wt%Ni coatings based on annealed (a) water atomized Ni powder (b) gas atomized Ni powder and as received (c) water atomized Ni powder and (d) gas atomized Ni powder 108

Table F 1: Raw data for EDS analysis on gas atomized Ni powder 113
Table F 2: Raw data for EDS analysis on water atomized Ni powder 113

Chapter 1

Introduction

1.1 Research background and motivation

Machine components used in different industries experience various types of wear during their operational lifetimes which may influence operational efficiency [1,2]. These components are widely comprised of steels and are frequently utilized in the mining, transport, power generation and tool industries [1,2]. A common wear phenomenon in all of these industries is slurry abrasion, where surface material is removed by hard particles either present within the slurry medium or inherent on one or both of the component surfaces which are in relative motion [3]. The wear life of the components used under slurry abrasion conditions is governed by the operational parameters, properties of the abrasive particles in the slurry, slurry medium properties and component material properties [4]. This type of wear has been shown to contribute to fracture of components, impede efficiency and in extreme cases, complete failure of the working components [3,4]. As steels are widely used industrially it is important that their operational lifetimes are not compromised, and possibly extended by finding methods to reduce their slurry abrasion wear rates.

A common and successful technique used to improve the wear resistance of steel components is the application of a hard tungsten carbide based (also known as hardmetal) coating onto the steel surface [5,6]. Hardmetal coatings are generally deposited using high temperature techniques such as high velocity oxy-fuel, laser cladding and plasma spray. An alternative to these high temperature processes is cold gas dynamic spraying (CGDS), which is a relatively recent technique finding increased industrial application due to the reduction in energy consumption. Cold gas

dynamic spraying is a process in which solid powders are accelerated in a de Laval nozzle toward a substrate [6]. If the impact velocity exceeds some threshold value, then the powder particles experience plastic deformation and adhere to the substrate surface. Different materials such as metals, ceramics, composites and polymers can be deposited using CGDS and it offers several technological advantages over thermal spray processes such as little to no oxidation and no decarburization, since it utilizes kinetic rather than thermal energy for deposition [6].Research into hardmetal coatings produced by CGDS has shown good results. Due to the low temperatures experienced during deposition, there is limited risk of decarburization, oxidation, dissolution of the WC and binder, and undesirable phase formation [7,8]. The physical and mechanical properties of these coatings have been shown to be similar and in some instances better than those of hardmetal coatings produced by high temperature processes [9]. To date, the majority of research in this field has been done on the use of high pressure CGDS [10–12], while limited research is available on the use of low pressure CGDS [5,10–12]. Thus the current research focused on the use of low pressure CGDS to develop WC-Ni coatings for potential application on steel components where slurry abrasion conditions are experienced. Nickel was selected as the binder due to its well-known corrosion resistant properties [12]. In addition, the research explored two different Ni powders, namely gas atomized and water atomized powders. It is well known that the feedstock powder properties influence the deposition kinetics and the resultant properties of a coating [13–15]. To the best knowledge of the author this type of comparison for WC-Ni cold spray coatings has not been done and thus the research should produce new scientific knowledge.

1.2 Research Aim and Objectives

The aim of this project was to determine if gas and/or water atomized Nickel powder may be used to produce low pressure cold sprayed WC-Ni coatings having a good

slurry abrasion resistance. This aim was achieved through the following objectives:

- Fabricating and optimizing low pressure cold spray WC-Ni coatings using two different types of Ni powder (gas atomized and water atomized).
- Characterizing the microstructure of the coatings.
- Determining the physical and mechanical properties of the coatings.
- Annealing the Ni powders to improve deposition efficiency.
- Assessing the slurry abrasion resistance of the coatings, and identifying the associated wear mechanisms.
- Correlating the wear properties to the material properties of the coatings.

1.3 Contribution to knowledge

It is believed that through this research a better understanding has been established on the influence of annealing the feedstock Ni powders prior to coating deposition. The Ni binder matrix properties were altered such that the coating's slurry abrasion properties were improved.

1.4 Layout of research

This dissertation is structured as follows: Chapter 1 presents and explains the background and significance of the research work undertaken. Chapter 2 reviews the published literature on the cold gas dynamic spraying technology, tungsten carbide-based cold sprayed coatings, abrasive wear, abrasion of WC-based coatings, annealing of WC and Ni-based coatings, and lastly a summary of the literature reviewed. Chapter 3 presents the experimental procedures employed such as powder and coating characterization, deposition parameter optimization, coating deposition, annealing of the Ni powders and slurry abrasion testing. Chapter 4 presents test results and analyses which are discussed in Chapter 5. Chapter 6 outlines the

conclusions drawn from the research work. Chapter 7 provides recommendations for future work while Chapter 8 lists all the cited references. Appendices A to F provides some detailed test results which are presented in summary form in Chapter 4, while Appendix H lists the conference presentations undertaken during the research project.

Chapter 2

Literature Review

2.1 Cold gas dynamic spraying

The cold spray process was originally developed in the mid-1980s at the Institute of Theoretical and Applied Mechanics of the Russian Academy of Sciences in Novosibirsk by Dr. Anatolii Papyrin and his colleagues [16]. They successfully deposited a wide range of pure metals, metal alloys, and composites onto a variety of substrate materials, and demonstrated the feasibility of the cold spray process for various applications [6,16,17].

Cold spray is a deposition process which fabricates thick, dense, adherent coatings by accelerating small metal or metal alloy particles (1-50 μm) to high velocities (300-1200 m/s) at low temperatures (20–650 °C) [5,13]. The temperature of the working gas (typically air, helium or nitrogen) is low, yielding particle temperatures much lower than their melting points. The cold spray process can be separated into two different categories namely high pressure and low pressure cold spraying. Cold spraying at high pressure is defined as a process which typically employs a working gas at pressures in excess of 2 MPa, while low- pressure cold spraying typically uses working gas pressures below 1 MPa. The pressurized gas which is heated, usually with electrical energy, to temperatures generally in the range of (200 – 800 ° C) is passed through a converging-diverging nozzle to create a supersonic gas jet [17]. The low processing temperatures (<1000 ºC) of cold spray allows for metallic coatings to be produced with minimal or no oxidation which has led to increased research in this area in recent years [13]. Fig. 2.1 illustrates an example of a cold spray system [18].

Unlike traditional thermal spray processes, the reason for heating the cold spray process gas is not to melt the feedstock powder. Rather the gas is heated primarily to increase the sonic velocity of the gas in the 'throat' (point of smallest diameter, indicated by double arrow in Fig. 2.1) of the converging-diverging nozzle, which creates a higher spray jet velocity, while also reducing process gas consumption. Due to the expansion of the gas in the diverging portion of the nozzle which rapidly cools the gas, it exits the spray gun nozzle at a much lower temperature compared to the entry temperature. Hence the name 'cold' spray.

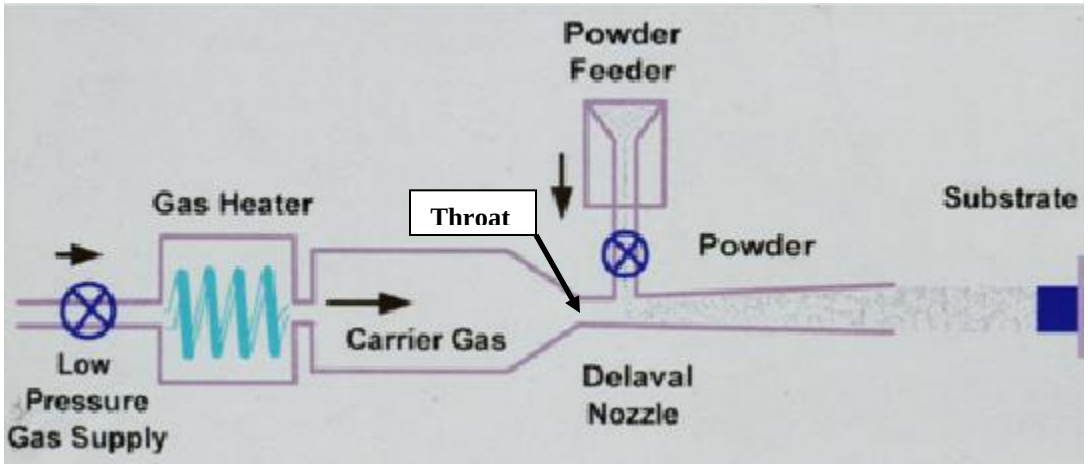


Figure 2.1 Low pressure cold spray system [21].

The high velocities promote plastic deformation of the particles and bonding through adiabatic shear instabilities at the particle-substrate or particle-particle interface during deposition, together with interlocking between the substrate and particles [17]. However, it is difficult to deposit brittle or hard materials, such as ceramics and tungsten carbides, unless they are co-deposited with a ductile matrix material [17]. This is because when the hard and brittle material are deposited at an angle of 90°, the impact may result in brittle fracture of the particles, as well as possible erosion of the previously deposited coating layers [19]. Cold spray requires at least limited ductility of the substrate to produce well-bonded coatings; hence, cold-sprayed coatings over ceramic substrates show limited bond strength [20]. The cold spray process has several benefits including a high deposition efficiency, dense coatings, flexibility in the substrate-coating selection, minimal thermal input to the substrate,

high bond strength, no phase changes and limited oxidation [17,21]. Disadvantages of the process include the use of expensive gas such as helium in order to achieve some of the velocities necessary for deposition of certain metals, and the difficulty in spraying the coating onto complex shapes and internal surfaces as the cold spray process is a line-of-sight process [6,17,22]. In some cases, there is need to conduct post spray annealing for the enhancement of the microstructural and most importantly the mechanical properties [23].

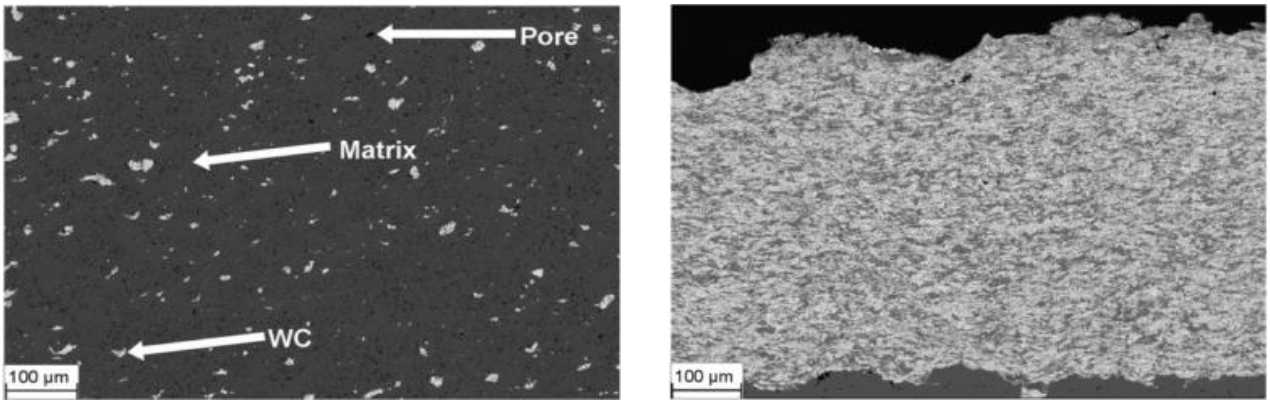
2.2 Tungsten carbide-based cold spray coatings

Tungsten carbide-based coatings have a wide application range because of their unique combination of hardness and toughness, which yields excellent wear resistance [6]. Typical industrial applications include general manufacturing, gas turbine, petroleum, chemical processes, paper/pulp and automotive industries [6,21]. These coatings are often preferred over their bulk counterparts because it is often more feasible to coat a prepared part than it is to prepare and machine a bulk WC-Co alloy [9].

The development of WC-based cold spray coatings has shown that due to the hard and brittle nature of WC, a metallic binder is required to co-deposit the carbide [6,7]. This is based on the plastic deformation required during cold spray deposition which allows the metallic powder particles to adhere to the substrate to form the coating. The hard WC particles, which do not plastically deform, generally tend to shatter on impact and/or to erode the previously deposited coating layers [12]. Typical binder metals used to produce cold spray hardmetal coatings include Al, Cu, Co and Ni, with Co remaining the most commonly used binder material as it provides the highest toughness [22,23]. Majority of the research on cold spray hardmetal coatings thus far has focused on the use of high pressure deposition systems [5,12,22] with limited research into the use of low pressure machines [12]. It is generally more challenging to achieve the adhesion of WC-based coatings using low pressure [10]. The deposition of hardmetal coatings has been shown to depend on the spray

parameters, such as gas temperature and pressure, standoff distance (SOD), substrate properties, powder particle size and morphology, and binder content [5,7,10]. In addition, it has been shown that decarburization, deleterious phase changes, high temperature oxidation and grain growth, all of which normally occur under high temperature deposition conditions, do not occur during cold spraying [3,6,17,19,22,24–26].

Lioma *et al* [10] successfully deposited various blends of WC-Ni using a low pressure CS machine, with Fig. 2.2 showing two of the coating microstructures obtained with the lowest and highest Ni contents respectively. X-ray diffraction (XRD) analysis of the coatings revealed that no phase transformations or grain refinement took place during deposition as no peak broadening was observed. There was low porosity with a non-homogenous distribution of the carbide phase. As the Ni content increased, the volume of carbide particles retained within the Ni matrix decreased, and consequently so did the hardness.



(a) (b)

Figure 2. 2: Microstructures of (a) WC + 50wt.%Ni and (b) WC + 4wt. %Ni coatings [5]. The white regions are the WC phase, while the Ni binder is the grey region.

Nunthavarawong *et al* [11] used a low pressure cold spray machine to investigate the effect of powder feed rate on the mechanical properties of a WC-5wt%Ni coating. Three different feed rates were employed while keeping the other deposition

parameters constant. The highest hardness was attained using a feed-rate of 75%. This feed rate also produced coatings where the highest retention of WC was achieved, the smallest average WC grain size, smallest binder mean free path and the lowest porosity. From XRD analysis no phase changes, decarburization, deleterious phases or oxidation effects were observed. In further research done by Nunthavarawong et al [27] the effect of substrate type on the material properties of WC-5wt%Ni cold spray coatings was investigated, where mild steel and stainless steel samples were used. It was found that the coatings deposited on mild steel had a higher porosity and longer binder mean free paths than the coatings on the stainless steel substrates. The hardness of the coatings on the stainless steel was 10% higher than that of the coating on the mild steel [11].

Melendez *et al* [5,9] employed low pressure cold gas dynamic spraying for developing WC-based metal matrix composite (MMC) coatings, with varying Ni binder contents. Unlike the results observed by Nunthavarawong *et al* [11], Melendez noticed a non-homogenous distribution of the hard WC reinforcing particles within the Ni matrix; this was observed for each coating. No phase changes were detected. An increase in the WC content led to a decrease in the porosity and an increase in the WC deposition efficiency. An inversely proportional relationship between hardness and binder mean free path was observed, and this agrees with work done by Lioma et al [10]. The authors also performed toughness tests and found that as the WC content increased, the likelihood of cracking decreased significantly from 100 % in the coatings with less than 19 wt% WC to 22 wt% in the coatings that contained 66 wt% of reinforcing WC hard particles.

Magagula *et al* [3] used a low pressure cold spray machine to deposit WC-4wt%Ni coatings onto mild steel substrates. An inhomogeneous distribution of the WC phase within the Ni matrix was observed. The authors suggested that the smaller WC particles observed in the coatings were due to the fracturing of the carbide phase during deposition when the particles impacted the substrate. A low retention of

41wt% WC was found in the final coating despite the high 95wt% WC content used in the feedstock powders; this trend was observed by all researchers [3,27].

Silva *et al* [28] used cold gas spray (CGS) to deposit WC-12Co and WC-25Co coatings onto AA 7075-76 alloys. Results showed dense structures with low porosity from the cross-sectional images. Coating thicknesses were 65 µm for WC-12Co and 118 µm for WC-25Co. XRD showed that no new phases were formed in the coatings. Results also showed well distributed ceramic phases, no cracks and no interconnected pores. Silva concluded that the compressive effect of applying the particles using the CGS technique, the appropriate amount of binder, and optimization of spray parameters, resulting in less porous coatings, were the main factors responsible for the high mechanical performance of the WC-25Co coating.

Lee *et al* [29] used CGDS to deposit boron carbide (B_4C), titanium carbide (TiC) and tungsten carbide (WC) based metal matrix composite (MMC) coatings. Nickel was used as the matrix and each carbide powder was mechanically blended with Ni powder prior to spraying. Mathematical modelling showed that the average momentum of the WC particles was more than two times greater than that of the B_4C particles and almost six times greater than that of the TiC particles. The higher momentum of the WC particles led to a higher level of work hardening of the matrix, which resulted in an improvement of the hardness and wear resistance of the MMC coatings. Furthermore, it was found that the high momentum and high fracture toughness of the WC particles increased the roughness of the coating surface and compacted the coating, which led to higher deposition efficiency for this carbide-metal powder blend on previously deposited coating layers. Fig. 2.3 shows the relationship between the carbide content in the starting powder and the carbide retention in the coating. WC shows the highest retention in the resulting coatings with B_4C showing the lowest retention. Fig. 2.4 compares the relationship between porosity and carbide content for the coatings based on WC and TiC. The WC showed

a decrease in porosity as the carbide content increased whereas TiC showed the opposite trend.

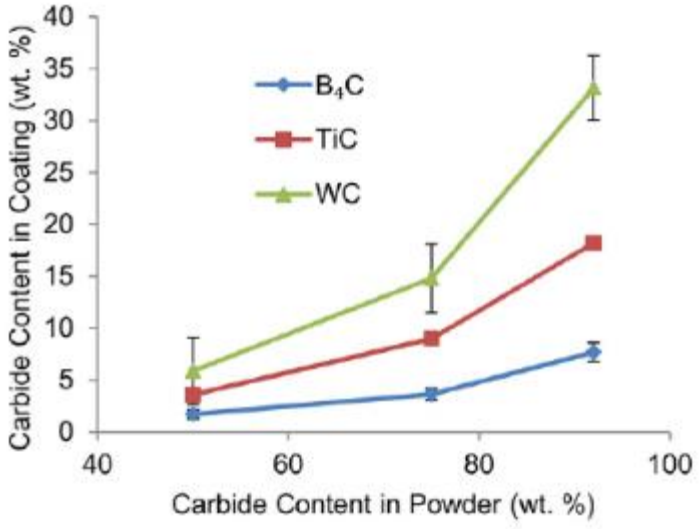


Figure 2. 3: Curves of reinforcing carbide particle content in the coating versus carbide particle content in the powder [29].

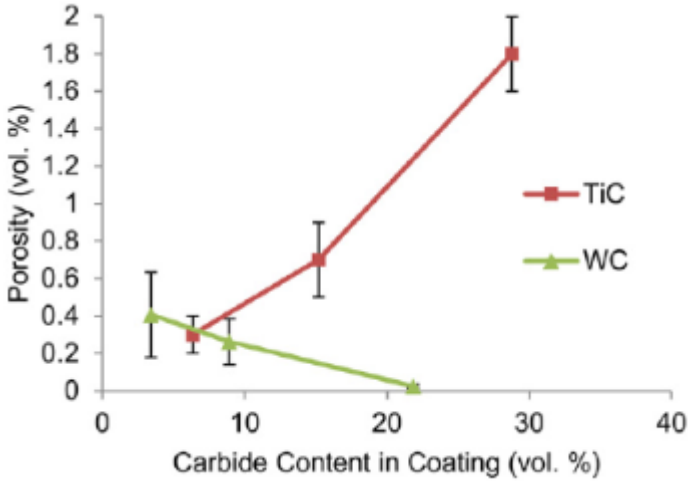


Figure 2. 4: Relationship between porosity and reinforcing carbide particle content in the coating [29].

Alidokht *et al* [30] fabricated Ni-WC coatings using the cold spray method. The WC and Ni powders were fed to the de Laval nozzle from separate hoppers with independent feed rates. The feed rates were adjusted, and a blend of Ni-36.2vol%WC was sprayed which resulted in a composite coating of Ni-10.5vol%WC. Mechanical

properties of the coatings were improved by incorporation of WC into the Ni matrix. Results also revealed that the presence of hard particles in the Ni-WC coating facilitated fast development of the mechanically mixed layer (MML) as well as stabilized the MML, characterized by less plastic flow, fewer cracks and higher hardness. It was also seen that inclusion of the WC phase decreased deposition efficiency and also reduced bonding between Ni particles.

Ji *et al* [31] focused on the deposition behavior of individual bimodal WC-12Co particles impacting on stainless steel and WC-12Co substrates. Results showed partial penetration of WC-12Co particles into the stainless steel substrate; similar results were reported by Nunthavarawong *et al* [11]. Flattening of the particles occurred due to impact on the WC-12Co substrate. During the impacting and flattening process of the powders, WC particles moved accompanied with plastic flow of the Co binder. The coating exhibited a microstructure with a wide range of WC particle sizes varying from less than 100 nm up to a micron scale. XRD analysis showed that no new phases were formed. It was concluded that the hardness of the substrate exerted an important influence on the deformation and flattening behavior of the powders. Obtained multimodal coatings exhibited both a high hardness and high fracture toughness.

Wang *et al* [32] deposited three multimodal WC-17Co CGDS coatings with different contents of nano-sized WC (10%, 30% and 50% in wt.%). Results demonstrated that the multimodal WC-17Co deposits exhibited a dense microstructure with some areas composing of Co and nano WC. Phase structures were similar to that of the feedstock powders. The micro-hardness and fracture toughness of the multimodal WC-17wt. % Co deposits respectively increased and decreased with increasing content of nano-sized WC. Some fracture of the WC occurred during deposition.

Ang *et al* [7] examined the WC particle size and its influence on the deposition of Co-based cermets. Micron and nanostructured powders with similar Co content were

employed. Results showed that micrometer-structured WC-Co feedstock powders did not permit coating build up when processed under comparable or thermal spray parameters used for the nanostructured WC-Co feedstock powders. In addition, micrometer-structured WC-Co coatings exhibited a conjoint erosion and deposition effect on the surface. Fine WC particles (< 1µm) were observed near the substrate interface and larger WC particles (1-2 µm) in the vicinity of the coating surface. These observations indicated the existence of a critical WC particle size for deposition by the cold spray method and that the size criteria arises due to the formation and cohesion mechanisms within the coating layer. Particle refinement occurred and was reflected by broadening of the XRD peaks. It was concluded that there is a WC particle size limit above which the thickness of a CS coating does not build up. For example, micron structured PM-17 WC-Co powder agglomerate sprayed at a higher velocity did not permit coating build-up. In such instances, a higher content of the Co binder phase, which increases the ductility of the powder and allows more deformation for cohesion between the interacting surfaces, is required. Table 2.1 shows the powder compositions that were employed in the investigation. Note : PM = Praxair; IN = Inframet; BN = Buffalo Tungsten [7].

Table 2. 1: Nominal composition of respective powders.

Designation	Method	Nominal composition	Mean particle size	Porosity
PM17	Conventional, sintered and crushed	WC-17wt.%Co	30.67 µm	29 %
IN17	Wet chemically synthesized and agglomerated	WC-17wt.%Co	30.09 µm	11 %
BN17	Wet chemically synthesized and agglomerated	WC-17wt.%Co	31.40 µm	38 %

Subsequent PM17 particles did not possess sufficient metallic Co binder and critical velocities and thus these particles caused erosion of the substrates and reduction of WC particles caused their refinement and splat breakup. Interactions of the WC particles at high velocities caused the breakup and formation of fine grains at the primary layers of PM17 coatings as shown in Fig. 2.5.

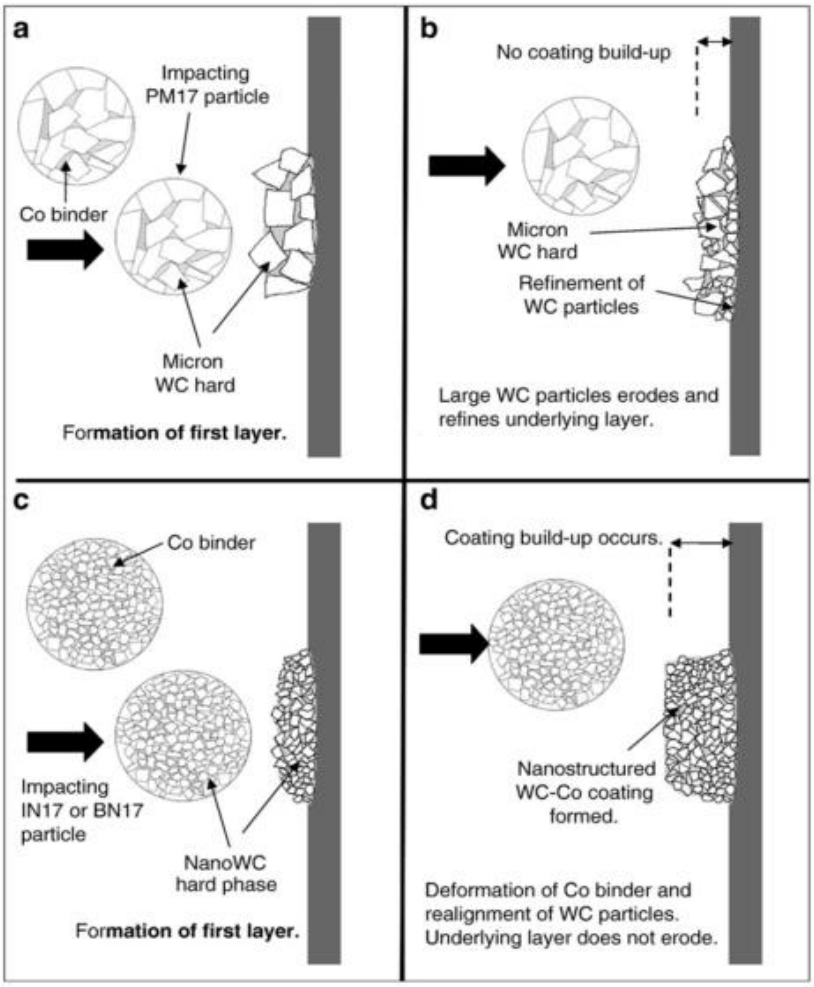


Figure 2. 5: Coating formation with different feedstock PM-17 (a, b) and nanostructured IN-17 or BN-17 (c, d) [7].

Kim *et al* [33] deposited WC-Ni cold sprayed coatings and changed contents of Ni for possible application to secondary water chemistry environment. Results showed WC-10wt. % Ni coatings having a hollow and broken form which failed to maintain spherical shape of the grains. WC-20wt. % Ni, however, maintained a spherical shape. The Ni amount was reported to have an effect on powder shape and lower

activation energy of composite powder due to form a spherical shape. Additional Ni powder to WC-10wt. % Ni lowered critical velocity and made it possible to coat on carbon steel. Relatively large powder lowered critical velocity of powder and plastic deformation occurred. It was concluded that increasing Ni contents in feedstock powders has an advantage for reducing porosity on coating surfaces.

Yin *et al* [34] used a high pressure CGDS system to fabricate WC-Co-Ni wear resistant coatings under moderate working parameters, and to clarify the coating formation mechanism. Mechanically mixed porous WC-17wt. % Co and dense Ni powders were selected as the feedstock with different WC mass fractions namely F1 (41.5%), F2 (64.5%) and F3 (74.7%). Results showed that the WC reinforcements had no phase transformation and were completely retained in the WC-Co-Ni coatings similar to the feedstock. Fracture of the porous WC-Co particles during the deposition process was found to be the reason for such high WC retainability dominating the coating formation mechanism.

2.3 Abrasive Wear

Abrasive wear is the progressive volume loss of material from a surface arising from mechanical action by solid particles, whereby the softer surface experiences material degradation by interacting with the harder surface or harder particles [35]. There are two abrasive modes as illustrated in Fig. 2.6.

1. Two-body abrasion: this mode of abrasive wear is caused by hard protuberances on the counter face [36]. Stachowiak et al [37] likened the passing of hard asperities or rigid grit over the surface to a cutting tool. This is illustrated in Fig. 2.6(a).
2. Three-body abrasion: in this abrasive mode, hard particles are free to roll and slide between two sliding surfaces as illustrated in Fig. 2.6(b).

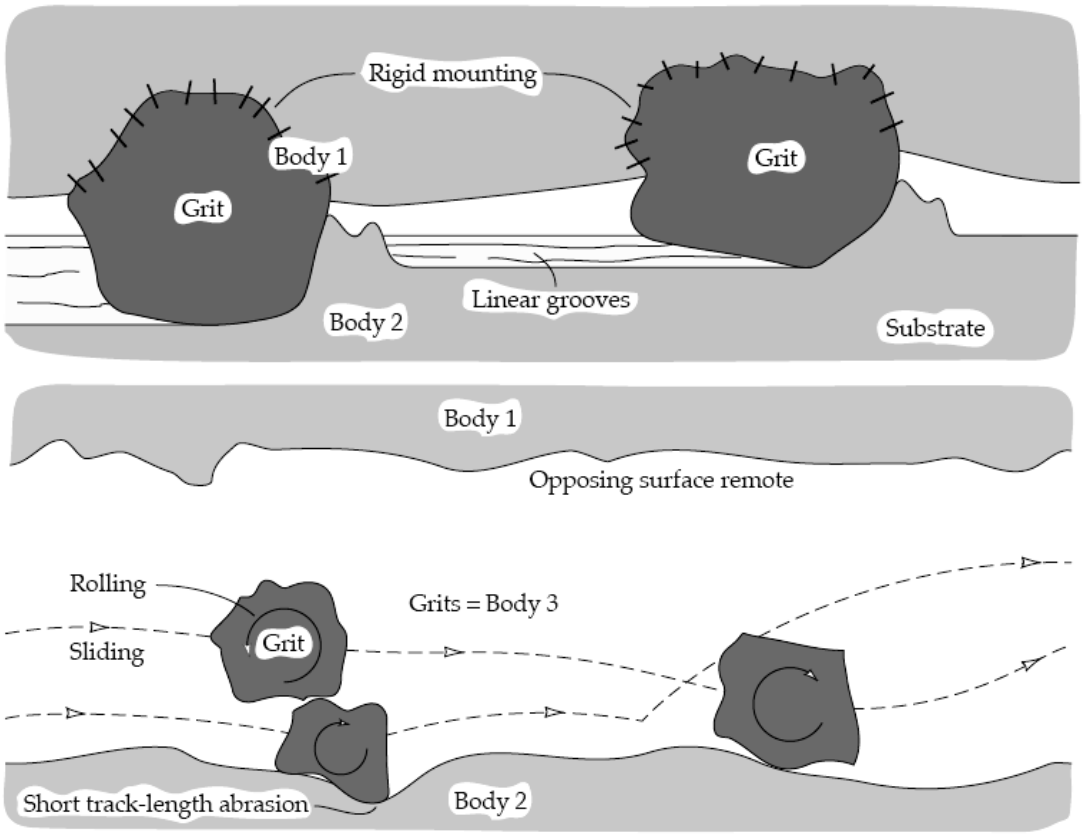


Figure 2. 6: Schematics showing (a) two-body abrasion and (b) three-body abrasion [38].

2.3.1 Slurry abrasion wear

Slurry abrasion is damage to a component surface which arises because of the motion relative to that of either harder asperities or perhaps hard particles trapped at the interface carried in a liquid medium [39]. Such hard particles may have been introduced between the two softer surfaces as a contaminant from the outside environment, or they may have been formed in situ by oxidation or some other chemical or mechanical process. Wear by slurry abrasion occurs in extruders, slurry pumps, and pipes carrying slurry of minerals and ores in mineral processing industries [4]. The wear life of components used under slurry abrasion conditions is governed by the process parameters such as, duration of exposure and amount of

abrasive particles. The properties of abrasive particles in slurry and material properties also affect the wear life [4]. Wear by slurry abrasion is a potential problem in engineering components subjected to particulate flow [40]. The most commonly used laboratory tests (Fig. 2.7) for abrasive wear employ either pin-shaped specimen sliding against fixed abrasive, or a rotating wheel sliding against a plane specimen with loose abrasive particles being continuously fed between the two [36,39].

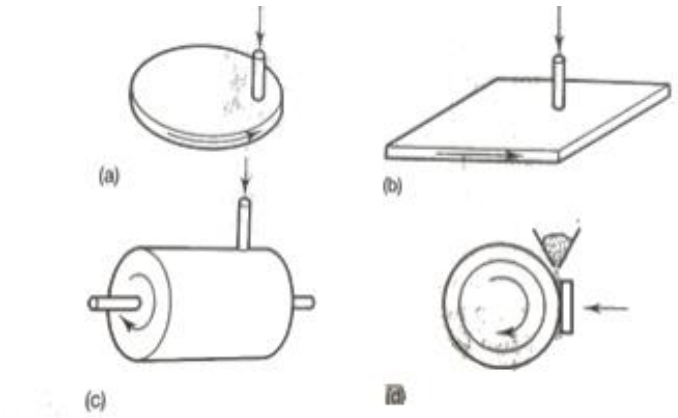


Figure 2. 7: Schematic illustration of four common methods used to measure abrasive wear rates of materials: (a) pin on abrasive disc; (b) pin on abrasive plate; (c) pin on abrasive drum; (d) rubber wheel abrasion test [36].

Fig. 2.8 (a) to (c) shows three common variants of the method in which a specimen pin slides against fixed abrasive particles, giving two-body wear [36]. Apparatus of this type are specified in a German national standard procedure for abrasion testing of rubber (DIN 53516) [36]. Fig. 2.8 (d) illustrates schematically the second common type of abrasive wear test. The specimen is in the form of a plate or a block, pressed under constant load against the rim of a rotating wheel, this process follows the US standard (ASTM G65; *Standard Practice for Conducting Dry-Sand/Rubber Wheel Abrasion Tests*) [36].

Hutchings [36] defines three distinct modes of deformation due to a rigid two-dimensional wedge (an idealized abrasive particle) sliding over a rigid-plastic material. Fig. 2.8 shows the different cutting modes

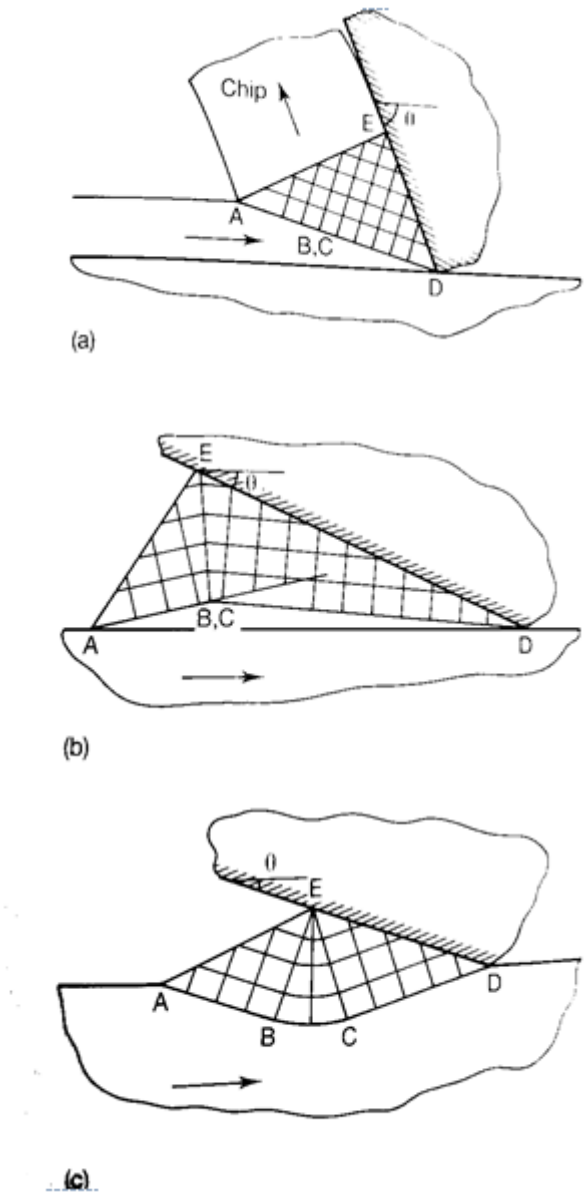


Figure 2. 8: Slip line fields for the deformation of a perfectly plastic material caused by the sliding of a rigid two-dimensional wedge from right to left. Three distinct modes can be identified, (a) cutting; (b) wedge formation; (c) ploughing. The angle Θ is termed the 'attack angle'[36].

2.4 Abrasion of WC-based coatings

Cermet coatings are widely used in wear situations because they combine several advantageous properties such as resistance to abrasion, erosion, high temperature and corrosive atmospheres [25,41]. Various compositions and microstructures of these coatings have been tested successfully in several high energy wear situations such as sliding, fretting, abrasion and erosion [2]. For this research work, the wear mechanism which was investigated was slurry abrasion; hence a review will be done of the abrasive wear of cemented tungsten carbide coatings.

2.4.1 Abrasion of high temperature cemented tungsten carbide coatings

Fig. 2.9 shows graphs of comparative wear rates for WC-based coatings which were subjected to high-stress (Fig. 2.9 a) and low-stress (Fig. 2.9 b) abrasion. The y-axis represents wear rate defined as volume per unit distance. The alloy names represent different Co binder contents and hardness values as listed in Table 2.1. The hardness increased with a decrease in binder content.

Microstructure studies revealed that the coatings under the APS (air spraying) group code were more porous than those with the VPS (partial vacuum spraying) code, hence the lower hardness values. Table 2.2 shows hardness values of the coatings associated with the WC quantity in the coatings; a larger amount of WC led to a larger hardness value.

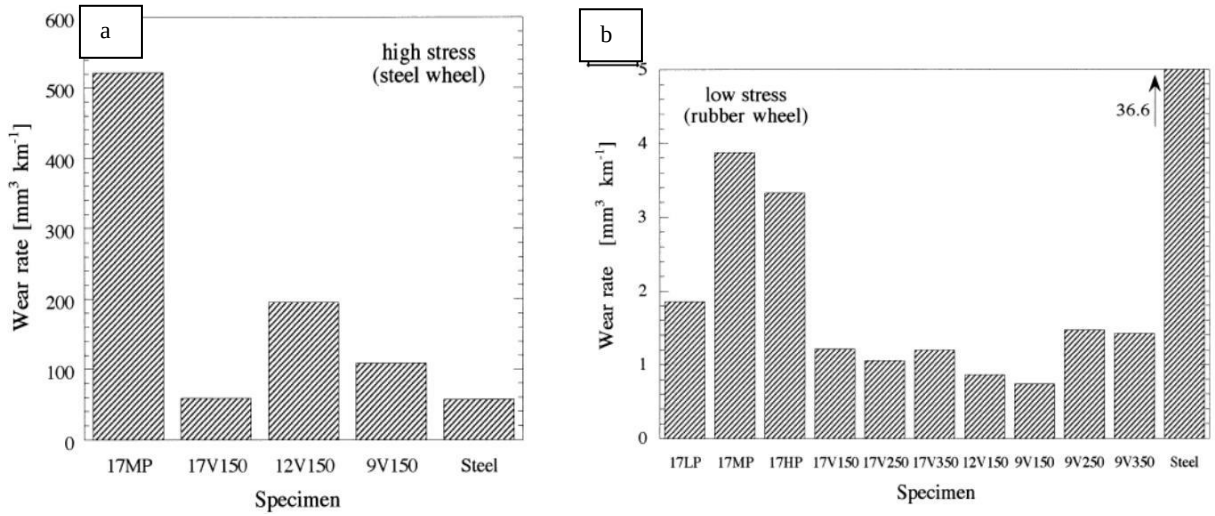


Figure 2. 9 Wear rates of WC-Co coatings under (A) high-stress, and (B) low-stress conditions [25].

Table 2. 2: WC-Co coatings hardness values [25].

Powder	**Group code**	**Coating code**	**Coating hardness HV at 2.94N**
WC-17%Co	17APS	17LP	592±60
		17MP	661±66
		17HP	661±66
	17VPS	17V150	859±86
		17V250	832±83
		17V350	854±85
WC-12%Co	12VPS	12V150	825±82
WC-9%Co	9VPS	9V250	956±96
		9V250	945±949
		V350	846±85

Higher wear rates were observed under high-stress abrasion compared to low-stress abrasion and the wear rates were aligned with the hardness values and this was in agreement with the work done by Machio *et al* [1] who replaced part of the WC hard phase with a VC phase thereby increasing the hardness which led to good wear

resistance. The wear response was explained in terms of the differences in the inter-pass bond strength of the coatings, the carbide particle distribution, and the coating porosity. For example, coating 17V150 had homogeneously distributed rounded WC grains while coating 9V150 had clusters of small angular carbides. All the VPS coatings showed a greater wear resistance than the APS coatings. However Liao *et al* [41] reported VPS coatings to have less abrasive resistance when compared to HVOF deposited coatings. Among the VPS coatings deposited from 17wt% Co powder at different pressures, little difference was evident in the wear resistance. However the wear resistance of the 9V150 coating was significantly better than that of 9V250 and 9V350, which were deposited at higher pressure.

Liao *et al* [41] investigated the influence of the abrasive grain size on the abrasive resistance of WC-Co coatings deposited by APS (atmospheric plasma spraying), HVOF (high velocity oxy-fuel) and VPS (vacuum plasma spraying). Results showed that the larger the abrasive particle size, the lower the abrasion resistance of the coatings. Under the same abrasion test parameters, HVOF based coatings gave the best abrasion resistance with VPS based coatings giving the least abrasion resistance. Alumina grits used in the investigation were of 30 µm, 60 µm and 100 µm particle sizes respectively with ASTM B611 – 85 standards being adhered to. Liao *et al* [41] reported that in order to increase the abrasion resistance of these materials, it is very important to increase the cohesion between the carbide particles and the cobalt matrix as was achieved by Chen *et al* [25] who deposited a homogenous WC-17%Co coating that displayed good abrasive resistance. Cohesion is related to the amorphous or nanocrystalline interaction phases in the coatings at the interphase between the carbides and the matrix.

Machio *et al* [1] deposited WC-12wt.%Co and WC-17wt.%Co as well as experimental WC-10wt.%VC-12wt.%Co and WC-10wt.%VC-17wt.%Co coatings, on stainless steel substrates using a high pressure (HP/HVOF) Tafa® JP5000™ thermal spraying system. The wear behavior of the WC-VC-Co coatings from

optimized powders was compared with commercial WC-Co coatings with the WC-VC-Co coatings exhibiting the higher abrasion resistance. Fig. 2.10 shows the mass loss curves from slurry abrasion tests. There was a tendency for all four coatings to have a reduced mass loss as the abrasion tests approached the hour mark. The powder blend that was reinforced with 10 wt. % VC had the lowest mass loss with WC-10wt. %VC-17wt. %Co and WC-12wt. %Co displaying almost similar mass loss readings. Here it is evident that replacing part of the WC hard phase in WC-Co by VC led to better abrasion resistance and Machio [1] had similar findings in both dry and slurry abrasion conditions with silica sand having elongated morphology used as the abrasive. This improvement in abrasion resistance was mainly caused by the VC hindering WC grain growth [1]. These findings are similar and were reported by H. Liao *et al* [41].

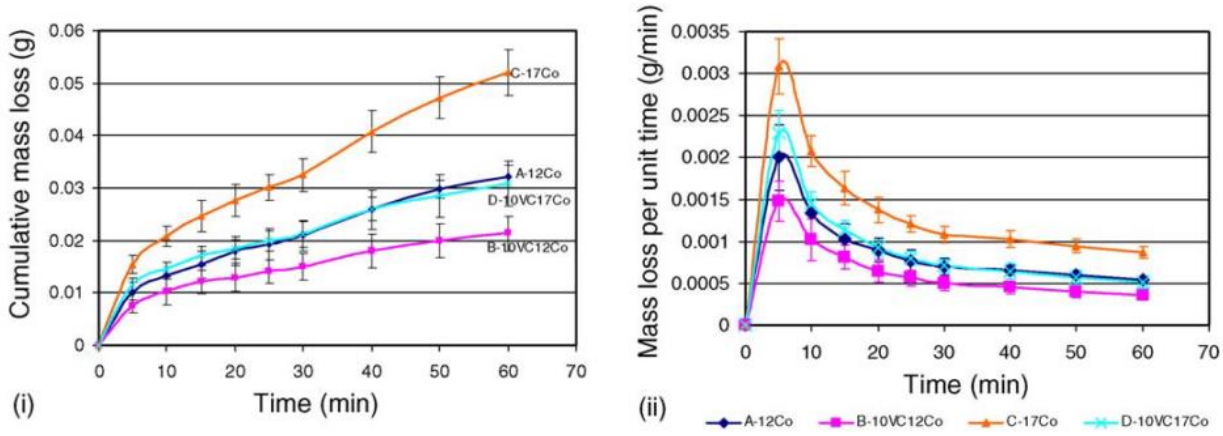


Figure 2. 10: Mass loss curves in wet abrasion. (i) Cumulative mass loss curves, (ii) Mass loss per unit time curves [1].

Kumari *et al* [42] deposited WC-10Co-4Cr coatings using HVOF and pulsed combustion. The study was focused on a detailed exploration of the influence of the coating microstructure on the abrasive wear mechanism. Alumina was used as the abrasive. The authors reported on the importance of binder mean free path affecting the resistance of good quality (low porosity) coatings. Results showed that a lower binder mean free path gave a higher abrasive wear resistance because the abrasive wear mechanism of the coatings was dominated by preferential removal of the binder

phase, followed by pullout of grains. This was in agreement with Liao *et al* [41] who reported on the importance of binder matrix and carbide cohesion.

Wang *et al* [26] (2008) deposited WC-12wt.%Co coatings using a HVOF system. Multimodal and conventional materials were used to fabricate the coatings. Results indicated that multimodal coatings showed slightly higher micro-hardness, denser microstructures and better abrasive wear resistance than the conventional coatings. Wang *et al* [26] also reported that thermally sprayed carbide-based phase coatings have excellent wear resistance when compared to hard chrome coatings which was in agreement with work done by Liao *et al* [41]. It was also concluded that both multimodal and conventional WC-12wt. %Co coatings exhibit more excellent abrasive resistance in comparison with mild steel and hard chrome plating. Fig. 2.11 shows micrographs of the powders that were used in the investigation and the multimodal powder shows a clear spherical morphology in Fig. 2.11(a) whereas the conventional powder shows an irregular morphology.

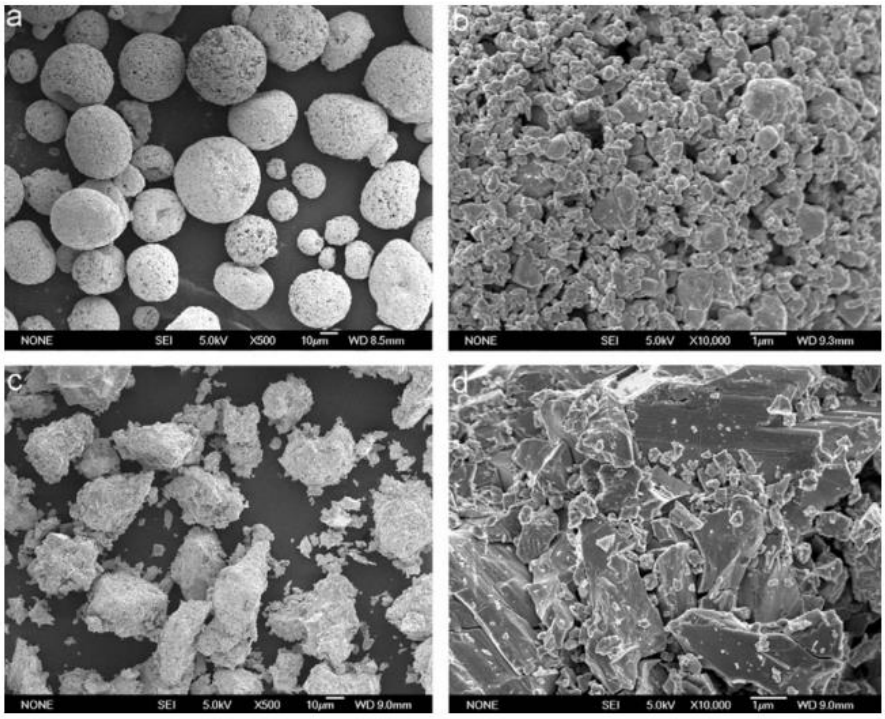


Figure 2. 11: Micrographs of multimodal and conventional WC-12Co powder at different magnification (a and b) multimodal powder and (c and d) conventional powder [26].

2.4.2 Abrasion of cold sprayed cemented tungsten carbide coatings

Limited research has been done on the abrasion of cold sprayed WC-based coatings. Magagula *et al* [3] performed slurry abrasion testing on WC-Ni and WC-Ni-Mo cold sprayed coatings where the effect of synthetic mine water was assessed. The corrosive effect of the mine water increased the slurry abrasion rates by 50%. The addition of Mo did not improve the wear properties of the coatings. The mechanisms of material removal in the coatings were found to be those commonly associated with hardmetals, namely selective removal of the binder likely caused by plastic deformation and fatigue due to repeated action of the abrasive particles followed by undermining of the carbide particles resulting in eventual pull out of the carbide grains.

Research on the dry abrasion response of low pressure cold sprayed WC-Ni coatings was conducted by Melendez *et al* [9] for a range of WC-based metal matrix composites. The binder mean free path between the WC grains was used to explain the improvements in wear rate and the relationship is illustrated in Fig. 2.12. The coatings with the highest WC content and smallest binder mean free path had the lowest wear rates. This result was found to be comparable to coatings deposited by high velocity oxy-fuel (HVOF) and high pressure cold spray.

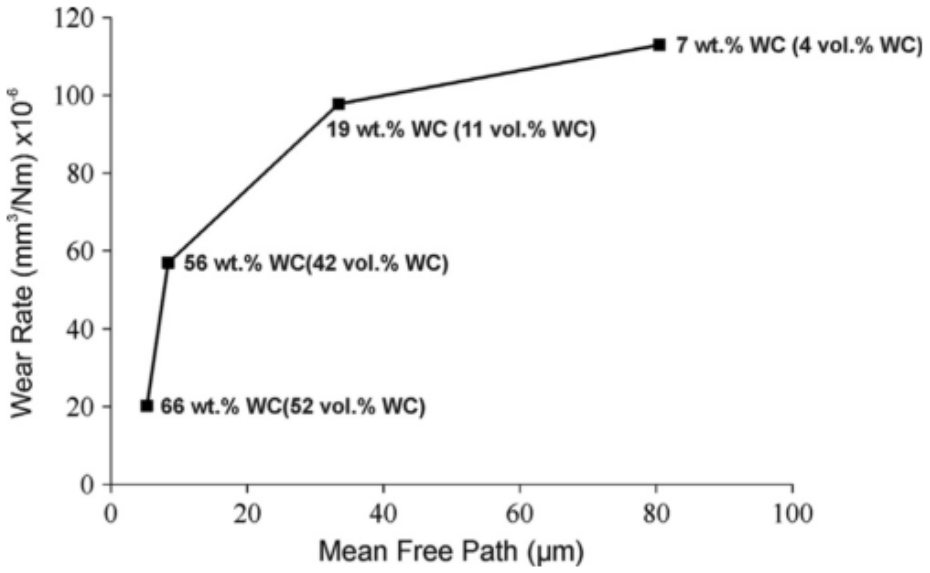


Figure 2. 12 Influence of binder mean free path on wear rate [9].

Ji *et al* [31] used CGDS to deposit bimodal WC-12wt.%Co onto stainless steel substrates. Characterization showed that the WC-12wt.%Co particles partially penetrated into the stainless steel substrate. A movement of small WC particles accompanied with a plastic flow of the Co binder occurred during the impacting and flattening process of the powders. The obtained multimodal coating exhibited both a high hardness and high fracture toughness. The authors reported that the cold sprayed coating exhibited a greatly enhanced wear resistance in comparison to the conventional HVOF sprayed WC-12wt. % Co coating.

Wang *et al* [32] used CGDS to deposit three multimodal WC-17Co deposits with different content of nano-sized WC (10 %, 30 % and 50 % in wt.%). The effect of micro/nano ratio of WC particles on the microstructure, phase composition and properties such as microhardness, fracture toughness and wear performance of cold-sprayed multimodal WC-12Co coating was investigated. The experimental results demonstrated that the cold-sprayed multimodal WC-17Co deposits exhibited dense microstructure with their phase structures similar to that of the feedstock. The

abrasive wear resistance of the coating was evaluated using a pin-on-disk tester. During the tests, the pin specimen was loaded against a rotating disk covered with a SiC abrasive paper 300 grit. The applied load was 10 N and the wear distance was 16 m. The wear resistances of three multimodal WC-17Co deposits were compared using a two-body abrasive wear tester. It was found that the wear weight loss of the three deposits decreased from 5.53 ± 0.11 mg to 2.67 ± 0.15 mg and the deposit exhibited the lowest wear weight loss. However, the wear weight loss of all deposits was much less than that of stainless steel bulk (28.2 ± 3.11 mg) in identical wear condition.

In general for slurry abrasion systems the hard particles which cause wear may come from the material itself or from the outside environment. In addition to hardness, the abrasive particle size and the slurry medium type will also influence the abrasion response of the coatings [3]. Small abrasive particles tend to preferentially wear the matrix around the WC particles, with the toughness of the matrix favoring micro-cutting; this induces a periodicity in the surface roughness and when the matrix has been removed around the carbide particles, the latter is pulled out and holes appear on the surface.

2.5 Annealing of WC and Ni-based coatings

Annealing is a term used to describe a variety of softening heat treatments by changing the microstructure of an alloy [43]. Annealing is used mainly to remove stresses, to alter ductility, to induce softness or to produce amongst other things a defined crystalline grain structure [43]. Coatings that undergo annealing have their mechanical properties improved, especially an increase in hardness and fracture toughness [44]. During annealing gas pores slowly expand, thus lowering their internal pressure until an equilibrium between the gas pressure and the strength of the coating at the annealing temperature has been reached [45]. This section will review how annealing has been used to improve coating properties.

Huang *et al* [46] subjected a Ni-Ti (at the atomic ratio 50/50) cold sprayed coating to annealing in order to form intermetallic phases for healing non-bonded gaps after deposition. When the coating was heat treated at 700°C, it was confirmed that the Ni particles became large and a different contrast from both Ni and Ti appeared at both boundaries. The high temperatures employed during heat treatment also caused a higher diffusion of Ni in Ti compared to Ti in Ni. By changing the heat treatment conditions, the uniform intermetallic phases were obtained, which increased the coating porosity rapidly at an elevated temperature due to the Kirkendall effect.

Vashishta *et al* [47] investigated the effect of heat treatment (300 – 950 °C) on the abrasive wear behavior of WC-12Co and Cr_3C_2-25NiCr HVOF coatings. Figs 2.13 and 2.14 show the effect of heat treatment temperature on the abrasive wear rate of the two coatings as a function of the applied load used in the abrasive wear tests. Both coatings demonstrate a general increase in abrasive wear rate with increasing heat treatment temperature for the 45 N and 60 N loads, however there is a general decrease in abrasive wear for temperatures below 600°C for loads of 15 N and 30 N. Above 600 °C the abrasive wear increased for the cold sprayed coatings by a factor of 10-15% up to 950 °C. Phase transformations and variations in mechanical properties

predominantly influenced the abrasive wear resistance. It was concluded that the low temperature heat treatment may be used to increase the wear resistance of the coatings under benign abrasive wear conditions.

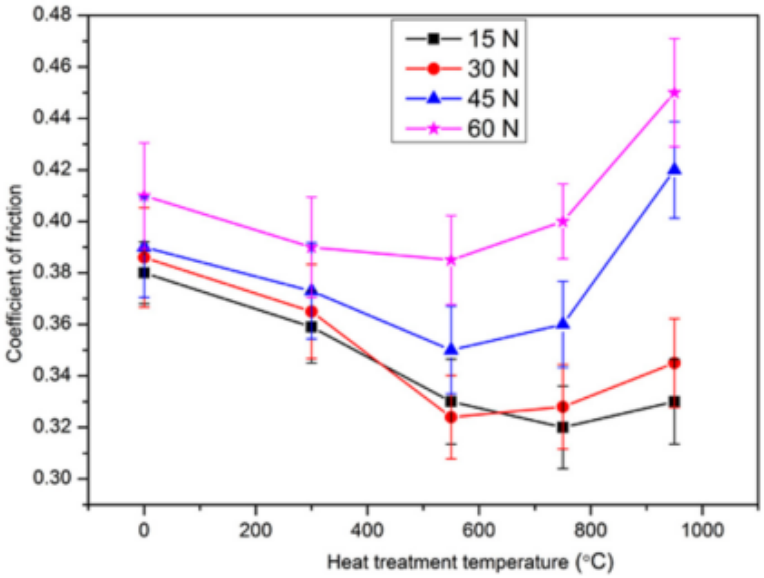


Figure 2. 13: Abrasive wear rate Vs heat treatment temperature of WC-12Co [47].

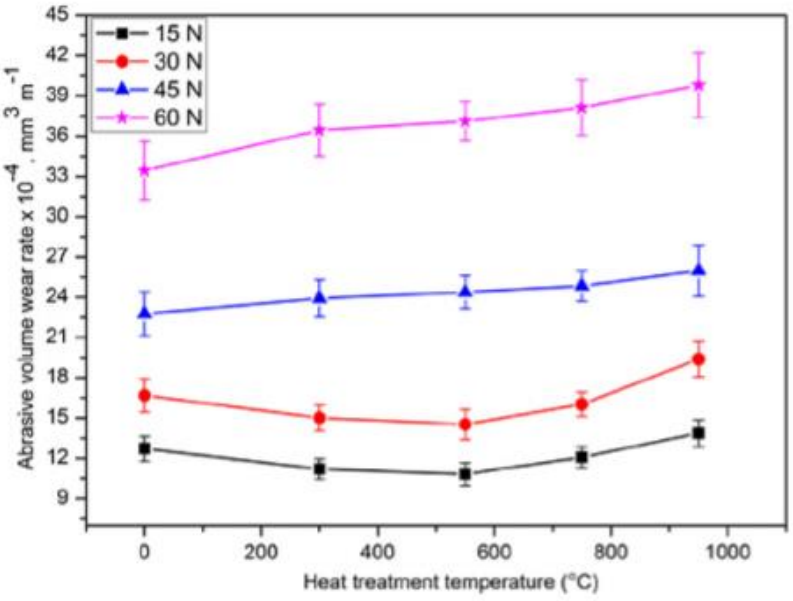


Figure 2. 14: Abrasive wear rate Vs heat treatment temperature of Cr_3C_2-25NiCr [47].

Fig. 2.15 shows a map outlining the abrasive wear rates and severity of contact for two different coatings namely WC-12Co and Cr_3C_2-25NiCr [47]. The map is divided into three different zones namely, plastic deformation, intermediate (plastic deformation and brittle phase) and lastly brittle fracture. The wear damage associated with each zone and severity of contact region is also shown. The graph also shows different stages vertically, namely, mild, medium, severe and very severe. The mild stage of abrasive wear is associated with extrusion of binder, fatigue and microcracking and this is usually experienced once a surface comes into contact with an abrasive surface. Both coatings experienced this in Zone 1 of plastic deformation. The WC-12Co coating did not experience severe abrasive wear. WC-12Co showed a better wear behavior as it only experienced medium abrasive wear at annealing temperatures of 750 °C and 950 °C however; it experienced Zone 3 – brittle fracture at over 10 x 10^6 level of severity of contact. The Cr-based coating experienced Zone 3 –brittle fracture very severe abrasive wear rate at over 16 x 10^6 level of severity of contact at annealing temperatures of 750 °C and 950 °C.

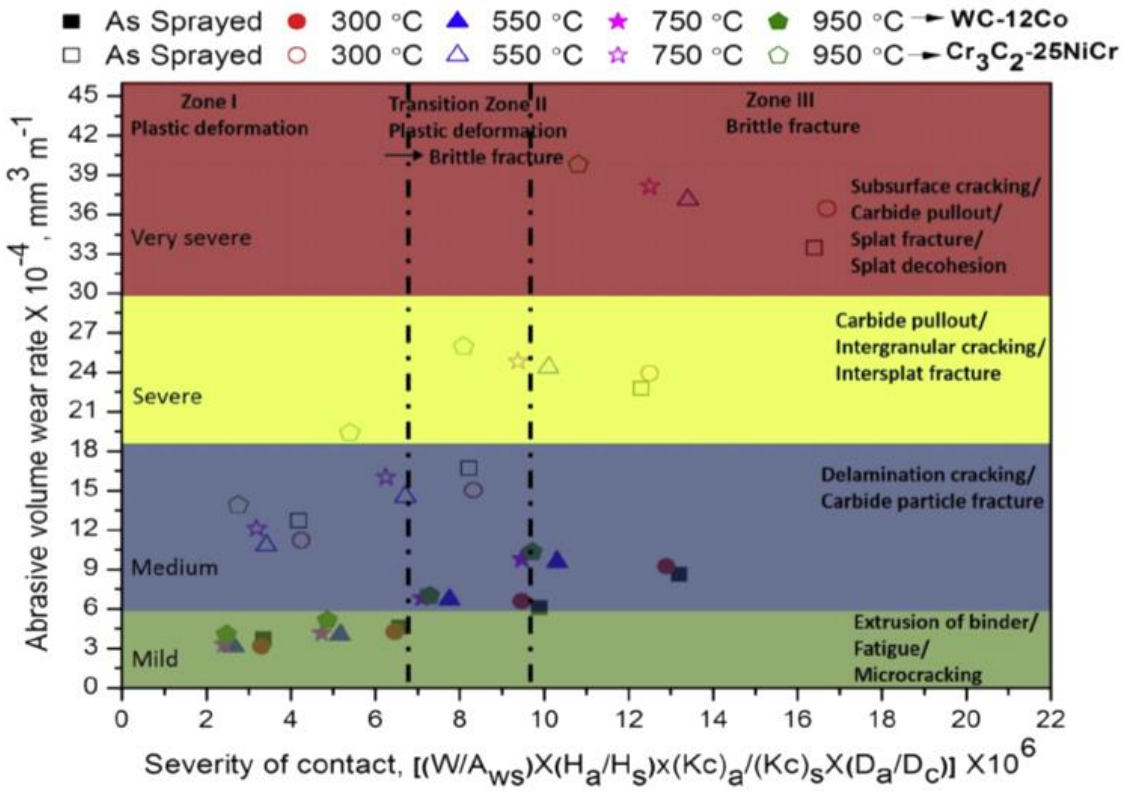


Figure 2. 15: Abrasive wear rate of WC-12Co and Cr_3C_2-25NiCr vs. severity contact of SoC [47].

Stewart *et al* [48] subjected WC-17wt%Co HVOF coatings to annealing at temperatures between 250 – 1100 °C prior to wear testing. At all temperatures changes in the integrity and residual stress state of the coating occurred due to thermal expansion coefficient mismatch between the coating and substrate. Above 600 °C, significant phase changes were found within the coating. The annealed coatings showed improved wear behavior compared to the as-sprayed coatings. Improvements in the wear resistance of up to 35 % were detected at temperatures as low as 250 °C. It was concluded that the abrasive wear behavior can be correlated to the residual stress state, coating integrity and microstructure.

Janka *et al* [49] investigated the influence of annealing on the microstructure, mechanical properties and abrasive wear of a HVOF Cr_3C_2-NiCr coating. The wear resistance was evaluated in low and high-stress abrasion regimes, the latter in a temperature range of up to 800 °C. Fig. 2.16 (a) shows the relationship between Vickers hardness and annealing temperatures while Fig. 2.16 (b) shows the mass loss comparison between the annealed and un-annealed as-sprayed coating. The as-sprayed coatings had the highest hardness, while a non-linear decrease in hardness was observed as the annealing temperature increased. The mass loss of the annealed coating was higher as expected from the hardness values. Precipitation of secondary carbides from the supersaturated as-sprayed binder matrix due to heat treatment was at the core of the observed changes in the coatings wear resistance.

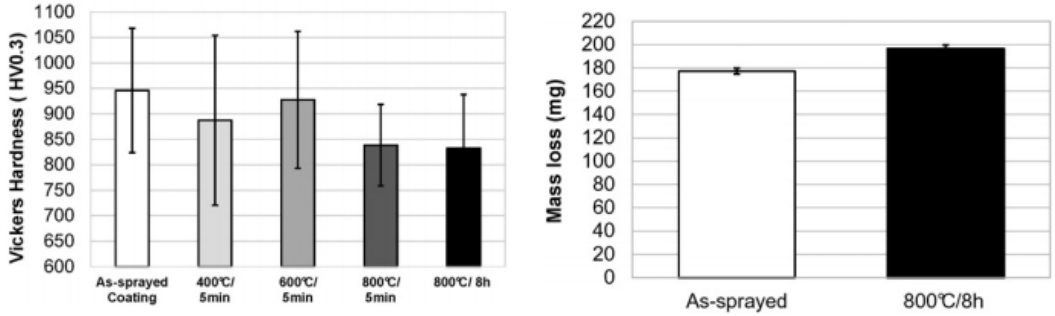


Figure 2. 16: Vickers hardness as a function of temperature and (b) mass loss of as-sprayed and heat treated coatings [49].

Wang *et al* [50] annealed HVOF WC-12Co coatings at temperatures of (550, 750, 900 and 1150) °C respectively for an hour in an Argon atmosphere. Various coating properties such as hardness, fracture toughness, abrasive wear resistance, phase composition and microstructure were investigated before and after heat treatment. X-ray diffraction analyses showed that the as-sprayed coating was comprised mainly of WC, an amorphous phase, a small amount of W_2C and trace metals W. For the annealed coatings, as the temperature increased the amorphous phase was found to gradually transform into eta phases such as CO_3W_3C, CO_6W_6C and CO_2W_4C, coupled with an increase of W_2C and WC phases. Elemental diffusion and new phase generation processes at the coating-substrate interface and within the coating were

shown by XPS, SEM and TEM analyses. As shown in Fig. 2.17 hardness increased initially with an increase in the heat treatment temperature followed by a decrease, whereas the reverse trend was found for fracture toughness. Slurry abrasion testing (refer to Fig 2.17) showed that the WC-12Co heat treated at 950 °C had the highest wear resistance among all the coatings due to formation of the hard and crystalline CO_6W_6C phase and tough Co phase while conserving the WC phase.

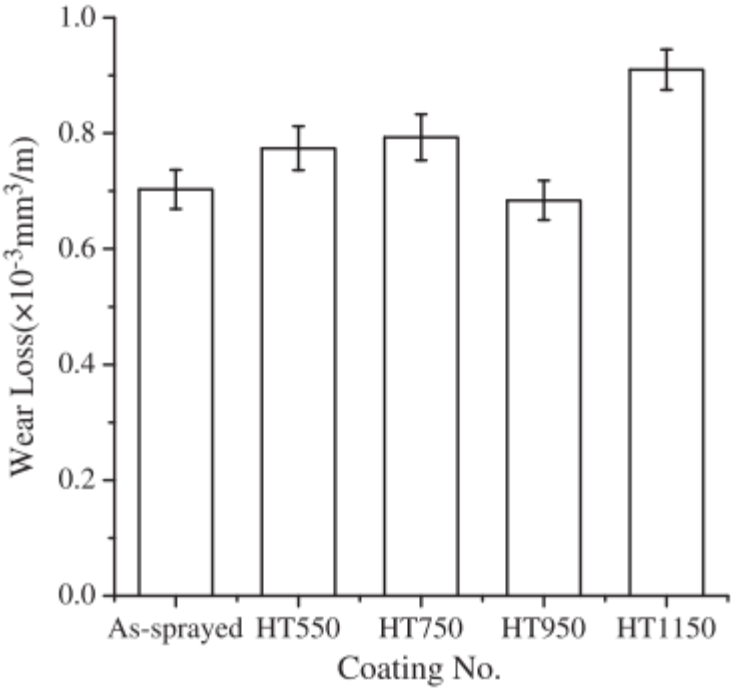


Figure 2. 17: The effects of heat treatment on the abrasive wear rate of as-sprayed and heat treated coatings [50].

Picas *et al* [51] studied the high-temperature performance of an HVOF Cr_3C_2-CoNiCrAlY coating which was also subjected to annealing at temperatures between 900 °C and 1100 °C prior to testing. The results showed precipitation of the carbide particles in the matrix phase after the 900 °C heat treatment of the coating thereby increasing the coating hardness. Higher temperatures led to the growth of carbide particles, with coalescence of grains leading to the formation of an extensive carbide structure that caused a hardness increase inside the coating. The use of the bond

coating (CoNiCrAlY) between the Cr_3C_2-CoNiCrAlY coating and the steel substrate reduced the difference in their thermal expansion coefficients, thereby minimizing stress generation and improving the thermal shock resistance, coating adherence and wear resistance at high temperature. Fig 2.18 shows the microstructure of HVOF-sprayed CoNiCrAlY bond coat after heat treatment in air at 900 °C. Fig 2.18 (a) shows typical two-phase γ/β microstructure clearly visible after 4 hours of heat treatment. It is reported that the reappearance of the β-phase was attributed to the fact that the heat treatment alleviates the stresses that were initially responsible for the dissolution of the β-phase. The second possibility is that the coating was held at 900 °C for sufficient time to allow diffusion and the excess of Al in the γ phase (blue arrow) caused the nucleation and growth of the β phase (black arrow). This causes the system to get closer to its equilibrium. Fig 2.18 (b) shows at a higher temperature of heat treatment (1100 °C) the oxidation of the coating progresses and the oxide scale (red arrow) thickness is observed both in the inter-splat boundaries as in the bond-coat coat interface (blue arrow) at approximately 2 µm .

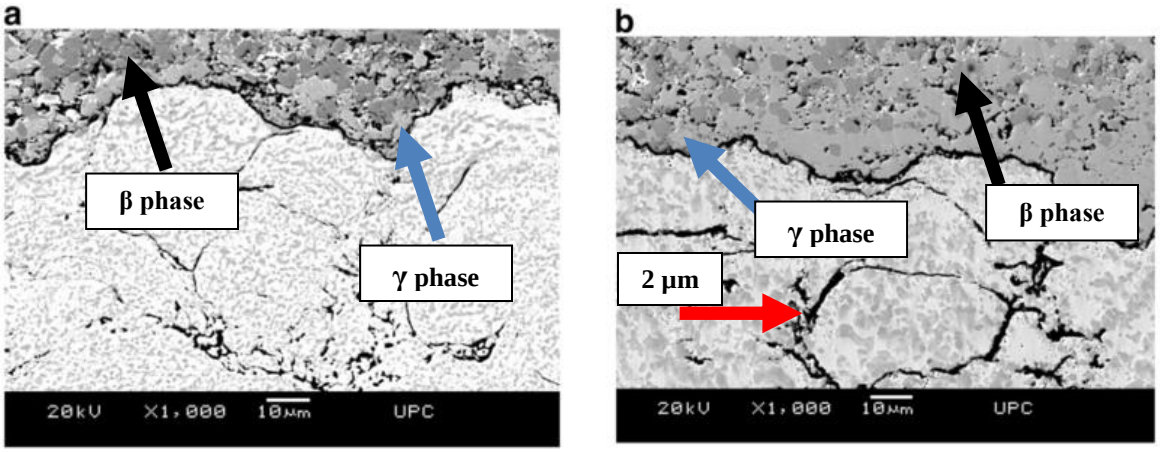


Figure 2. 18: BSE images of the microstructure of HVOF-sprayed CoNiCrAlY bond-coating after heat treatment in stationary atmospheric conditions at (a) 900 °C and (b) 1100 °C.

2.6 Summary

In summary, literature has shown that it is possible to use a low pressure cold spray system to deposit WC-based cold spray coatings with good properties. Various WC-binder blends have been investigated in order to study the effect of binder content and retention levels of the reinforcing WC hard particles. Different substrates have been studied as different materials have different physical, mechanical and thermal properties, all of which influence deposition kinetics and coating properties. The variation in spray parameters has been investigated, and these include feed rates, stand-off distance, temperature and pressure. Powder manufacturing methods, however, do not appear to have been investigated when using low pressure CGDS to deposit WC-Ni coatings. The ductile component, also known as the Ni binder, in the powder blend is immensely important because the hard brittle WC phases would otherwise not adhere to the substrate. Therefore it is important to investigate the effect of different powder production methods on the cold spray coating properties.

Chapter 3

Experimental Procedures

This chapter presents the experimental methods and apparatus used during the course of the project. The chapter begins with powder preparation and characterization, steel substrate description and the deposition parameter optimization procedure. Thereafter the cold spray coating deposition process is described followed by the coating characterization tests. The chapter concludes with the annealing process of the nickel powders and the slurry abrasion tests.

3.1 Powders

Three different Ni powders were used in this study. A spherically shaped gas atomized Ni powder with an average particle size of 34 µm and irregularly shaped water atomized Ni powder with an average particle size of 31 µm were purchased from Praxair Surface Technologies. The third Ni powder, irregular shaped 13 µm particle size that appeared to have agglomerated, was purchased from Centerline, which is the company name of the cold spray machine used in this study. This third Ni powder was included in this research work so as to employ the supplier recommended spray parameters as a starting point for mapping the optimized spray parameters for the gas and water atomized Ni powders. An irregularly shaped WC powder with an average particle size of 4 µm was purchased from Pilot Tools (Pty) Ltd.

The WC powder was blended with each of the Ni powders in a mechanical mill to form WC-5wt%Ni feedstock powders. The mill duration was 2 hours, with a ball to powder ratio of 2:1 and 30% alcohol of blend mass was used. A Carl Zeiss Sigma field emission scanning electron microscope (FESEM) was used to determine the powder morphology while energy dispersive spectroscopy (EDS) was used to verify the elemental composition. The phases in the powders were identified using x-ray diffraction (XRD) and the powder particle size was mapped using a Malvern Mastersizer 2000 machine with a stirrer and distilled water as the dispersant. The Vickers hardness of the powders was determined using a force of 300 gf and a dwell time of 10 seconds; 8 indentations were made per powder sample.

3.2 Steel substrate

Mild steel substrates with the dimensions 18 x 18 x 4 mm were used as the substrate material. Steels and specifically mild steel is highly used in different industries namely manufacturing, transport, mining, agricultural and aerospace. As steels are widely used industrially it is important that their operational lifetimes are not compromised, and possibly extended by finding methods to reduce their slurry abrasion wear rates. FESEM was used to obtain images of the mild steel substrate so has to reveal the microstructure.

3.3 Deposition Parameter Optimization

Table 3.1 lists cold spray machine supplier recommended spray parameters for the Centerline Ni powder. These parameters were used to construct an initial Design of Experiments (DoE) matrix for depositing the gas and water atomized Ni powders; refer to Table 3.2.

Table 3.1: Centerline Ni recommended spray parameters [18].

Spray parameters	**Recommended Range**
Temperature	450 – 550 °C
Pressure	0.7 – 1.72 MPa
Standoff Distance	10 – 25 mm
Gas	Compressed Air or Nitrogen
Feed rate (gram/min)	12 – 18 (gram/min)
Gun transverse speed	10 – 250 mm/s depending on process settings and target coating thickness
Surface preparation	SST-G0002 commercial blast
Spray nozzle	UltiLife ™

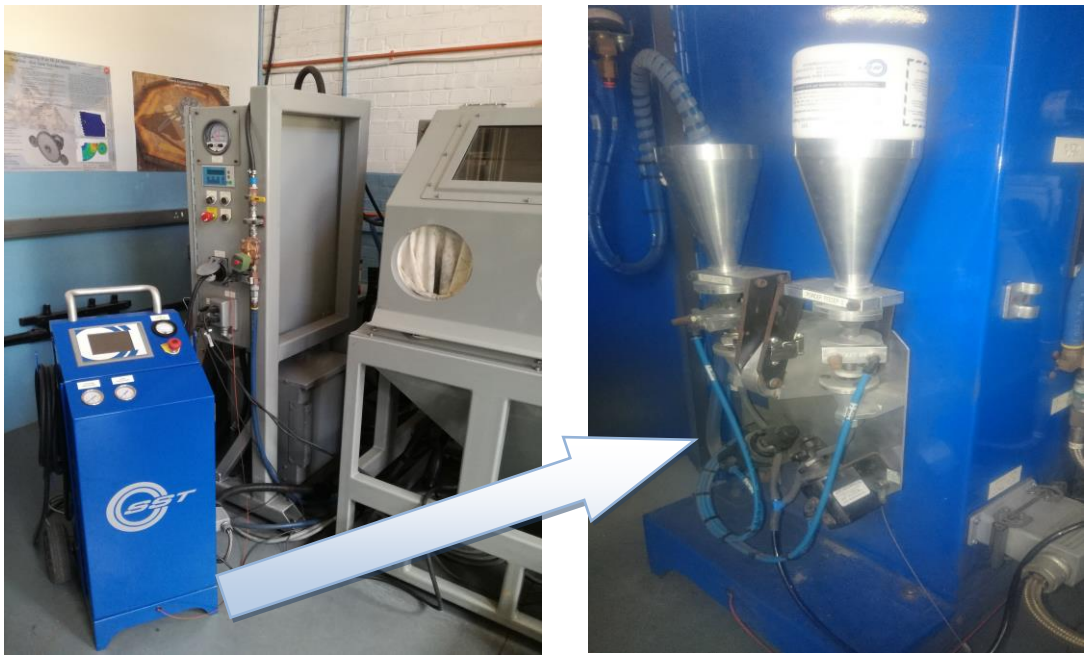
Five parameters were considered for mapping the DoE matrix namely temperature, pressure, standoff distance, powder feed rate and the number of passes. The output response selected was thickness because attempted deposition of the respective Ni powders onto the mild steel was the initial objective. Thus the trial which produced the thickest coatings would be considered as the set of optimized spray parameters.

Table 3. 2: Design of Experiments matrix.

Trial	Temperature (°C)	Pressure (MPa)	Standoff distance (mm)	Feed rate (%)	Passes	Coating thickness (mm)
1	500	1.21	15	25	2	X
2	500	1.21	15	25	4	X
3	500	1.21	15	25	8	X
4	500	1.21	15	25	16	X
5	500	1.21	15	25	25	X
6	500	1.21	15	25	30	X
7	500	1.21	15	25	32	X
8	500	1.21	15	30	8	X
9	500	1.21	15	35	8	X
10	500	1.21	10	25	8	X
11	500	1.21	20	25	8	X
12	500	1.00	15	25	8	X
13	500	1.10	15	25	8	X
14	400	1.21	15	25	8	X
15	450	1.21	15	25	8	X

3.4 Coating Deposition

The mild steel substrates were grit blasted using (169 µm) alumina grit prior to deposition. This stage is essential for enhancing the adhesion of the coatings onto the surface of the substrate. The Alumina grit roughens the surface and thereby creates crevices for the splats to form and adhere. The substrates were ultrasonically cleaned for 20 minutes to remove oils and dirt accumulated during the handling. A Supersonic Spray Technologies Low Pressure Cold Spray Machine shown in Fig. 3.1 was used to deposit the coatings using a gravitational powder feeder. Air was used as the carrier gas and a traverse speed of 120 mm/s employed. A WC spraying nozzle was used.



(a) (b)

Figure 3. 1: (a) Cold spray machine and (b) gravitational powder feeder.



Figure 3. 2: WC spray nozzle

Initially the three different Ni powders were each deposited onto mild steel plates to assess the adhesion characteristics of each powder. The deposition parameters used were; a temperature of 500 °C, pressure of 1.21 MPa, standoff distance of 15 mm, feed rate of 30 % and 2 passes. Thereafter the WC-5wt%Ni powder blends were deposited using the parameter sets listed in Table 3.2 based on the DoE matrix. Following initial material characterization tests on the coatings, additional coatings were produced using the deposition parameter set which produced the thickest coatings. These coatings were then subjected to detailed materials characterization and slurry abrasion tests.

3.5 Coating Characterization

3.5.1 Sample preparation

The Ni-only coatings were sectioned using an aluminum oxide cut-off wheel whereas the WC-5wt%Ni coatings were sectioned using a diamond cut-off wheel. A Struers Secotom 10 cutting machine was used to cut both types of coatings. The cutting parameters used were a cutting distance of 40 mm, cutting wheel feed rate of 0.010 m/s, and speed of 3 000 rpm. Water was used lubricant. The samples were hot mounted using an OPAL 410 machine. Samples for FESEM and optical microscopy were mounted in Polyfast powder. The mounted samples were polished down to a 1 µm surface finish using a SAPHIR 520 automatic grinding and polishing machine. The complete grinding and polishing procedure is listed in Table 3.3. Steps 1 to 3 represent the grinding stage while steps 4 to 6 represent the polishing stage.

Table 3. 3: Grinding and polishing procedure

Step	**Size/µm**	**Force/N**	**Lubricant**	**Duration/min**	**Rotational speed**
1	Struers MD Piano 220	25	Water	6	150
2	Struers 1200	25	Water	6	150
3	Struers MD Piano 2000	25	Water	8	150
4	Struers MD Largo	40	LECO Premium Diamond Suspension (9 µm)	8	150
5	Struers MD Dur	40	LECO Premium Diamond Suspension (3 µm)	8	150
6	Struers MD Nap	40	LECO Premium Diamond Suspension (1 µm)	8	150

3.5.2 Thickness

The thickness of the coatings were initially measured using a the LEICA CTR-6000 As some coatings were too thin to be measured using this instrument, an OFM BX63 field microscope was used in order to obtain more accurate readings while a FESEM was used to verify these measurements. The mean coating thickness was determined from the average of 5 measurements per sample.

3.5.3 Hardness

The hardness of the coatings and mild steel substrate were measured using a Future Tech FM700 hardness testing machine. For the coatings a micro indenter was used with a 300 gf load and a dwell time of 15 seconds. The average hardness was calculated from a total of 12 indentations per coating sample according to ASTM C1327 [52]. The macro-Vickers hardness of the mild steel substrate was measured using a load of 5kgf and dwell time of 10 seconds. The average hardness was calculated from a total of 12 indentations per sample according to ASTM C1327 [52].

3.5.4 Phase analyses

X-ray diffraction was used to identify the phases in the coatings using a Bruker D2 Phaser with a Lynx Eye detector. For the analysis, a cobalt anode, with X-ray generator settings of 30 kV and 10mA was used. The measurements were made from 10° to 90° at a rate of 0.026° per second and EVA software was used for identifying the phases present.

3.5.5 Microstructure

Microstructure images of the coatings were captured using the FESEM and these images were used to calculate various microstructural parameters. The WC grain size was measured using Image J software version 1.5f. The mean grain size was determined from the average of 1800 grains for the coatings based on annealed gas atomized Ni powder and an average of 50 grains for the rest of the coatings. This was mainly because of the thickness of the coatings. The percentage porosity was also determined using the Image J software. The Ni binder mean free path was calculated using lineal analyses according to equation 3.2 [53]:

$$\lambda_{Ni} = d_{WC} [V_{Ni}/(1 - V_{Ni})(1-C_c)] \qquad (3.2)$$

Where d_{WC} is the grain size of the WC particles, V_{Ni} is the volume fraction of the Ni phase and C_c is the WC contiguity calculated according to equation 3.3 [53];

$$C_c = 2N_{\alpha\alpha}/ (2N_{\alpha\alpha} + N_{\alpha\beta}) \qquad (3.3)$$

Where ($N_{\alpha\alpha}$ and $N_{\alpha\beta}$) are the average number of intercepts per unit length of test lines with the traces of carbide-carbide grain boundaries and carbide-binder interface respectively.

3.5.6 Crack density

The crack density (c) of the coatings was calculated using the fraction of the dispersed phases and pore areas according to equation 3.4 [54], where, x_i is the major length of the i_{th} crack, and A is the total area of each random image.

$$c = \Sigma x_i/A \qquad (3.4)$$

3.5.7 Fracture toughness

The fracture toughness (K_{IC}) was calculated by applying the following equation proposed by Beshish [55]. The Vickers hardness values of the coatings were considered and the Young's modulus values of the coatings. The crack lengths propagated during indentation were measured using an OFM. Equation 3.5 was used for calculating the fracture toughness [56]:

$$K_{IC} = 0.016\ (E/H)\ ^{\wedge}0.5(P/C^{\wedge}3/2) \qquad (3.5)$$

Where K_{IC} is the fracture toughness, MPa.m^0.5; P is the indenter load, 49.05 kgf, E is the Young's modulus, GPa and it was obtained from [57,58]; H is the hardness of the coating, GPa; and C is the mean crack length (mm) propagated on the coatings during indentation.

3.5.8 Elastic Modulus

The Young's modulus (E_C) of the coatings was determined using equation 3.6 [59].

$$E_C = S\ (E_i a_i V_i/V_m) \qquad (3.6)$$

Where E_i is the Young's modulus of WC and Ni, a_i is the atomic fraction of WC and Ni obtained from EDS analysis. V_i is the molar volume of W, C and Ni obtained from [60]. V_m is the average molar volume of elements obtained from [60]. Individual calculations were done for the WC and the Ni phases respectively and the mean Elastic modulus value was considered according to [59].

3.5.9 Plasticity Index

The plasticity index was calculated using the ratio in equation (3.7)

$$PI = E/Hv \qquad (3.7)$$

Where E is the Young's modulus, GPa of the coatings discussed in 3.5.8 and Hv is the hardness of the coatings, $HV_{0.3}$ discussed in 3.5.3.

3.5.10 Atomic Force Microscopy (AFM)

AFM was performed on the coatings using a Veeco Dimension 3100 Atomic Force Microscope (AFM). The AFM was used for mapping surface images in 3D. The images were taken from an area of 20 µm by 20 µm. AFM was also used to map 3D images at different angles so as to view the coatings deposition pattern and the features of the coating/substrate interface. The image frame sizes that were taken were 40 x 40 µm for the coatings based on the annealed gas atomized Ni powder and 20 x 20 µm for the rest of the coatings. AFM was used to generate surface roughness values from the images that were taken. For each coating, 10 images were considered.

3.6 Annealing of Nickel powders

Annealing was performed on the as-received Ni powders in order to investigate if the coating thickness could be improved. A tube furnace was used at a temperature of 500 °C, chamber pressure of 100 kPa and Argon air as the carrier gas for an annealing duration of 2 hours. After annealing, XRD, FESEM (refer to sub-section 3.1), Raman spectroscopy (refer to sub-section 3.6.1) and EPMA (refer to sub-section 3.6.1) were used to assess changes in the powder properties.

3.6.1 Raman Spectroscopy

Raman spectroscopy was performed on the as-received Ni powders and on the respective annealed Ni powders. This analysis was used to characterize the Ni powders after annealing. For each powder type, eight spots were sampled and images were taken by a charge coupled device (CCD) camera. The raw data was plotted in Microsoft Excel and the peaks were matched with previous work [61]. The laser was focused on (0, 0) coordinates in the middle of the image and the spot diameter was 1 μm.

3.6.2 Electron Probe Micro-analyzer

Electron Probe Micro-analyzer (EPMA) was used to show the difference in powder elemental compositions. A back scattered electron detector (BSE) as well as secondary electron detector (SE) were used to take images. An operational current of 20 nA was used while Wavelength dispersive-spectroscopy (WDS) and EDS were used to identify which elements were present in the powder samples.

3.7 Slurry Abrasion Testing

Slurry abrasion testing of the coatings was conducted according to ASTM B611-91 [62]. A schematic of the machine is shown in Fig. 3.3. Four samples were tested simultaneously using an applied load of 22 N per sample with the abrasion wheel rotating at 0.66 m/s. Silica sand with an angular morphology (refer to Fig. 3.4) and an average hardness of 1375.8 ± 164 HV was used as the abrasive medium with a load of 22 N per sample and a particle size of 150 μm. The silica sand was mixed with distilled water in a ratio of 1:20 to produce the abrasive medium. The WC-5wt%Ni coatings based on the annealed gas atomized Ni powder were tested for 6 hours and weighed at hourly intervals while those based on the annealed Ni powder, un-annealed gas and water atomized Ni powders were tested for 30 minutes and weighed at 5 minute intervals. Different time intervals were used because of the coating thickness; the coatings based on the annealed were significantly thicker and therefore were able to be tested for up to 6 hours. The rest of the coatings were relatively thin and therefore were able to be tested for up to 30 minutes. After each time interval, the samples were dismounted and ultrasonically cleaned before getting weighed. The average wear rate of each coating was calculated according to equation 3.8:

$$Q = KN/H \quad (3.8)$$

Where Q is the volume removed per unit sliding distance, N is the normal load on the contact (distributed over all the contacting particles) used according to ASTM B611-91 [62], and H is the indentation hardness of the surface being worn (refer to sub-section 3.5.3).

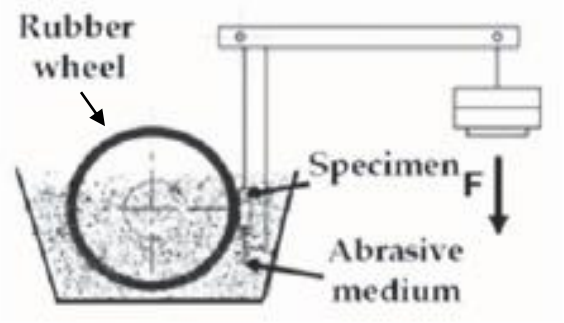


Figure 3.3: Schematic of the slurry abrasion test setup [1].

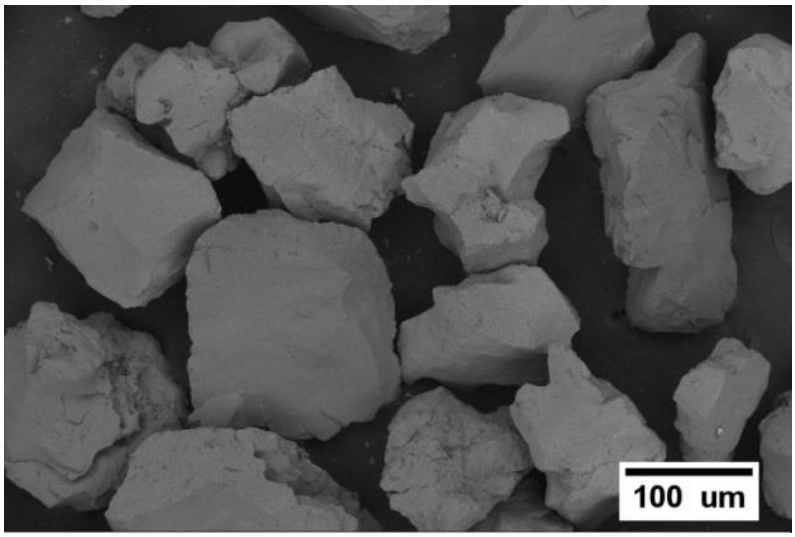


Figure 3.4: Silica sand used as abrasive in slurry abrasion tests.

After the slurry abrasion tests, the worn samples were studied using FESEM in planar and cross-sectional views to determine the wear mechanisms. The type of abrasion, i.e. hard versus soft, was determined by calculating the H_a/H_s ratios where H_a is the hardness of the abrasive and H_s is the hardness of a surface [36]. If $H_a/H_s > 1.2$ then hard abrasion associated with plastic indentation is expected to occur on the surface and if $H_a/H_s < 1.2$ then soft abrasion where the abrasive remains intact without any crushing or plastic deformation occurring. The applied stress experienced during slurry abrasion was calculated according to equation 3.9:

$$\text{Applied stress} = F/A \quad (3.9).$$

Where F is the applied stress, N, according to ASTM B611-91 [62], and A is the coating area, mm^2, measured by a Vernier caliper.

Chapter 4

Results

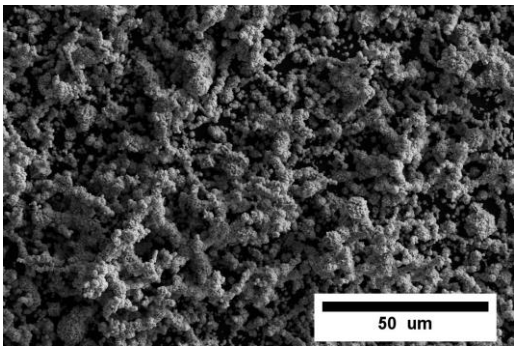
This chapter presents detailed results of the experiments that were conducted for this work. Sections 4.1 – 4.7 present full analyses done on the powders used for this work, followed by optimization using design of experiments, characterization of coatings based on un-annealed Ni powders proceeds to annealing of Ni powders followed by coatings based on annealed Ni powders and lastly slurry abrasion tests.

4.1 Powder Characterization and Hardness

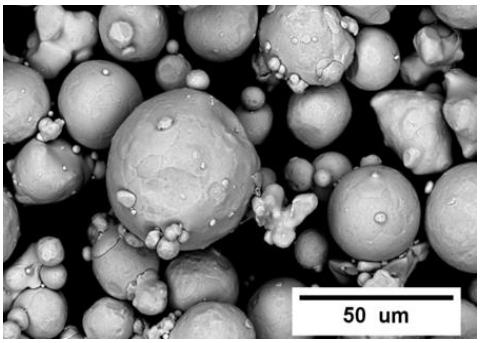
This section presents the FESEM images showing the morphology of the starting powders utilized in this work. The particle size distributions of the powders are also presented.

4.1.1 Morphology of nickel powders

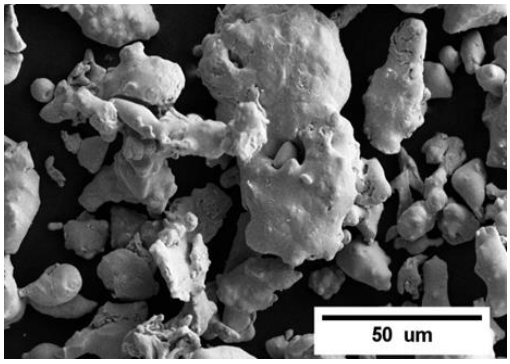
The FESEM images of the different nickel powders used in this work are presented in Figs. 4.1a-c. The images show the morphology of Centerline, gas atomized and water atomized nickel powders. It can be seen that the Centerline and water atomized Ni powder had an irregular shape, while the gas atomized powder had a spherical morphology. It was reported that the morphology of powder seems to influence more significantly the coating's hardness than the operational parameters [23].



(a)



(b)

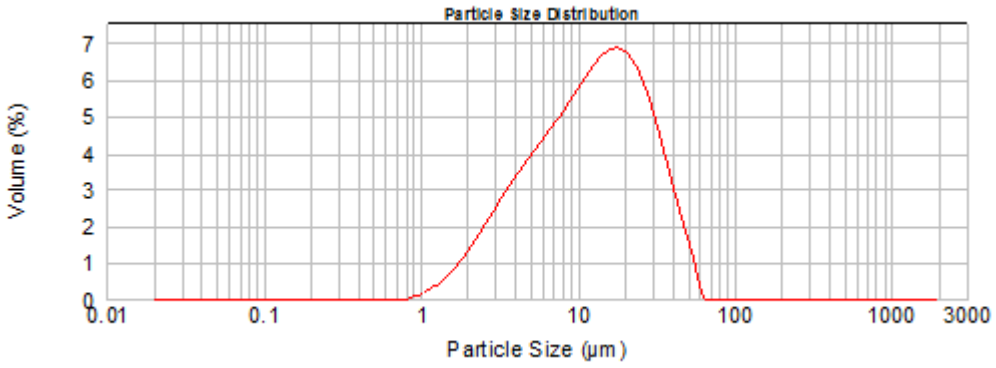


(c)

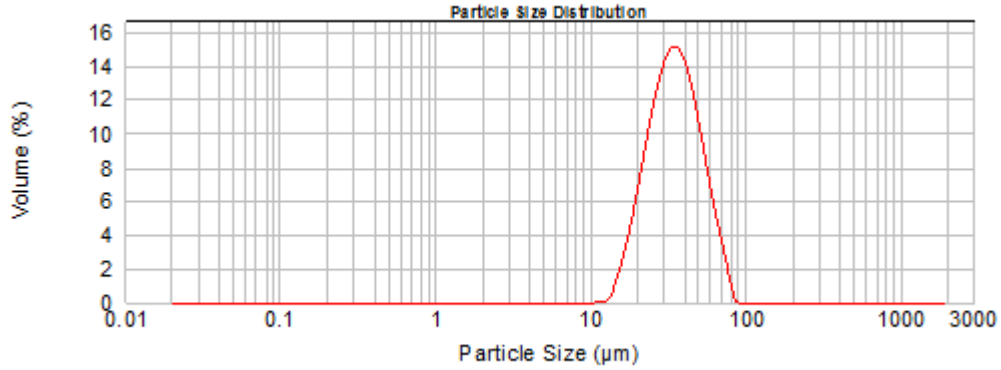
Figure 4. 1:Scanning electron images of different nickel powders showing different morphologies a) Centerline nickel powder, b) gas atomized nickel powder and c) water atomized nickel powder

4.1.2 Particle size distribution of nickel powders

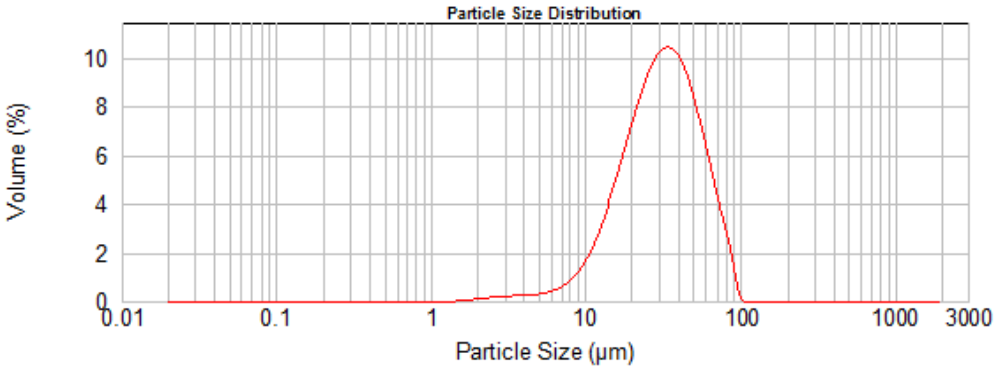
Fig. 4.2 shows the particle size distribution of the different nickel powders. It can be seen that the gas atomized Ni powder has the largest particle size of approximately 34 µm when compared with Centerline Ni and water atomized Ni powders.



(a)



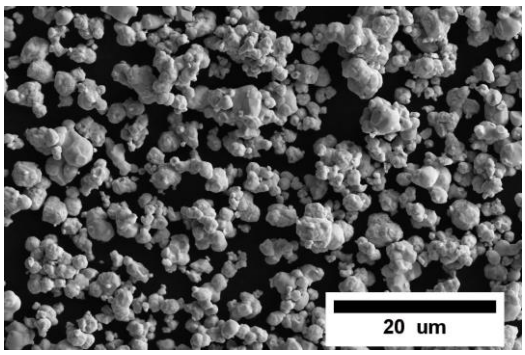
(b)



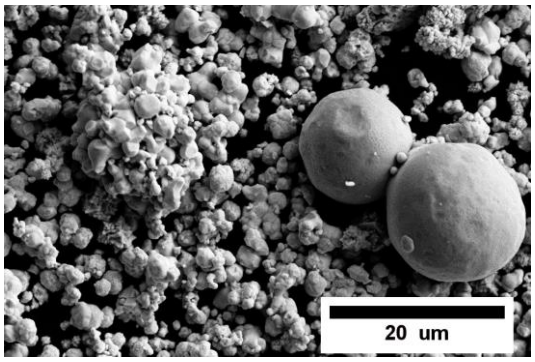
(c)

Figure 4. 2: Particle size distribution a) Centerline nickel powder, b) gas atomized nickel powder and c) water atomized nickel powder

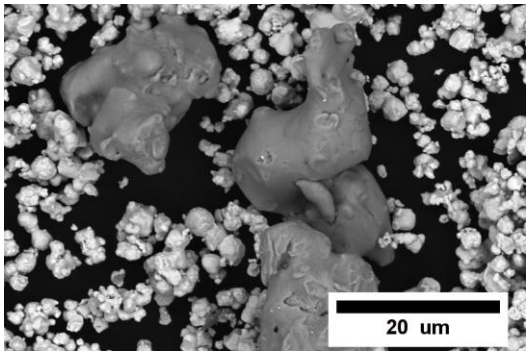
4.1.3 Morphology of WC and WC-5wt%Ni powder blends



(a)



(b)

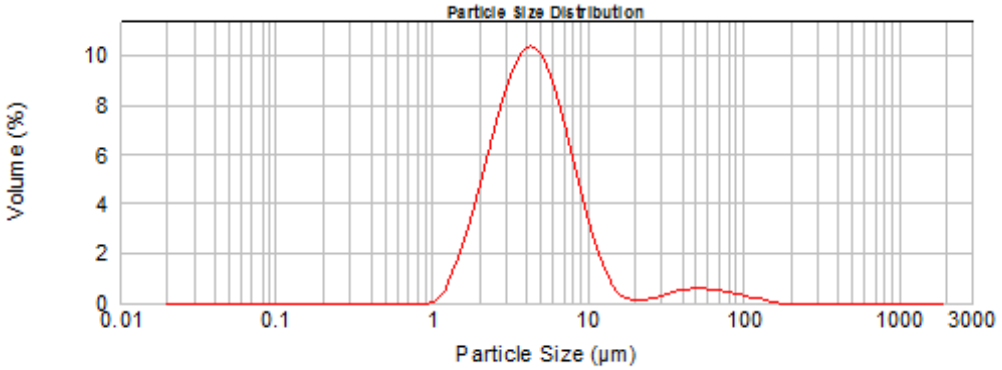


(c)

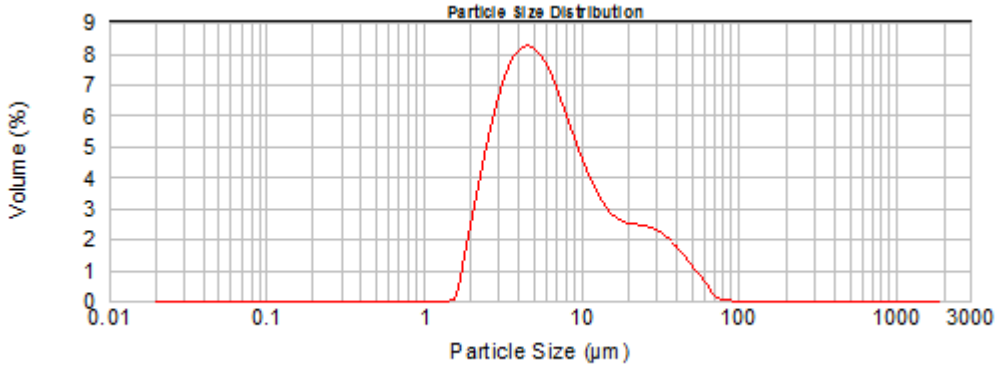
Figure 4. 3: Scanning electron images of different nickel powders showing different morphologies a) WC powder, WC-5wt%Ni based on b) gas atomized Ni powder and c) water atomized Ni powder.

4.1.4 Particle size distribution of WC and WC-5wt%Ni powder blends

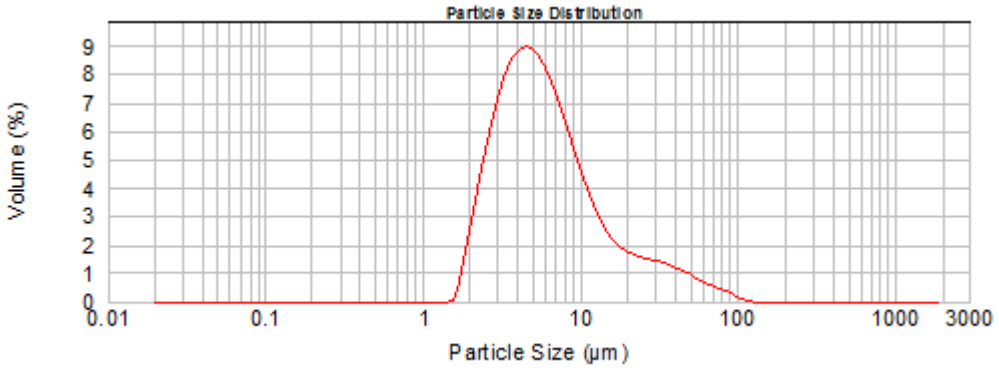
Fig. 4.4 shows the particle size distribution of the WC powder and the respective WC-5wt%Ni blends. Fig. 4.9 shows the particle size distribution of the WC powder. The average particle size was 4μm, it was finer than the respective Ni powders. The WC powder was relatively more finer with a particle size of 4 μm. The WC powder was more compacted compared to the respective Ni powders, this was due to its higher density also it did not form a suspension when immersed in distilled water while performing particle size distribution tests. The WC-5wt%Ni powder blends based on the gas atomized Ni powder maintained its relativley larger particle size compared to the WC-5wt%Ni based on the water atomized Ni powder.



(a)



(b)



(c)

Figure 4. 4: Particle Size distribution a) WC powder, WC-5wt%Ni powder blends based on b) gas atomized Ni powder and c) water atomized Ni powder

Fig. 4.5 shows the Vickers hardness of the powders used in this study. The water atomized Ni powder had a hardness of 59.98 ± 59.5 $HV_{0.3}$, while the gas atomized Ni powder had a hardness of 56.46 ± 59.5 $HV_{0.3}$. The WC-5wt%Ni blended with the water atomized Ni powder also had hardness higher than that of the WC-5wt%Ni blended with the gas atomized Ni powder. The silica sand had a relatively high Vickers hardness. The measured Vickers hardness can be attributed to the powder manufacturing process. Water atomization gives irregular particles, which have better shape retention ability whereas gas atomization yields spherical particles and high packing density [63]. Figs. 4.1b & c show Ni powder shapes based on atomization.

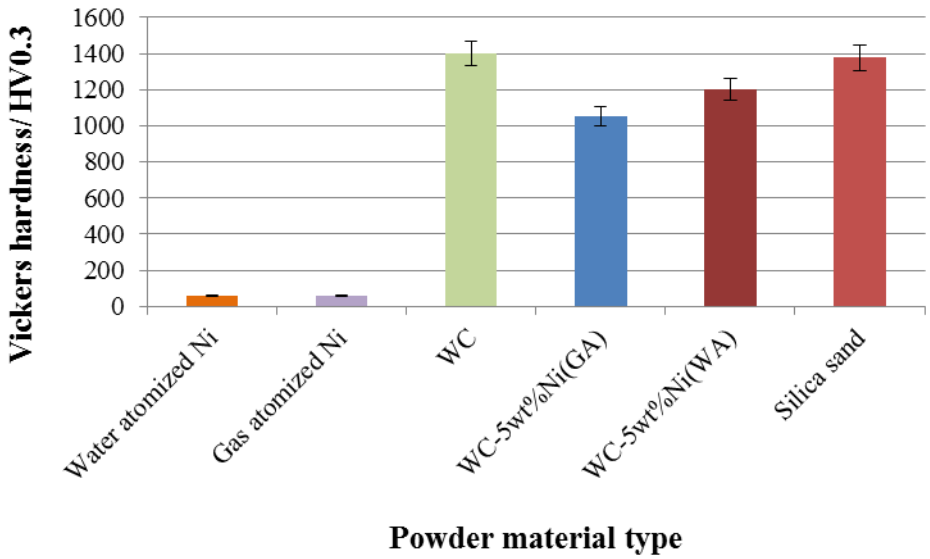


Figure 4. 5: Powder and silica sand Vickers hardness

4.2 Design of Experiments Optimization

Having established the morphology and particle size distribution of the different starting powders and their blends, optimization of spray parameters using DOE was performed to determine near optimal deposition parameters. The DOE designation was mixed level, and this was due to powder consumption control.

Table 4.1 represents the thickness results obtained for the gas atomized Ni powder from the spray parameters considered. The aim was to find the thickest coatings and apply the same spray parameters to the WC-5wt%Ni coatings. Thickness was used as the output response for the DOE matrix. The thickest coatings were obtained from trial 8. Spray passes exceeding 8 seemed to have an eroding effect on the already deposited layers and this was also demonstrated by the water atomized Ni powder coatings.

Table 4. 1: Experimental matrix for coatings based on gas atomized Ni powder.

Trial	**Temperature (°C)**	**Pressure (Mpa)**	**Standoff distance (mm)**	**Feed rate (%)**	**Passes**	**Coating thickness (mm)**
1	500	1.21	15	25	2	2.9 ± 0.9
2	500	1.21	15	25	4	3.3 ± 1.3
3	500	1.21	15	25	8	18.8 ± 0.7
4	500	1.21	15	25	16	12.7 ± 1.5
5	500	1.21	15	25	25	18.8 ± 1.1
6	500	1.21	15	25	30	14.4 ± 0.8
7	500	1.21	15	25	32	27.9 ± 1.5
8	500	1.21	15	30	8	30.3 ± 3.7
9	500	1.21	15	35	8	15.7 ± 2.4
10	500	1.21	10	25	8	12 ± 0.8
11	500	1.21	20	25	8	3.8 ± 0.6
12	500	1.00	15	25	8	1.3 ± 0.7
13	500	1.10	15	25	8	3.1 ± 0.9
14	400	1.21	15	25	8	5.2 ± 0.5
15	450	1.21	15	25	8	3.9 ± 1.6

Table 4.2 represents the thickness results obtained for the water atomized Ni powder from the spray parameters considered. The aim was also to find the thickest coatings and apply the same spray parameters to the WC-5wt%Ni coatings. Thickness was used as the output response for the DOE matrix. The thickest coatings were obtained from trial 8.

Table 4. 2: Experimental matrix for coatings based on water atomized Ni powder.

Trial	**Temperature (°C)**	**Pressure (Mpa)**	**Standoff distance (mm)**	**Feed rate (%)**	**Passes**	**Coating thickness (mm)**
1	500	1.21	15	25	2	2.5 ± 1.2
2	500	1.21	15	25	4	1.6 ± 0.6
3	500	1.21	15	25	8	15.6 ± 2.5
4	500	1.21	15	25	16	9.8 ± 1.6
5	500	1.21	15	25	25	13.5 ± 1.3
6	500	1.21	15	25	30	15.6 ± 2.1
7	500	1.21	15	25	32	18.2 ± 2.8
8	500	1.21	15	30	8	24 ± 2.1
9	500	1.21	15	35	8	13.5 ± 1.3
10	500	1.21	10	25	8	10.7 ± 1
11	500	1.21	20	25	8	3.4 ± 0.2
12	500	1.00	15	25	8	2.3 ± 0.9
13	500	1.10	15	25	8	2 ± 1
14	400	1.21	15	25	8	1.8 ± 0.6
15	450	1.21	15	25	8	2.4 ± 1.1

4.3 Characterization of Ni-only coatings

The results for characterization performed on the Ni-only coatings are presented in this section. The Ni-only coatings were fabricated prior to the WC-5wt%Ni coatings for mapping of close to optimal spray parameters.

4.3.1 Nickel-only coating characterization

Fig. 4.6 shows a cross-sectional view of the coating fabricated using Centerline Ni powder. The fixed spray parameters were 500 °C, 1.21 MPa, 15 mm stand-off distance and 30% powder feed rate. The image shows a dense coating with minimal porosity evident. The top surface of the coating shows portions of discontinuity in the coating lamellae. Fig. 4.7 shows the high magnification image of the coating microstructure, the dark spots (black arrows) represent the voids and pores within the coating.

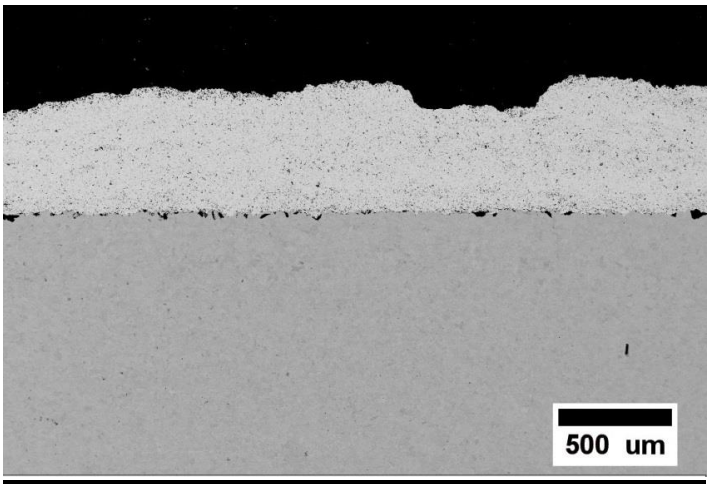


Figure 4. 6: BSE image of Centerline Ni coating cross-sectional view.

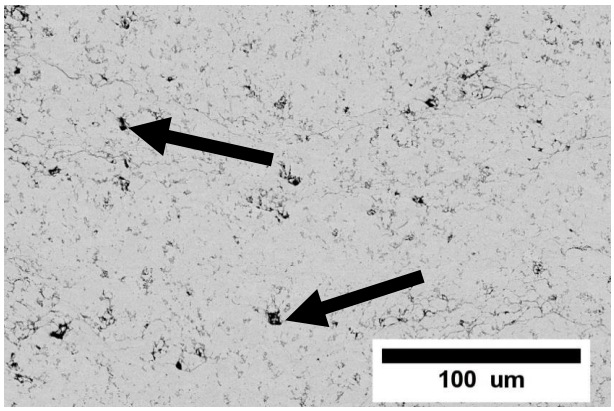


Figure 4. 7: BSE image of Centerline Ni coating microstructure.

Fig. 4.8 shows the elemental spectrum of the Centerline Ni coating, the results show no evidence of inclusion elements.

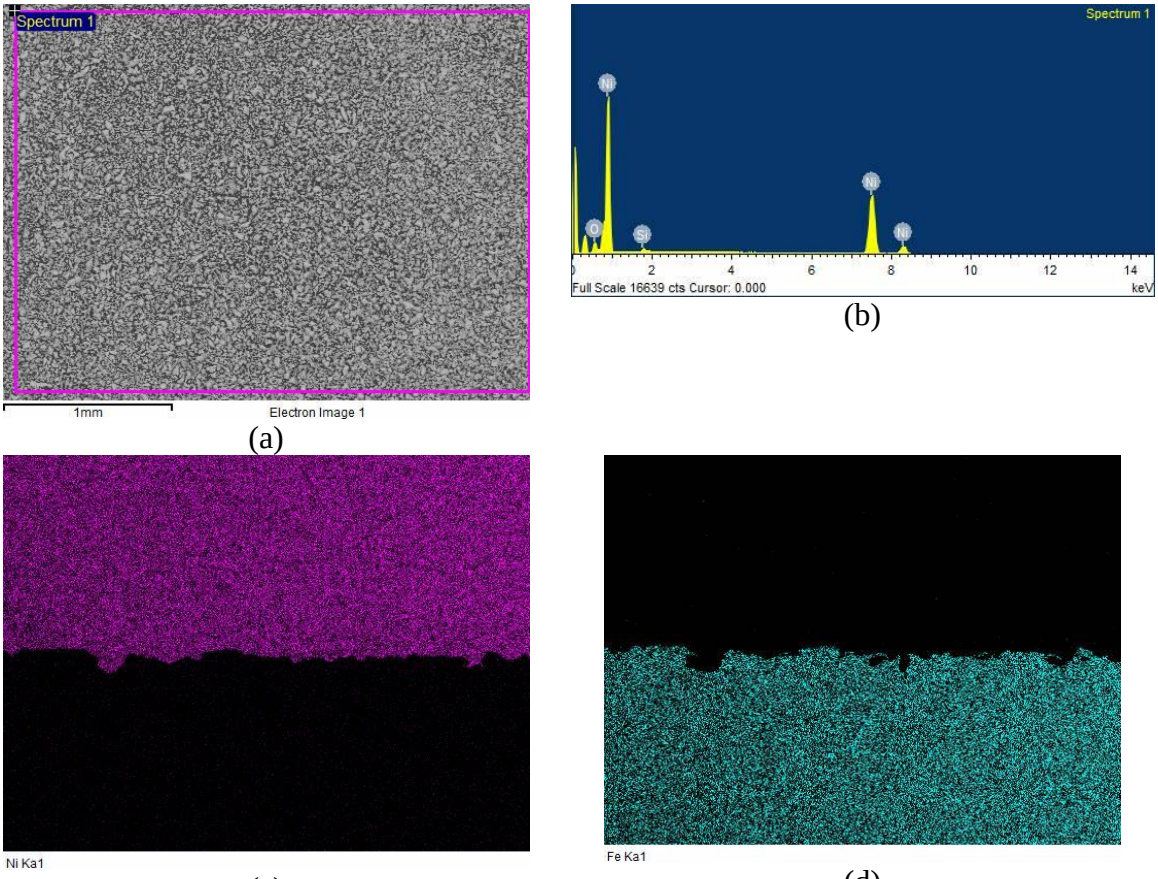
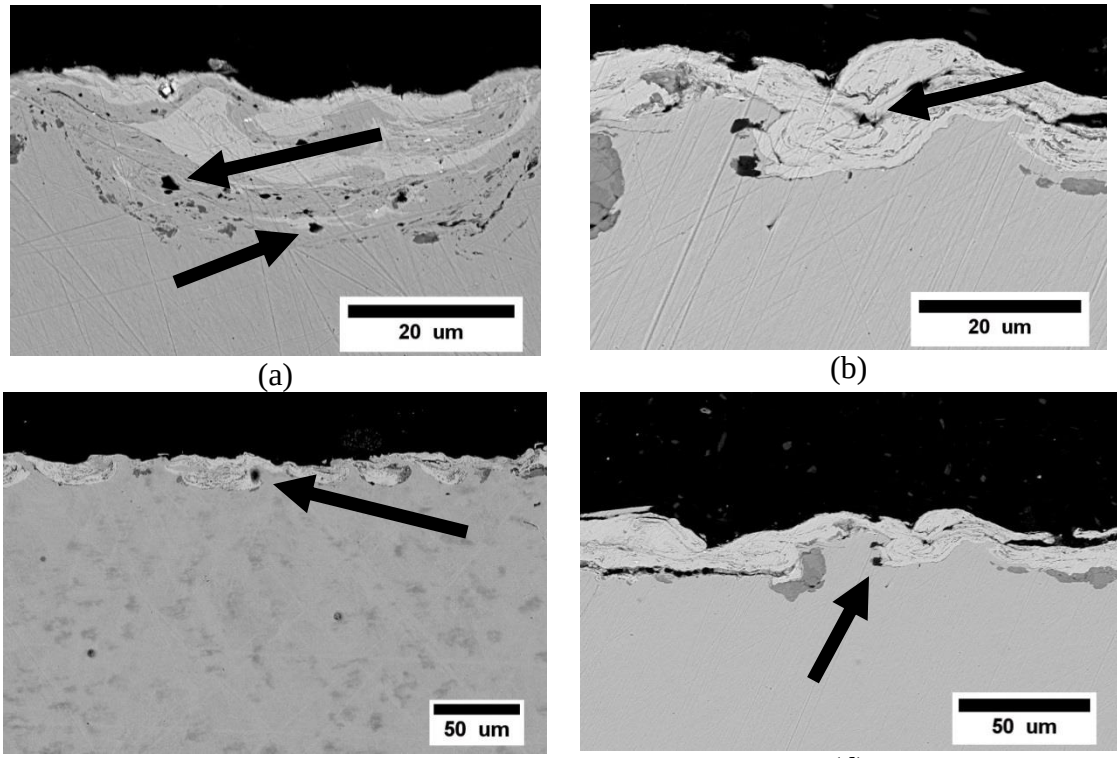


Figure 4. 8: EDS mapping for Centerline Ni coating showing (a) Ni powder, (b) elemental spectrum, (c) elemental mapping of Ni and (d) Fe.

Fig. 4.9 shows the coatings fabricated from gas atomized Ni powder Fig. 4.9 (a & c), and water atomized Ni powder in (b & d). Both powders showed minimal deposition. The images also show the powder impinging into the substrate surface; this is a normal phenomenon in cold spraying due to the high velocities generated [6,17,23,44]. The black spots represent porosity and voids.



(a) (b)

(c) (d)

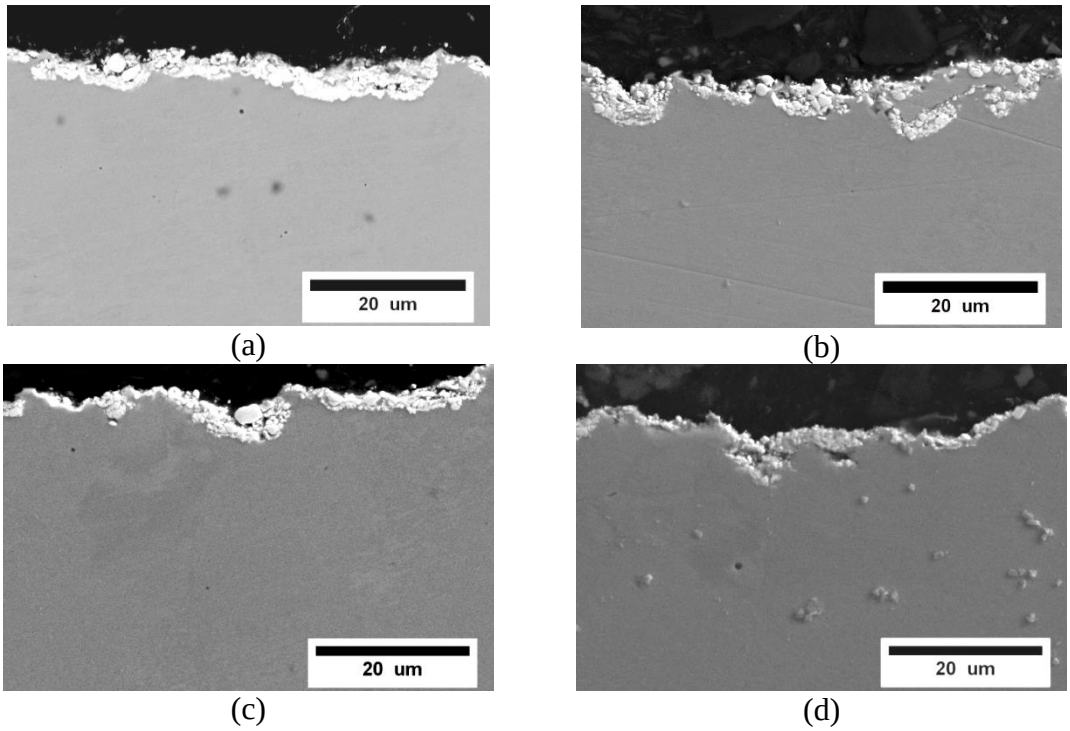
Figure 4. 9: Coating microstructures for Ni coatings deposited at (a-b) 2 passes and (c-d) 8 passes.

4.4 Characterization of WC-5wt%Ni coatings based on un-annealed Ni powders

This section presents coatings based on the WC-5wt%Ni powder blends. FESEM showed that the coating-substrate interfaces were, in general clean, however, voids and alumina grit inclusions could be seen. All the coatings presented different levels of porosity.

4.4.1 Coating microstructures

Fig. 4.10 shows the coatings microstructures that were obtained from un-annealed Ni powders. The FESEM images show the manner of deposition along the cross section of the mild steel substrate. The substrate/coating interphase can be seen. The penetration of the feedstock powder into the substrate material is clearly visible, supersonic speeds generated by the CGDS process make this possible [6,17,23]. Figs 4.11 and 4.12 show high magnification images of the coatings based on the gas atomized Ni powder and the water atomized Ni powder respectively. Both images show the dominance of the WC (white phase) in the coatings, this is verified by the high % WC retained, high hardness and low binder mean free path (refer Table 4.3). The gouging effect on the surface of the coatings is as a result of the bouncing off of particles that also caused eroding of previously deposited layers and substrate material [11,44].



(a) (b)

(c) (d)

Figure 4. 10: Coating microstructures WC-5wt%Ni coatings based on gas atomized Ni powder (a & c) and water atomized powder Ni (b & d).

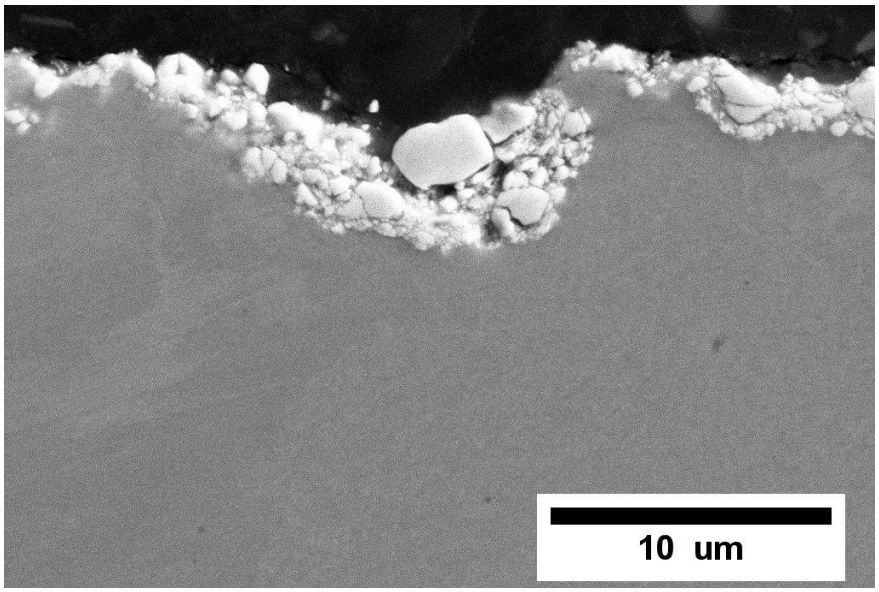


Figure 4. 11: High magnification image of WC-5wt%Ni based on gas atomized Ni powder.

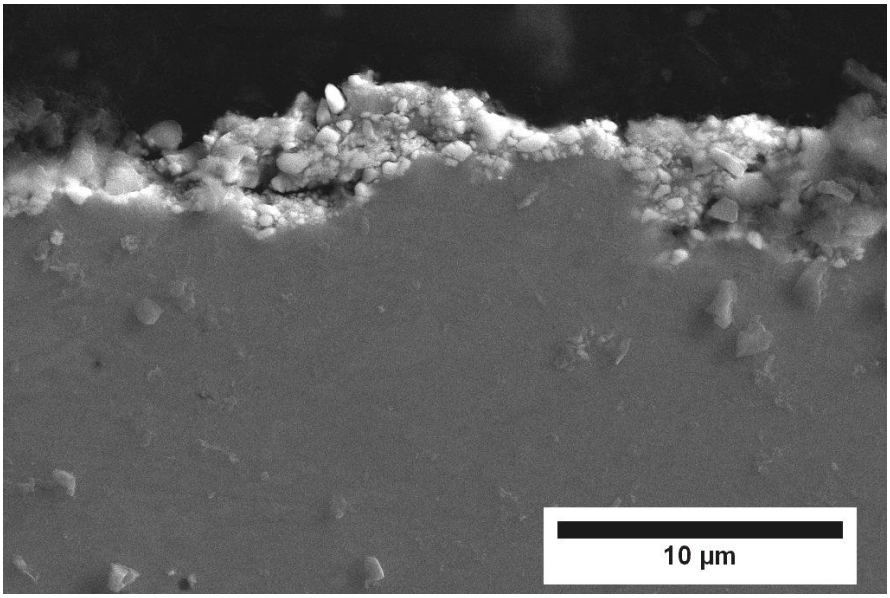


Figure 4. 12: High magnification image of WC-5wt%Ni based on water atomized Ni powder.

4.4.2 Phase analyses

Figs 4.13 and 4.14 show the phase analysis done on the coatings and they stacked above the starting powders XRD patterns. The XRD patterns almost matched, showing no decarburization or oxidation. No phase changes were detected.

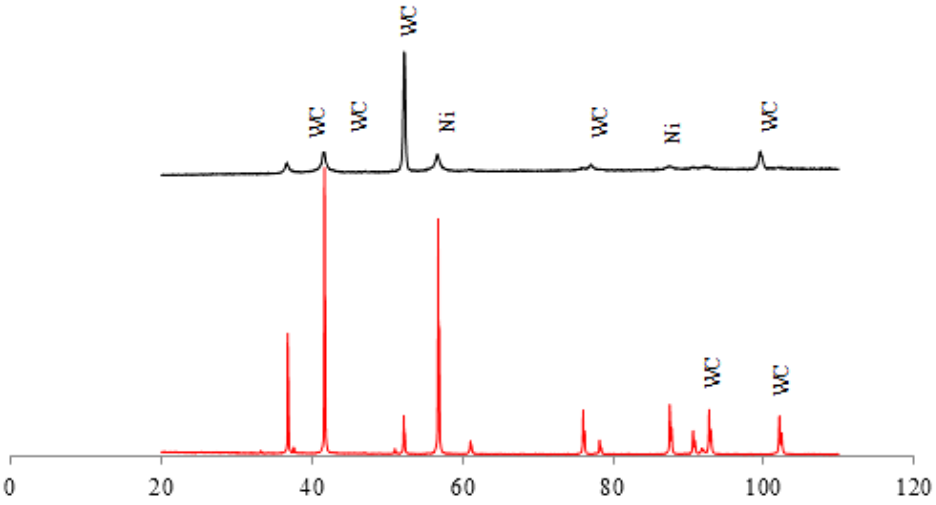


Figure 4. 13: XRD patterns for coating (black) and powder (red) for coatings based on un-annealed gas atomized Ni powder.

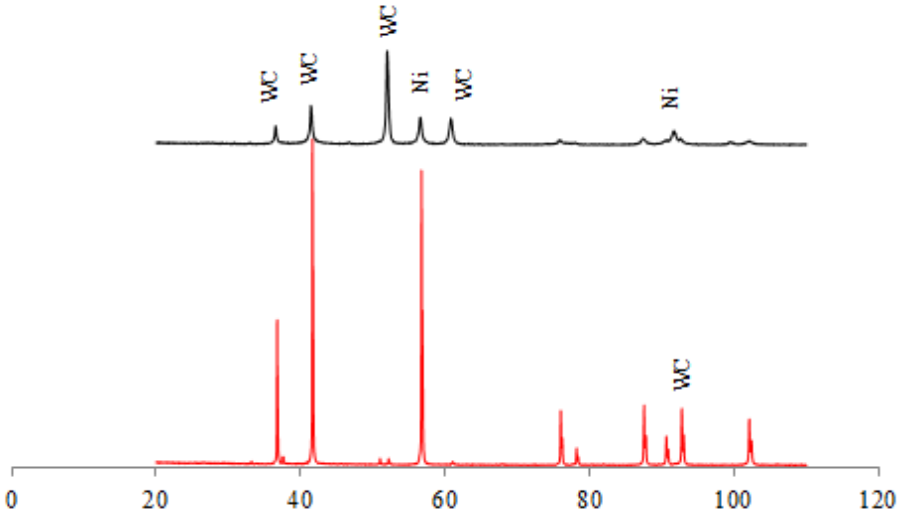


Figure 4. 14: XRD patterns for coating (black) and powder (red) in descending order for coatings based on un-annealed water atomized Ni powder.

Table 4.3 lists the coating properties for the coatings based on the un-annealed Ni powders. The thickness, WC retained, carbide grain size, binder mean free path and Elastic modulus of the coatings were similar. The water atomized Ni powder however, produced coatings with porosity in the same range as the gas atomized Ni powder.

4.4.3 Properties of WC-5wt%Ni coatings based on un-annealed Ni

Both WC-5wt%Ni coatings were relatively thin due to the difficulty in getting the coatings to adhere to the mild steel substrate surface. Both coatings had relatively high porosity as there was evidence of gouging and eroding of already deposited coating layers (refer Fig. 4.11 and 4.12). The circularity showed that almost perfect circular shape was achieved for the WC phase in the gas atomized Ni powder based coatings whereas the water atomized Ni powder based coatings had flat WC particles, almost parallel to the mild steel substrate surface. The equivalent pore diameter was similar for both coatings and this was because of similar deposition mechanisms that achieved similar thickness and porosity values. The WC retention was relatively high for both coatings as the white phase (WC) was dominant in the resultant coatings (refer Fig. 4.10).

The carbide grain sizes were similar for both coatings and the binder mean free path was very low due to the relatively very thin coatings, the Ni phase did not have much area to occupy. Both coatings achieved relatively high Vickers hardness due to the dominant WC phases seen in both coatings. The crack densities were relatively high and this was due to the bouncing off of feedstock powder particles that caused a grit blasting effect on the mild steel surface. This effect opposed the intended feedstock powder deposition and adherence. The relatively thicker gas atomized Ni powder based coatings had a higher roughness than that of the water atomized powder Ni based coatings. Both coatings however, showed a smooth surface because of the

significant minimal coating build up. The Elastic modulus of the gas atomized Ni powder based coatings was in range with the water atomized Ni powder based coatings and this was in agreement with the respective Vickers hardness values that were also in close range. The Plastic index was the same for both coatings.

Table 4. 3: Properties of coatings based on un-annealed Ni powders.

WC-5%wt%Ni coatings		
Properties	**(gas atomized Ni)**	**(water atomized Ni)**
Thickness (µm)	28.4 ± 3.5	24.2 ± 1.5 µm
Porosity (%)	6.5 ± 2.64	5.3 ± 3.8
Circularity	1.0 ± 0.0	0.3 ± 0.1
Equivalent pore diameter	0.14 ± 0.1	0.2 ± 0.1
WC retained (%)	57.8 ± 9	52.8 ± 10
Carbide grain size (µm)	0.2 ± 0.1	0.2 ± 0.1
Binder mean free path (µm)	0.011 ± 0.0001	0.015 ± 0.001
Hardness ($HV_{0.3}$)	470 ± 9	454 ± 12
Crack density (μm^{-1})	8.8 ± 7.1	19.3 ± 14.8
Roughness (Ra)	31.1 ± 4.8	18.7 ± 0.5
Elastic Modulus (GPa)	127 ± 6.6	115.8 ± 22.7
Plasticity Index	0.04	0.04

Fig. 4.15 shows the EDS analysis of the WC-5wt%Ni coatings based on the gas atomized Ni powder. The maps indicate clearly that the deposition was minimal. Disconnected lamellae of the coating are also shown, suggesting other region experienced more severe rebounding than others. This behavior was very similar from the water atomized based coatings (refer to Fig. 4.16); however the coating lamellae breakage was less.

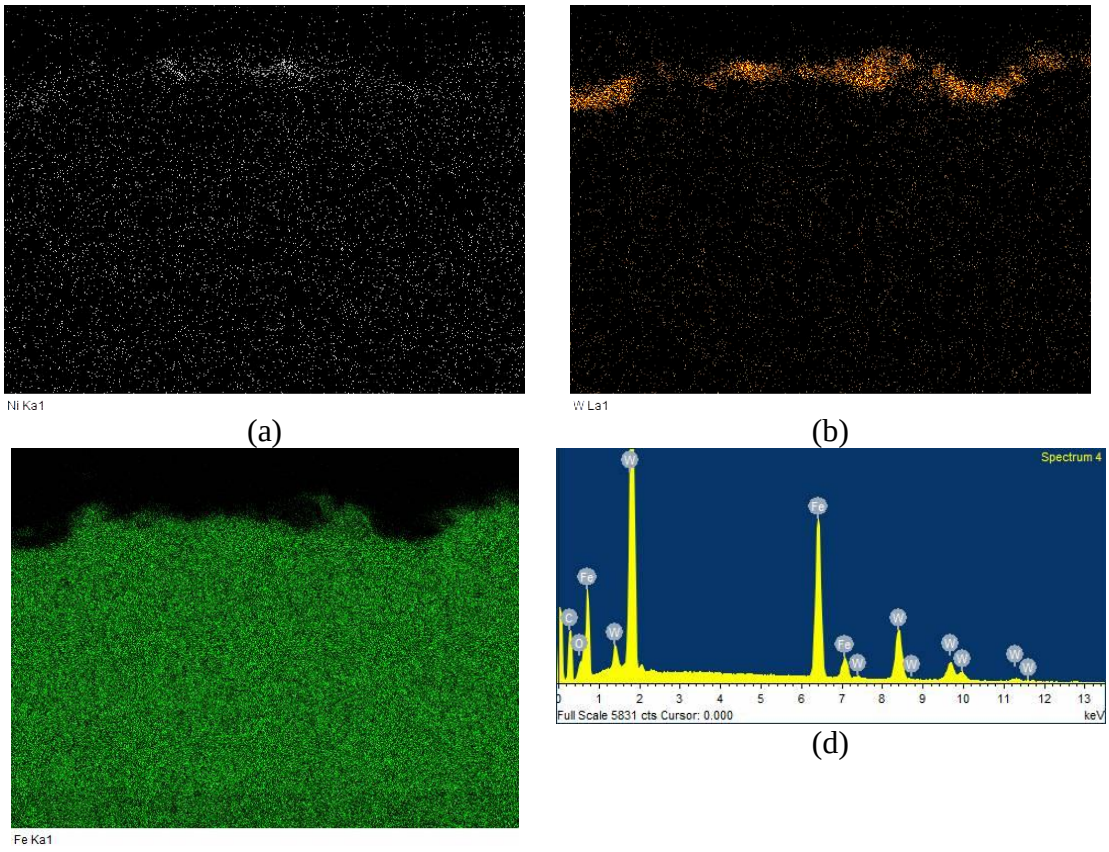


Figure 4. 15: EDS mapping for a WC-5wt%Ni coating based on gas atomized Ni powder, (a) Ni, (b) W, (c) Fe and (d) elemental spectrum.

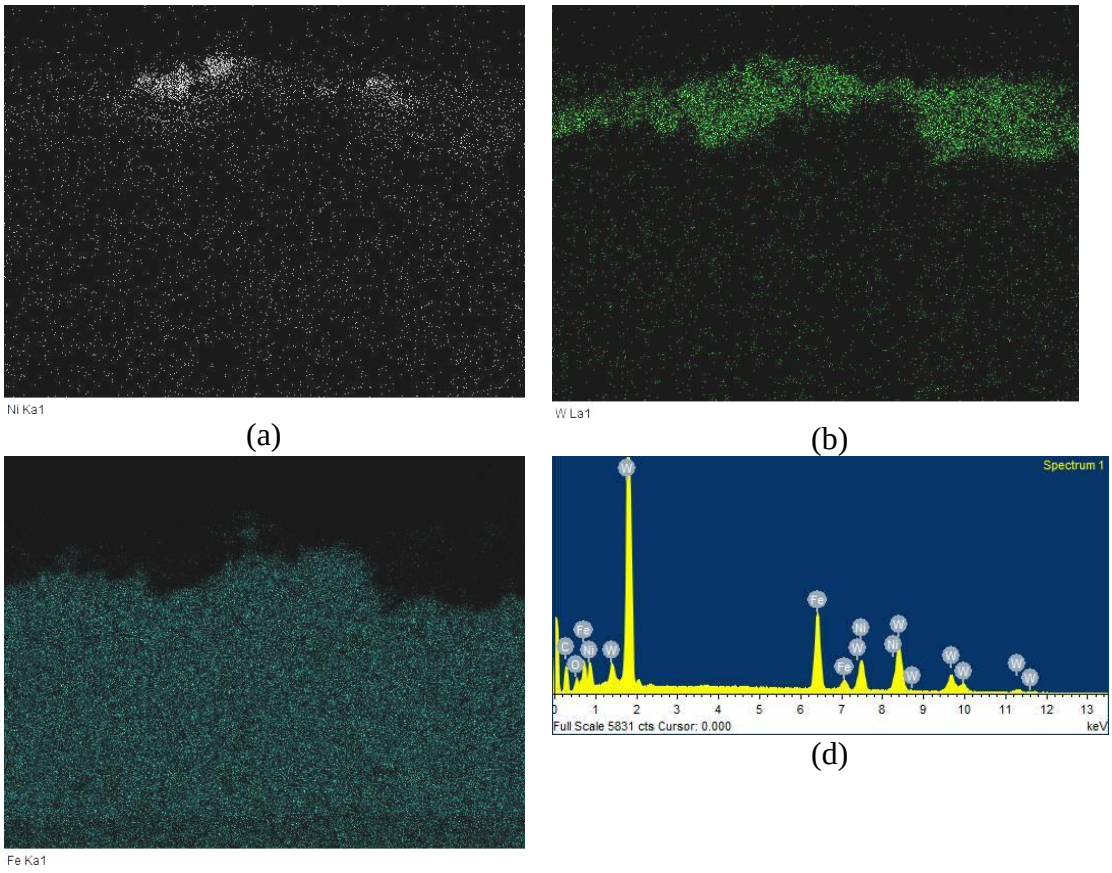


Figure 4. 16: EDS mapping for a WC-5wt%Ni coating based on water atomized Ni powder, (a) Ni, (b) W, (c) Fe and (d) elemental spectrum.

4.5 Annealing of nickel powder

This section presents a step that was introduced during the course of the research work. The gas atomized Ni and water atomized Ni powders were annealed so as to try and change the deposition properties while maintaining the powder properties.

4.5.1 Morphologies of Ni powders

The gas atomized Ni and water atomized Ni powders were taken for post-annealing analysis to verify if there have been any changes made on the powders. Figs 4.17 and

4.18 show the powder morphologies taken by BSE detector; both powders maintained their original morphology. The annealed gas atomized Ni powder showed a similar spherical morphology (refer to Fig. 4.17) as the un-annealed gas atomized Ni powder (refer to Fig. 4.1). The water atomized Ni powder (refer to Fig. 4.18) had a similar morphology to the un-annealed water atomized Ni powder (refer to Fig. 4.1).

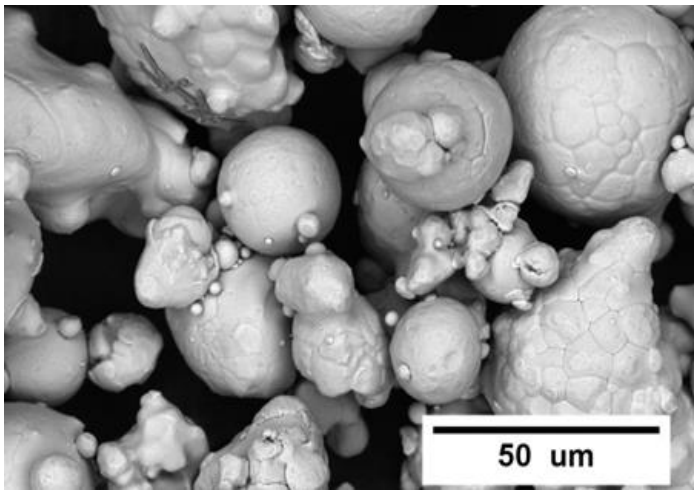


Figure 4. 17: Annealed gas atomized Nickel powder morphology.

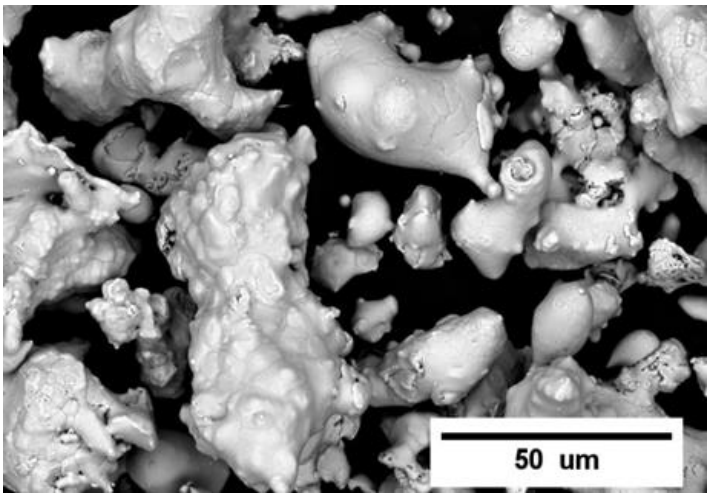


Figure 4. 18: Annealed water atomized Nickel powder morphology.

4.5.2 Phase analyses

Fig. 4.19 shows the phase analyses of the Nickel powders, no new phases were detected by this analysis.

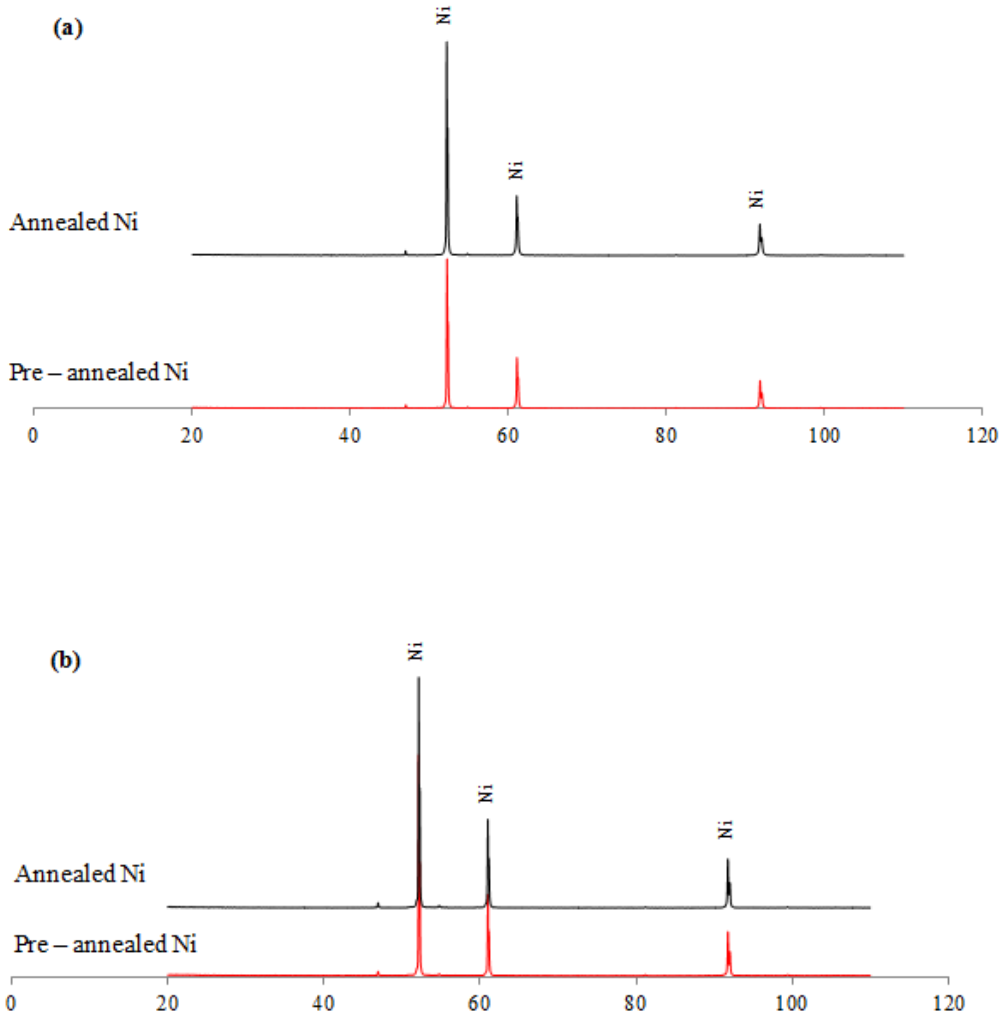


Figure 4. 19: XRD patterns of un-annealed and annealed powders based on (a) gas atomized Ni powder and (b) water atomized Ni powder.

Fig. 4.20 shows the Raman spectroscopy performed on the Nickel powders. Fig.4.20 (a) shows a NiO phase that was detected on the surface of the heat treated gas atomized Nickel powder. Fig.4.20 (b) shows no new phases on the surface of the water atomized Nickel powder.

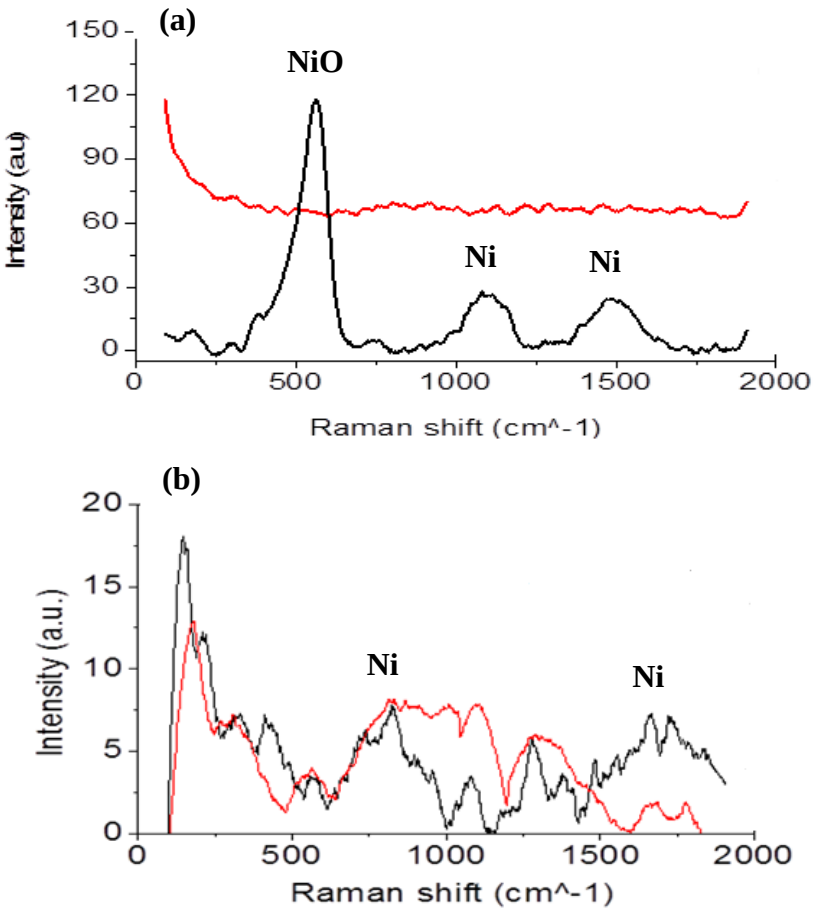


Figure 4. 20: Raman spectra for un-annealed and annealed powder based on (a) gas atomized Ni powder and (b) water atomized Ni powder.

Table 4.4 shows the hardness values for the Nickel powders and this shows a significant decrease from the starting Nickel powders.

Table 4. 4: Nickel powder hardness.

Powder	annealed water atomized Nickel	annealed gas atomized Nickel
Hardness ($HV_{0.3}$)	32.4 ± 32.2	29.8 ± 28.4

Appendix E shows the Rietveld analysis that was performed on the powders. The analysis shows that the powder size reduced after the annealing however for the milled WC-5wt%Ni powder blends indicated a similar particular size with the starting powders and this is unlike the outcome after milling where particle size is expected to reduce.

4.6 Characterization of WC-5wt%Ni coatings based on annealed Ni powders

Changes were seen in the gas atomized Ni powder based coating. There was significant reduction in particle rebounding and increased feedstock powder deposition. The water atomized Ni powder based coatings however, did not show major changes.

4.6.1 Coating microstructures

Figs 4.21 and 4.22 show the coating microstructures. Mainly the deformation and splat forming upon impact with the substrate surface was shown in the coatings based on the gas atomized Ni powder. Pores are indicated by red arrows and alumina grit is indicated by the light blue arrows.

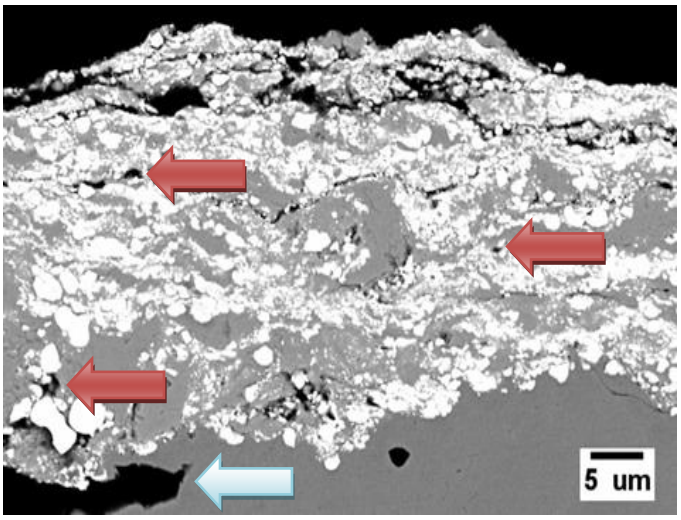


Figure 4. 21: Microstructures of WC-5wt%Ni coatings based on annealed water atomized Ni powder.

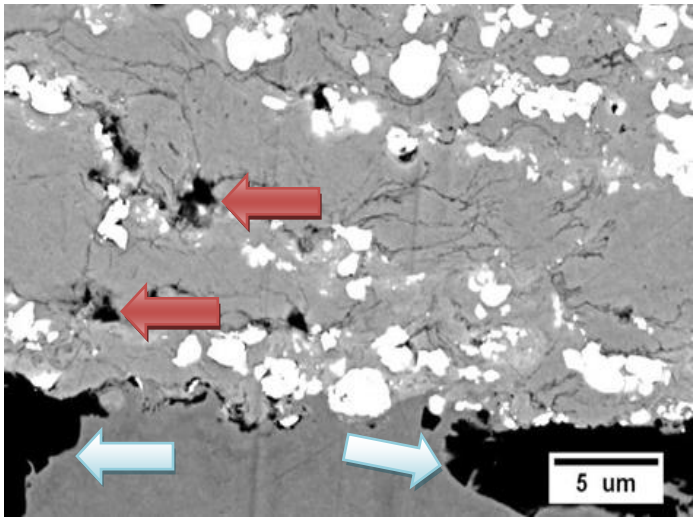


Figure 4. 22: Microstructures of WC-5wt%Ni coatings based on annealed gas atomized Ni powder.

4.6.2 Phase analyses

Figs 4.23 and 4.24 show the phase analysis done for the coatings and they are compared with the starting powders. The XRD patterns almost match, showing no decarburization or oxidation. No new phases occurred during the spraying.

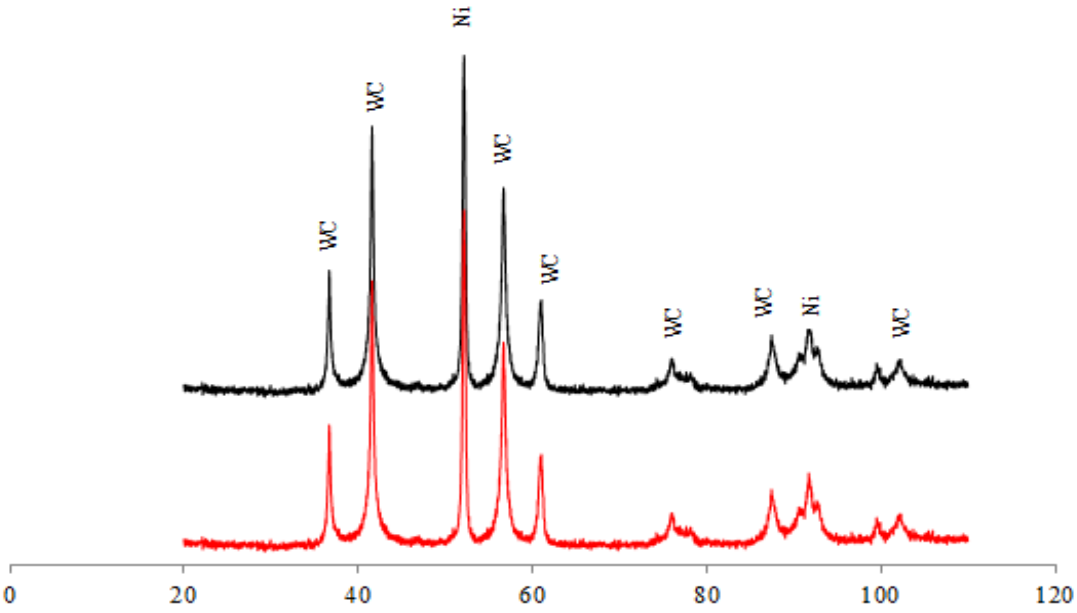


Figure 4. 23: XRD patterns for WC-5wt%Ni coating (black) and powder (red) based on gas atomized Ni powder.

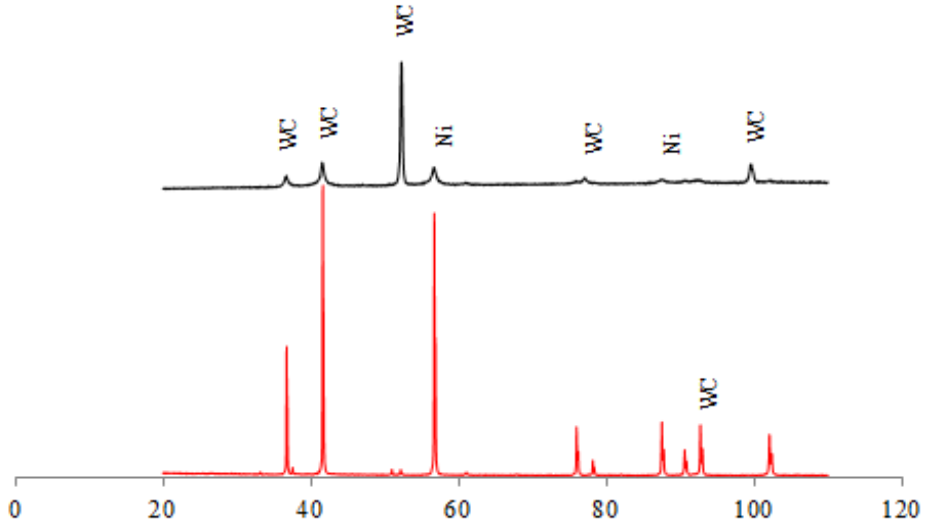
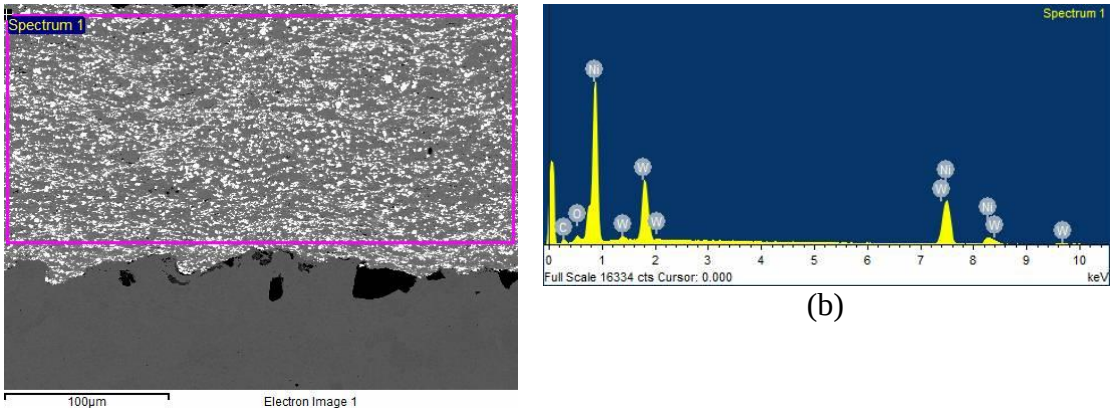


Figure 4. 24: XRD patterns for WC-5wt%Ni coating (black) and powder (red) based on water atomized Ni powder.

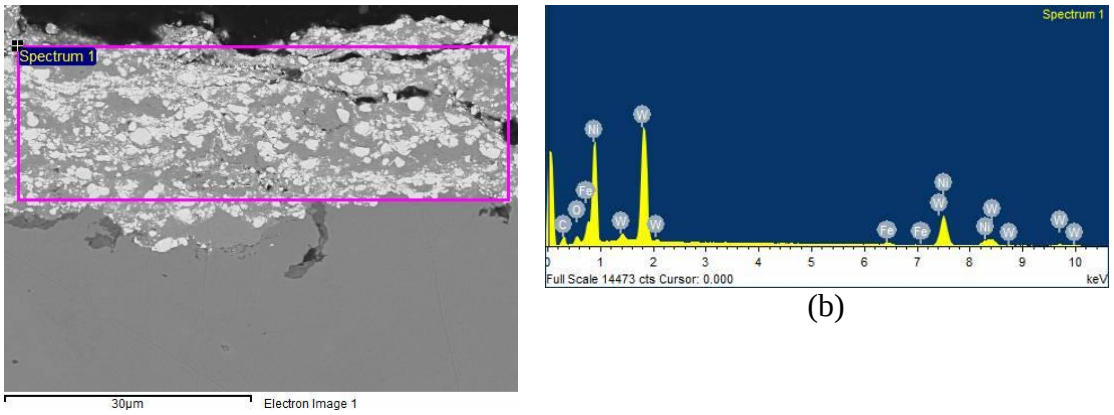
Figs. 4.25 and 4.26 show the coatings area considered and EDS spectra for the coatings WC-5wt%Ni coatings deposited using annealed Nickel powders. The phases

present in the resulting coatings are shown in the EDS analyses; the phases in the starting powders are also present in the resulting coatings.



(a) (b)

Figure 4. 25: (a) FESEM and (b) EDS for gas atomized based WC-5wt%Ni.



(a) (b)

Figure 4. 26: (a) FESEM and (b) EDS for water atomized based WC-5wt%Ni.

4.6.3 Topographical analyses (AFM)

Fig. 4.27 shows the Atomic force microscopy (AFM) images obtained for a typical coating/substrate interphase. An alumina grit particle is shown embedded in the substrate surface (white arrow); this phenomenon is common in the cold spray process due to the supersonic speeds attained during feedstock powder deposition.

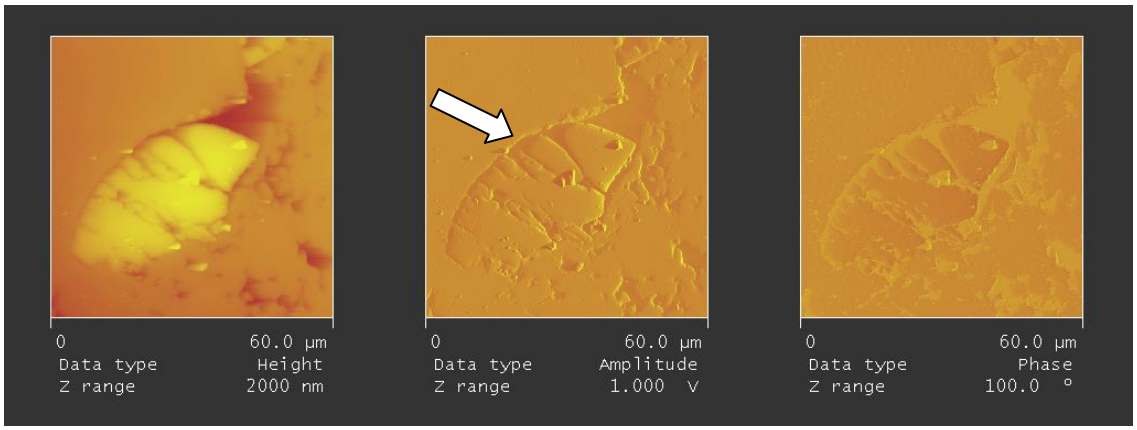


Figure 4. 27: AFM image showing alumina grit (white arrow) embedded in the substrate surface.

Fig. 4.28 shows a high magnification 3D image of the alumina grit embedded in the substrate surface. The alumina grit particle also forms voids in the areas surrounding the inter splat. White arrows indicate where the location of the alumina grit.

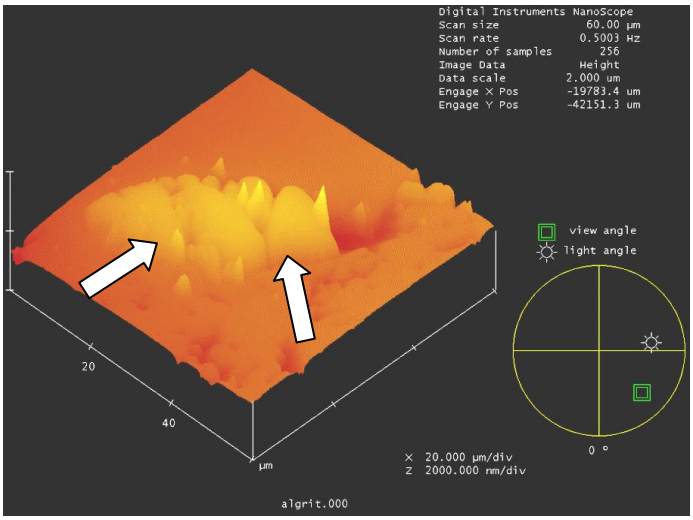


Figure 4. 28: 3D AFM image of alumina grit in the substrate surface.

Fig. 4.29 shows the surface 3D coating topographies taken by AFM. Coatings based on the respective annealed powders displayed rougher surfaces compared to the respective un-annealed based coatings.

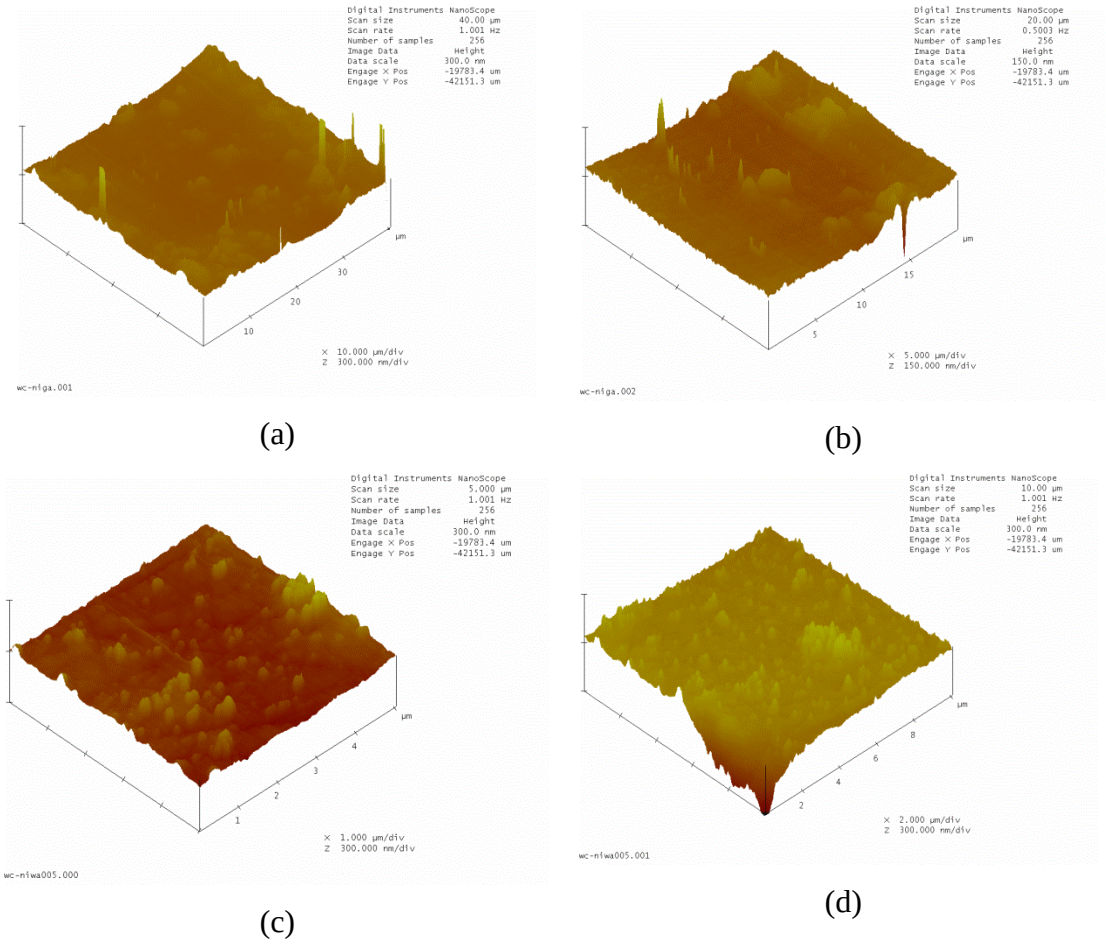


Figure 4. 29: 3D AFM topographies of coatings based on un-annealed and annealed (a & b) gas atomized Ni powder and (c & d) water atomized Ni powder.

4.6.4 Properties of WC-5wt%Ni coatings based on annealed Ni powder

Table 4.5 lists the coating properties of the coatings based on annealed Nickel powders. The coatings based on the gas atomized Ni powder were significantly thicker than the water atomized Ni powder based coatings, approximately 89 % thicker. The gas atomized Ni powder based coatings displayed good coating build during powder deposition and this led to dense coatings forming. The porosity was therefore low and consequently the crack density. The water atomized Ni powder based coatings had a higher porosity and the gouging effect on the coating surface seen during deposition facilitated pore formation. Appendix C shows the typical

images that were obtained from Image J software; the images represent the respective coatings based on annealed Ni powders. The images were used to identify and quantify the pores for each coating. The circularity showed that the WC particles assumed a circular shape for the gas atomized Ni powder based coatings more compared to the water atomized based Ni coatings (refer Fig. 4.21 and 4.22). The equivalent pore diameters were similar for both coatings. The water atomized based Ni coatings had a higher WC retention and this is shown in Fig. 4.22 where the coating area is dominated by the white phase (WC). The gas atomized Ni powder based coatings had a larger carbide grain size and this is because of the deposition mechanism, thicker coatings were achieved unlike for the water atomized Ni powder based coatings where some of the feedstock powder broke away and did not build up thick and dense coatings. The water atomized Ni powder based coatings had a smaller binder mean free path and this is because of the low retention of the Ni phase in the coatings coupled with thin coupled with very thin coatings. Consequently the Vickers hardness and Elastic modulus were higher than that of the gas atomized Ni powder coatings and this was in agreement with a lower Plastic index value for the water atomized Ni powder based coatings. Thicker coatings demonstrated rougher surfaces compared to very thin coatings because with minimal coating build up, the thin coatings had a smoother surface and thus the gas atomized Ni powder based coatings had a higher roughness.

Table 4. 5: Properties of coatings based on annealed Ni powders.

WC-5%wt%Ni coatings		
Properties	**Gas atomized Ni**	**Water atomized Ni**
Thickness (µm)	255 ± 33.5	28.5 ± 1.1
Porosity (%)	0.7 ± 0.3	1.3 ± 0.8
Circularity	0.9 ± 0.4	0.6 ± 0.0
Equivalent pore diameter	0.6 ± 0.2	0.6 ± 0.0
WC retained	42.9 ± 0.7	49.5 ± 2.5
Carbide grain size	1.8 ± 0.004	0.4 ± 0.1
Binder mean free path (µm)	0.10 ± 0.003	0.02 ± 0.0003
Hardness ($HV_{0.3}$)	361 ± 38	426 ± 12
Crack density (μm^{-1})	36.8 ± 24.3	328.8 ± 60.2
Roughness Ra	32.6 ± 32.6	15.9 ± 1.4
Elastic Modulus (GPa)	62 ± 3.5	88.3 ± 1.8
Plasticity Index	0.06	0.05

4.7 Slurry Abrasion Tests

Fig. 3.4 shows the FESEM image of the silica sand abrasive used for the slurry abrasion tests. The angular and sharp morphology is discernible. Fig. 4.30 shows the particle size distribution of the silica sand.

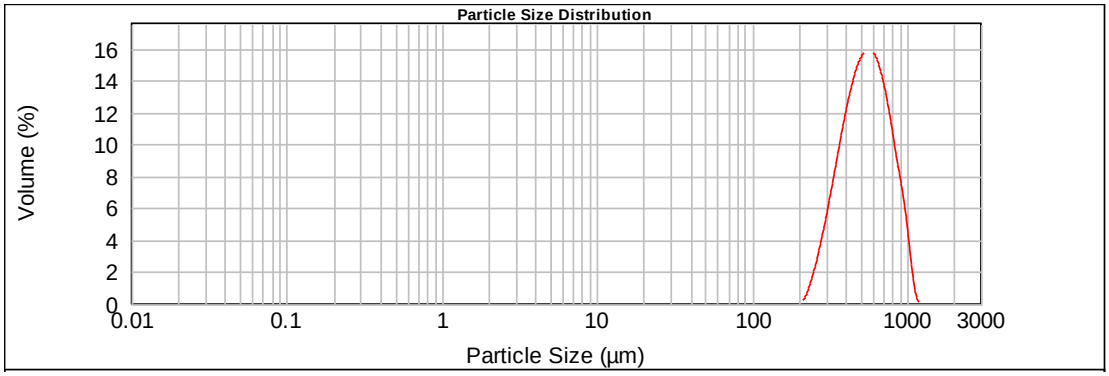


Figure 4. 30: Particle size distribution of silica sand.

4.7.1 Mass loss plots

Figs 4.31 and 4.32 show the mass loss vs. time plots for all four types of WC-5wt%Ni blends investigated in this research. Red line plots represent the coatings based on annealed Ni powders while the blue line plots represent the coatings based on un-annealed Ni powders respectively. The raw data of the mass losses are given in Appendix B. The rise in mass loss for both coatings is a normal phenomenon in wear tests because that is the initial recorded mass loss from (T_0) before tests begin. Fig. 4.31 shows that the annealed Ni-based coatings had better wear resistance. Firstly, the tests ran longer (6 hours) because the coating thickness allowed for such a relatively long duration. Secondly, as the slurry tests progressed, mass loss decreased, notably after 2 hours. The fracture toughness was 3.197 $MPa.m^{0.5}$ according to the Evans and Wilshaw model [64], this was comparable to the work carried out by [11]. The rest of the coatings did not have fracture toughness tested because of the thin coatings obtained. The un-annealed gas atomized Ni powder based coatings were tested for 30 minutes and showed a tendency for increased mass loss as the tests proceeded.

Fig. 4.32 shows mass loss curves for the coatings based on the water atomized Ni powder. The annealed Ni-based coatings showed a consistent mass loss until the 30^{th} minute when mass loss reduced noticeably and this may be the steady state conditions likely to be attained. The un-annealed Ni-based coatings showed a tendency for the mass loss to rising as the wear testing progressed. The porosity and crack density values for these coatings were the highest and the thicknesses were the lowest (refer to Table 4.3) this is seen in the severity experienced by the coatings which showed almost complete binder removal and total undermining of the carbide grains.

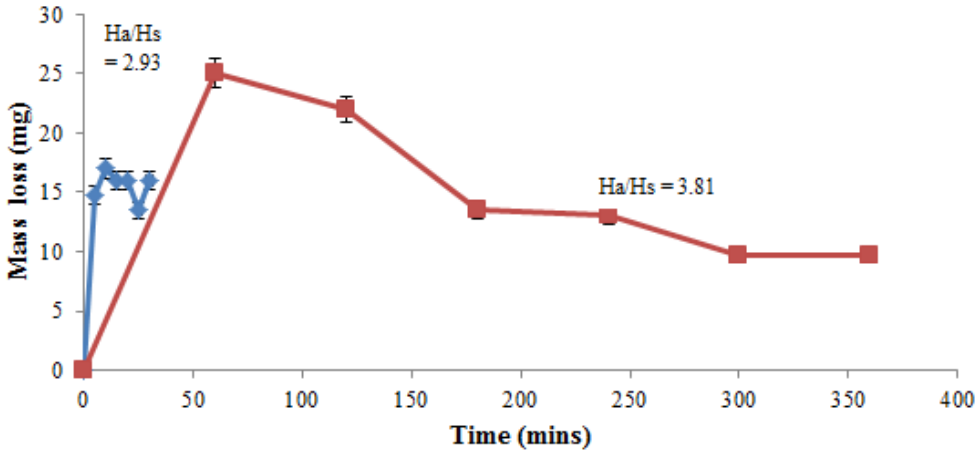


Figure 4. 31: Mass loss curve WC-5wt%Ni coatings based on gas atomized Ni powder.

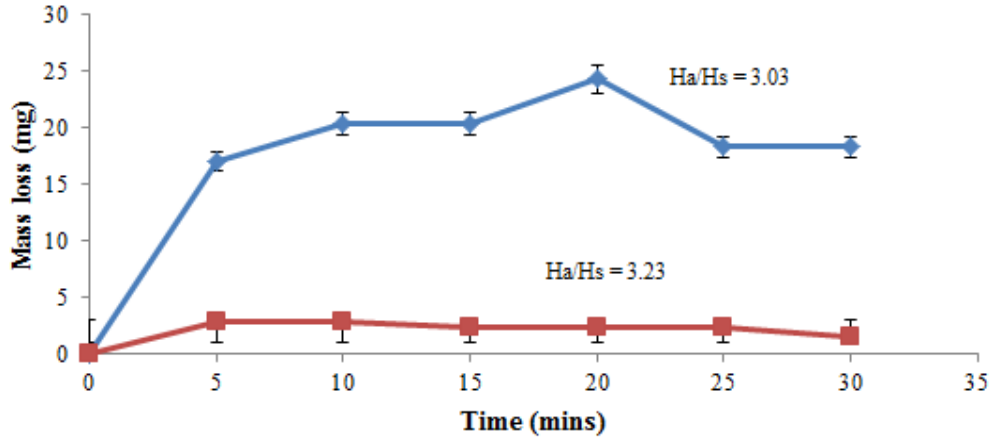


Figure 4. 32: Mass loss curve WC-5wt%Ni coatings based on water atomized Ni powder.

4.7.2 Worn surfaces

Fig. 4.33 shows the worn surfaces for all the WC-5wt%Ni coatings. Figs 4.33 (a-d) represent coatings based on the gas atomized Ni powder while Figs 4.33 (e-h) represent coatings based on the water atomized Ni powder. All the images are Backscattered (BS) images. There was severe scratching, preferential binder removal and carbide grain cracking for the coatings based on the un-annealed respective Ni powders and on the coatings based on the annealed water atomized Ni powder.

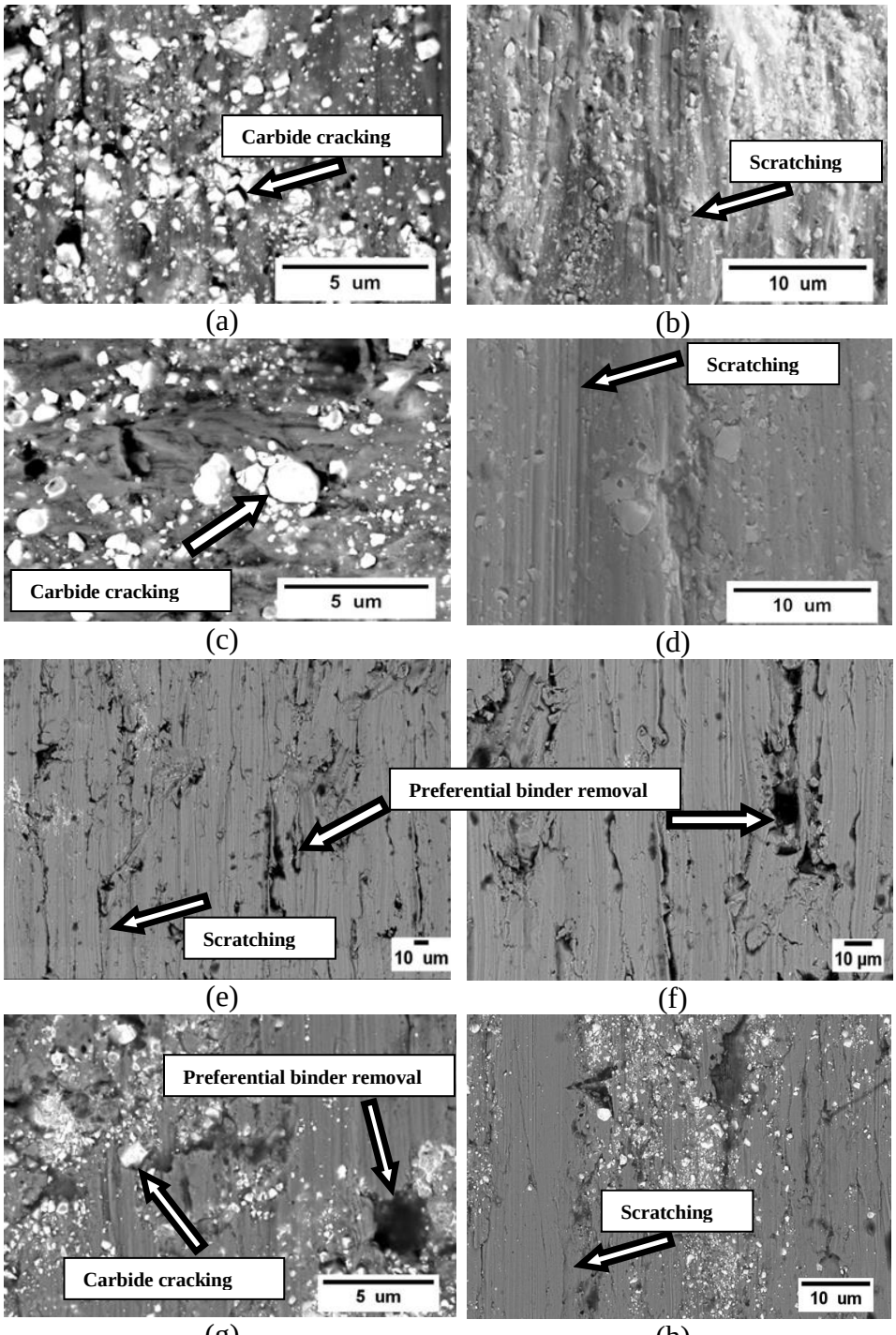


Figure 4. 33: Wear scars of WC-5wt%Ni coatings based on (a-d) gas atomized Ni powder and (e-h) water atomized Ni powder.

4.7.3 Wear rates

Fig. 4.34 shows the average wear rates for all WC-5wt%Ni coatings. The un-annealed Ni based coatings had higher average wear rates with the water atomized Ni powder based coatings having the highest wear rate. The coatings based on the annealed gas atomized Ni powder had the lowest average wear rate, therefore meaning they had best wear resistance.

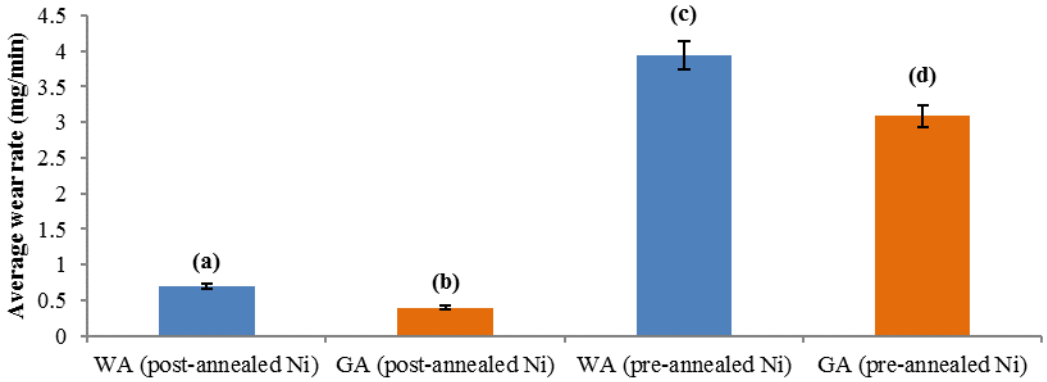


Figure 4. 34: Average wear rates of WC-5wt%Ni coatings.

Chapter 5

Discussion

This chapter presents detailed discussions of the results presented in Chapter 4. This chapter is divided into two sections namely:

- Gas Atomized versus Water Atomized Nickel Powders.
- Effect of Annealing Nickel Powder Prior to Coating Deposition

5.1 Gas Atomized versus Water Atomized Nickel Powders

This section presents a discussion on the un-annealed Ni powders, namely the gas atomized nickel and water atomized nickel. Section 5.1.1 presents the comparison between the properties of the nickel powders, while detailed discussion on the properties of coatings made from the powders is presented in 5.1.2. Lastly, section 5.1.3 discusses how the slurry abrasion of the different coatings compares.

5.1.1 Powder property comparison

The gas atomized Ni powder had a spherical shape while the water atomized Ni powder had an irregular shape, this can be seen on the FESEM images (refer to Fig. 4.1). Powder particle shape is determined by the method of production, gas atomization normally produces spherical shaped powders [65], while water atomization produces irregular shapes [63]. Both powders were in the same particle size range. The gas atomized Ni had $D_{10,\ 50,\ 90}$ values of 21, 35 and 57 µm respectively, while water atomized Ni had $D_{10,\ 50,\ 90}$ values of 14, 31 and 62 µm respectively. Similar sizes were reported for studies done on WC-12wt%Co powder blends [10]. Both Ni powders had a relatively narrow distribution of particle size

(refer to Fig. 4.2). Prisco *et al* [66] reported that a particle axial velocity is observed in the discharging jet, also in the case of a feedstock powder with a narrow distribution of particle size. The author went on to argue that this velocity distribution cannot be explained only in terms of the size-dependent distribution of velocity that arises inside the nozzle, also the slowest particles are observed outside the projected area of the nozzle. These particles experience a slower dragging fluid and, as a consequence, a smaller dragging force. This was observed when depositing the Ni-only coatings as the powders demonstrated an impeded flow. Feedstock powder particle size has a significant bearing on the velocity of particles thereby influencing the deposition characteristics. The work of Assadi *et al* [44] argued that the size of the particle as an influential factor on the velocity thereby influencing resulting coatings, several other reports suggested that the size of impacting particles influence the critical velocity [65,67,68]. In conclusion, it is essential for different powder particle sizes and particle distributions to attain their respective critical velocities so as to impact on substrate surfaces sufficiently for deposition to take place.

It is reported that irregular particles could contain a higher amount of impurities in the as-received state due to the method of production [69], in agreement to this, Lagutkin *et al* [70] reported that water atomization is not suitable for the production of clean powders. It is, therefore, a high possibility that unclean powders may have their properties altered by impurities. In this work, XRD analyses (refer to Fig. 4.19), showed that both Ni powders were in their pure form and EDS analyses confirmed no evidence of inclusion elements, the Vickers hardness, however, was changed, (refer to Fig. 4.5). The hardness of the water atomized Ni powder was in range with the gas atomized Ni powder. Powder hardness is associated with deformability and harder particles may not deform well upon contact with substrate surfaces. Both powders displayed limited ductility during deposition and instead had a grit blasting effect on the mild steel substrates thereby producing thin coatings. The Ni powder hardness, therefore, had a major impact on the deformation characteristics and subsequently, the coating build up.

5.1.2 Coating deposition and material properties

Fig. 4.9 shows minimal deposition for the Ni-only coatings. Most of the powder particles bounced off the mild steel substrate surfaces. Both WC-5wt%Ni coatings generally displayed difficulty in adhering to the mild steel surface initially. There was narrow tolerance on the critical number of powder passes that would allow for any significant coating build up which would lead to a significantly non-thin coating (refer Table 4.1 and 4.2). FESEM mode images shown in Figs. 4.10 – 4.12 displayed that there was an eroding effect during deposition and this led to the partial removal of the already deposited coating layers. This eroding effect which is relatively similar to grit blasting effect, contributed to the thin coatings. Critical velocity of approaching feedstock powders is important in ensuring that powder adiabatically shears and adheres to a substrate surface, [6,17,23,44,69]. There is a possibility that critical velocity was not attained from the spray parameters considered. Due to the dominance of the WC phase in the coatings, it can be concluded that there was not enough encapsulation of the WC phase by the binder matrix thereby leading to the rebounding of the feedstock powder. This is in agreement with Wang's work [20].

Table 4.3 lists the WC-5wt%Ni coating properties. Both Ni powders produced thin WC-5wt%Ni coatings and this can be attributed to the Ni powder properties discussed in section 5.1.1 coupled with the difficulty to attain critical velocities during deposition. Both Ni powders produced coatings with relatively high porosity. The gas atomized Ni powder based coatings had the highest porosity. The spherical shape of the gas atomized Ni powder may have influenced the resulting circularity of the WC phase as shown by the approximate 100% circularity value, whereas the water atomized Ni had a very low circularity value and this can be seen on the flattened shape of WC phase (refer to Fig. 4.12). Koivuluoto *et al* [71] report that flattened shape of primary particles indicates that high degree of plastic deformation occurred during spraying and also particles with dendritic structure break down during the particle impact on the substrate or other particles. The WC-5wt%Ni

coatings based on the water atomized Ni powder showed more particle breaking and thus a higher crack density, this was in agreement with Koivuluoto's [71] and Alidokht's work [30]. The WC retention was relatively high for both coatings and this was higher than WC-5wt%Ni coatings deposited by CGDS in previous work [11] and the Vickers hardness was about 50% higher. The higher hardness values can be ascribed to high WC retention.

The Elastic modulus and Plastic index were in the same range for both WC-5wt%Ni coatings. The gas atomized Ni powder based coatings had a relatively higher roughness, the coatings were thicker, therefore, a higher roughness was expected, Moridi *et al* [6] however report on higher surface roughness causing for less porosity due to good interlocking and voids reduction.

5.1.3 Slurry abrasion comparison

Both WC-5wt%Ni coatings experienced severe wear, and this was seen on the wear scars refer to Fig. 4.33 b) & d) for the coatings based on the gas atomized Ni powder and Fig. 4.33 f) & h) for the coatings based on the water atomized Ni powder. Both coatings experienced hard abrasion as exhibited by the Ha/Hs calculations (refer to Fig. 4.31 and 4.32). The FESEM images for the worn surface indicate that in most cases there was almost total binder removal thereby leading to carbide grain pullout [3,25]. The thickness was low for both coatings and therefore the high rise in mass loss shown after just 5 minutes of slurry abrasion testing. The gas atomized based Ni coatings showed that the coatings had a tendency of having an increase in mass loss. The Mass loss recorded at the 30^{th} minute mark was more than the mass loss at the 25^{th} minute mark. For the water atomized Ni powder based coatings however, there was a tendency of reduction in the mass loss as the slurry abrasion tests progressed. The trends displayed on the mass loss graphs (refer to Figs. 4.31 and 4.32) could also

mean that before the 30 minutes of slurry abrasion testing was reached, the water atomized Ni powder based coatings was almost completely worn away. This would mean that for the gas atomized Ni powder based coatings there was still a coating on the surface.

Even though both coatings showed poor wear behavior, the gas atomized Ni powder based coatings had better wear behavior and this can be attributed to relatively thicker coatings, higher WC retention and Vickers hardness, low crack density, and high Elastic modulus. This is in agreement with Chen's work [25] where under high-stress abrasion, coatings with relatively low Vickers hardness experienced higher wear rates. Kumari *et al* [42] report on how a low binder mean free path would impose higher abrasive wear resistance. This was not the case with the WC-5wt%Ni that had significantly low binder mean free path and also very low abrasive wear resistance. Oladijo *et al* [24] reported on coatings with the highest hardness also the having highest wear rate, much similar to the water atomized based coatings that had significantly high hardness but highest wear rate. In conclusion, the WC-5wt%Ni coatings generally did not display good microstructural and mechanical properties. After being exposed to hard abrasion, the wear resistance was minimal.

5.2 Effect of Annealing Nickel Powder prior to coating Deposition

This section presents a discussion on the effects of annealing the Ni powders prior to coating deposition. This section is divided as follows; firstly powder property comparison, followed by coating deposition and material properties then lastly slurry abrasion comparison. The three sections will also include comparisons with results from un-annealed Ni-based coatings.

5.2.1 Powder property comparison

The gas atomized Ni powder and the water atomized Ni powder both maintained their morphologies after annealing (refer to Figs. 4.17 & 4.18). The spherical shape is still seen for the gas atomized Ni powder while the water atomized Ni powder still had an irregular morphology. This suggests that the annealing performed on the powders did not have significant effects on powder morphology. The gas atomized Ni powder had a particle size slightly larger than that of the water atomized Ni powder (refer to Appendix E). The particle sizes for both Ni powders were similar to the un-annealed Ni powders particle size.

The size reduction was detected on the nanometre (nm) scale suggesting very minimal effect imposed by the feedstock particle size on resultant coatings. Fig. 4.19 shows the phase analyses; the XRD patterns are stacked so as to match phase peaks in the annealed and un-annealed powders. The XRD patterns show that there were no new phases formed. Raman spectroscopy, however, showed a new NiO phase on the surface of the gas atomized Ni powder, (refer to Fig 4.20a). Similar findings were reported by Valladares *et al* [61], the authors annealed Ni powder at 400 °C and detected NiO, the analysis, however, showed no new phases for the water atomized Ni powder, (refer to Fig 4.20b). For this research, the Ni powders were annealed at a maximum temperature of 500 °C, Valladares annealed to a maximum temperature of 700 °C. The authors reported that there were significant changes made on the powders at higher annealing temperatures, especially on the crystalline size. It can be suggested that the water atomized Ni powder had stronger interlocking compared to the gas atomized Ni powder thereby assuming at higher temperatures significant changes would be seen on the water atomized Ni powder. The hardness for the annealed Ni powders both decreased with the water atomized Ni powder maintaining a higher hardness. Annealing decreases the hardness and increases the ductility, this is in agreement with Koivuluoto's work [72]. The technique used does not expose fully the powder after mounting it in the transparent thermoplastic powder; this may

lead to slightly wider error values. The EDS analysis showed a 76% increase in the oxygen content of the gas atomized Ni powder, compared to the 14% increase seen for the water atomized Ni powder. Appendix F shows the EDS data that was used to calculate this change in oxygen content. The gas atomized Ni powder demonstrated the most response to the annealing as demonstrated by the new NiO phase and the increase in oxygen content. The water atomized Ni powder displayed minimal response to the annealing, and this may be attributed to the annealing parameters namely temperature and holding time, the powder properties may also be a contributing factor. The carbon content shown on the EDS analysis for the annealed Ni powders was selected during analysis, whereas for the un-annealed Ni powder, the carbon was not selected. Carbon is usually detected because powder samples are placed on carbon tape when doing EDS analysis and thus it is picked up. Carbon has a low density so quantifying it with EDS detector is difficult.

5.2.2 Coating deposition and material properties

The WC-5wt%Ni coatings based on the water atomized Ni powder did not demonstrate significant changes. The deposition characteristics were almost maintained with powder flowability and rebounding on the substrate surface being maintained. Fig. 4.21 shows a similar coating to the coatings based on the un-annealed water atomized Ni powder (refer to Fig 4.12). Minimal coating deposition associated with eroding of underlying coating layers was experienced and this led to thin coatings. It can be suggested that critical velocity was not attained therefore the deformation characteristics upon impact with the mild steel substrate did not result in coating build up. The coatings showed significant porosity and voids, alumina particles were seen on the coating/substrate boundaries, this was also observed by Machio *et al* [1]. The splat boundaries in the Ni matrix were not as discernible as in the coatings based on the gas atomized Ni powder.

The WC-5wt%Ni coatings based on the gas atomized Ni powder demonstrated much improved deposition characteristics. Good coating build-up led to thick and dense coatings (refer Fig 4.22), the FESEM images showed a homogenous coating with minimal porosity and voids. The coatings had approximately 89% increase in thickness, thicker coatings from the same feedstock powder blend and CGDS technique were reported elsewhere [11]. The decrease in gas atomized Ni powder hardness contributed to the increase in deformation of the WC-5wt%Ni feedstock powder upon impact with the mild steel substrate surface, this can be attributed to the increase in ductility. Vashishta *et al* [47] reported that there was an improvement of coatings after an increase in ductility of binder matrix, the author, however, mentioned that there was a decrease in binder matrix ductility at temperatures beyond 550 °C due to the recrystallization of the amorphous binder with the formation of various eta carbides. In this research, however, this was not displayed by the WC-5wt%Ni coatings based on the annealed Ni powders.

Table 4.5 lists the properties of the WC-5wt%Ni coatings based on the annealed Ni powders. The porosity of the gas atomized Ni powder based coatings was in range with the water atomized Ni powder based coatings and approximately 90% less porous than the coatings based on the un-annealed gas atomized Ni powder. This reduction in porosity can be attributed to the tamping effect as a result of plastic deformation of powder particles upon impact [30]. Tamping effect results in densification of porous regions that once were the top layer of the coating, this was also observed by Ajdelsztajn *et al* [73]. The coatings based on the water atomized Ni powder did not display tamping effect due to the particles rebounding off the surface, therefore, densification could not be attained and this led to relatively higher coating porosity (refer to Table 4.5). The circularity was above 50% for both annealed Ni-based WC-5wt%Ni coatings with the gas atomized Ni powder based coatings having 90% circularity of the WC particles. A lower circularity means particle flattening was achieved to a larger extent during deposition. The water atomized Ni powder based coatings from both annealed and un-annealed Ni powder exhibited lower circularity

and this is in agreement with breaking of WC particles upon impact which also led to minimal deposition. Appendix D shows the probability and cumulative curves for the carbide grain size for annealed Ni-based coatings. The plots show that the WC-5wt%Ni coatings based on the gas atomized Ni powder had larger carbide grain size compared to the water atomized Ni powder based coatings. The particle area size of the WC-5wt%Ni coatings based on the gas atomized Ni powder covered a larger particle area size and this is seen in the FESEM images showing the coating areas (refer to Figs. 4.21 and 4.22).

The equivalent pore diameter was the same for both coatings was relatively high. The equivalent pore diameter for both coatings was relatively higher compared to coatings deposited using un-annealed Ni powders. For the gas atomized Ni powder based coatings this can be attributed to thicker coatings that allowed for larger but fewer pores [69,74,75]. For the water atomized Ni powder based coatings this can be attributed to the softening of the Ni matrix that was insufficient to bring about good deposition characteristics which would minimize equivalent pore diameter [17,23]. The equivalent pore diameters for the WC-5wt%Ni coatings based on un-annealed Ni powders were relatively low and this can be attributed to coatings that were characterized by rebounding of particles, high porosity and relatively thin [17]. Porosity is associated with cracking and it is usually a direct correlation, authors have reported on this [65], many authors have also reported similar findings [7,76]. The WC-5wt%Ni coatings based on the annealed water atomized Ni powder, however, had the highest porosity and relatively very high crack density. This can be ascribed to the possibility that the WC-5wt%Ni feedstock powder went through stronger impacts which led to a more severe strain on the coating surface. The lowest porosity achieved by the gas atomized Ni powder based coatings saw a lower crack density, however; the 3D AFM images (refer to Fig. 4.29) show that the pores were deeper. In the 3D images the peaks are clearly seen and these represent the topographical makeup of the coatings where the rest of the three coatings (refer to Figs. 4.29 a), c) and d)) had a more flat topography thereby suggesting relatively less deep pores.

The WC retention was relatively lower compared to the WC-5wt%Ni coatings based on un-annealed coatings. During deposition, the hard phase WC dominated in rebounding and partially depositing on the mild steel substrates, this led to a compromise of the Ni retained in the un-annealed Ni-based coatings. The FESEM images (refer to Figs. 4.11 and 4.12) show the dominance of the white phase (WC) and this is in agreement with the high WC retention. Higher WC retention led to higher hardness of the coatings. The annealing caused softening of the Ni binder and consequently decreased hardness for the respective WC-5wt%Ni blends (refer to Fig. 4.5). Effects of reduced hardness due to annealing was also reported on by previous researchers [47,48,71].

The annealed Ni-based coatings had relatively more homogenous coatings and this reduced the WC retention as the coatings had a larger representation of the two phases namely WC and Ni binder matrix. The WC-5wt%Ni coatings based on the gas atomized Ni powder had the highest binder mean free path. The rest of the coatings had a similar and relatively low binder mean free path. This can be attributed to the thicker coatings obtained for the gas atomized Ni powder based coatings meaning the Ni binder matrix occupied a larger area compared to the other coatings. The larger binder mean free path also contributed to the homogenous coatings that resulted. The WC-5wt%Ni coatings based on the annealed gas atomized Ni powder had the highest surface roughness while the coatings based on annealed water atomized Ni powder had the lowest surface roughness. The greater roughness can be attributed to the greater coating build up that was shown by the gas atomized Ni based coatings, as the layers build up accommodated by shear stresses and intersplats, the resulting surface will be rougher compared to very thin coatings seen for the water atomized Ni based coatings. The roughness was relatively higher compared to previous work [11]. The authors used the same WC-5wt%Ni powder blend and same CGDS machine but however, the substrate material was stainless steel.

The Plasticity index is an essential parameter that helps to predict the onset of plasticity [77] and coating durability in tribological behavior [78]. The coatings based on the respective un-annealed Ni powders had a similar value for plasticity index (refer to Table 4.3). Their hardness values were in a closer range compared to their annealed counterparts. The coatings based on the annealed gas atomized Ni powder had a relatively higher plasticity index and this can be attributed to the lower hardness value. The lower plasticity index seen for the coatings based on the annealed water atomized Ni powder is therefore because of the higher hardness.

5.2.3 Slurry abrasion comparison

The WC-5wt%Ni coatings based on the gas atomized Ni powder displayed better wear behavior compared to the coatings based on the un-annealed gas atomized Ni powder (refer to Fig. 4.31). Both graphs show a sharp rise in mass loss in the initial testing periods and this can be attributed to the vast removal of loosely attached coating material. The same behavior is seen for the WC-5wt%Ni coatings based on annealed and un-annealed Ni powders (refer to Fig. 4.32). The same behavior is reported for abrasive wear of hardmetal-based coatings elsewhere [25,26,47,48]. The WC-5wt%Ni coatings based on the gas atomized Ni powder displayed the mass loss reducing as the slurry abrasion tests progressed; this can be attributed to the more densified coating layers that resisted particle removal more compared to the top layers.

The WC-5wt%Ni coatings based on the un-annealed gas atomized Ni powder displayed an increase in mass loss as the slurry abrasion tests progressed; this was the same case with the WC-5wt%Ni coatings based on the un-annealed water atomized Ni powder. This behavior can be attributed to the coatings having particles that were relatively less densified, characterized by high porosity and high crack densities (refer to Table 4.3) contributed to compromised wear resistance. The respective WC-

5wt%Ni coatings based on un-annealed Ni powders also showed almost complete removal of coating material, the severe breaking of carbide grains and removal of binder material. Fig. 4.33(b, d, e, f, g, h) shows the wear scars and damage done to the coating surfaces is displayed, whereas Figs. 4.33 a) & c) is for the coatings based on the annealed gas atomized Ni powder. The WC-5wt%Ni coatings based on the annealed water atomized Ni powder displayed mass loss that was almost constant with the last time interval displaying the lowest mass loss. Appendix A shows high magnification tilted FESEM images of the cross-sectional wear scars for all the four coatings. The images give a closer view of the particle removal areas and the state of the mild steel substrate after interaction with the silica sand abrasive. Severe abrasion is seen in Fig.A1 (b, c & d); in some areas, the coating material is completely wiped away. Fig.A1 (a) represents the annealed gas atomized Ni powder based WC-5wt%Ni coatings and while material removal was evident, there was still a relatively thick coating remaining after the slurry abrasion tests. The gas atomized Ni powder reacted more to the annealing stage compared to the water atomized Ni powder. The major changes were based on the phase analysis and the hardness. Fig. 5.1 compares the powder hardness relative to annealing. Both Ni powders, however, experienced a reduction in hardness. The decrease in hardness brought about an increase in ductility and this influenced the deposition characteristics. The increase in ductility is associated with improved deformation behavior, the gas atomized Ni powder had better deformation and this resulted in dense and thick coatings that had improved wear characteristics. The wear resistance also showed that the coatings had increased adherence, the relatively larger carbide grain size meant that a greater force would be needed to cause cracks or coating failure. In wear environments, the coatings delamination process and the initiation of crack development could be delayed [78].

The average wear rates are shown in Fig. 4.34 and the WC-5wt%Ni coatings based on the un-annealed water atomized Ni powder had the highest wear rate followed by the un-annealed gas atomized Ni powder based coatings, this was due to the ease that the abrasive had in removing coating material. Although the annealed water atomized

Ni powder based coatings had close and similar properties to the respective un-annealed Ni-based coatings, it showed a relatively low average wear rate, this can be attributed to the relatively low porosity and better-attached coating material. This counteracted for the high crack density on the already thin coatings. Improvements in abrasive wear behavior due to annealing have previously been reported [47,48] and it can be seen that annealing brought about good deposition characteristics for the gas atomized Ni feedstock powder and relieves off stress in the case of coatings thereby bringing better wear resistance.

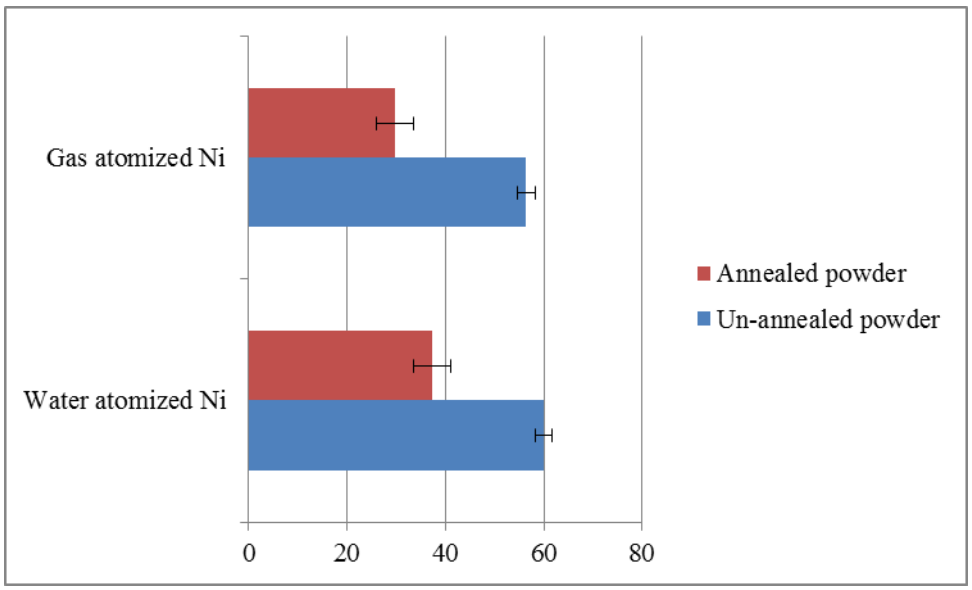


Figure 5. 1: Powder hardness relative to annealing

Chapter 6

Conclusions

A spherically shaped gas atomized Ni powder and an irregularly shaped water atomized Ni powder were used to make WC-5wt.%Ni powder blends and were each deposited onto mild steel substrates using a low pressure cold spray machine, the fabricated coatings were characterized. The shapes of the Ni powders were influenced by their respective powder production methods. The gas atomized Ni powder had a larger particle size compared to the water atomized Ni powder. An annealing stage was introduced so as to improve the deposition characteristics of the powders because the un-annealed Ni-based WC-5wt. %Ni coatings did not exhibit significant powder particle deposition. The synthesis process produced four types of WC-5wt. %Ni coatings based on un-annealed gas atomized Ni powder, annealed gas atomized Ni powder, un-annealed water atomized Ni powder and lastly annealed water atomized Ni powder. Initially, the respective Ni powders were deposited on the mild steel substrates so as to obtain near-optimal spray parameters.

Annealing of the Ni powders brought about changes in the powders and this was revealed by the characterization stage were oxygen content. For the gas atomized powder, NiO was detected on the surface of the powder. All coatings exhibited consistency with the phases in the powders as in the coatings; no new phases emerged from the spraying process. The alumina grit used for roughening the surfaces was detected in some cases embedded in the substrates and this is a condition well associated with the cold spray process; due to the supersonic speeds attained, particles break, fracture and get embedded in substrates surfaces.

The slurry abrasive wear resistance was significantly improved for the WC-5wt%Ni coatings based on the annealed gas atomized Ni powder. Both Ni powders decreased

in hardness; however, the gas atomized Ni powder attained a lower hardness compared to the water atomized Ni powder. The wear mechanisms in the slurry abrasion were found to be similar for all four coatings but with varying severity. The wear mechanisms included preferential binder removal, grain pull out, carbide grain cracking and undermining, smearing and plastic deformation of deposited particles. The WC-5wt. %Ni based on the annealed gas atomized Ni powder had the best wear resistance due to the lower average wear rate and a reduction in the mass loss during slurry abrasion progression. The WC-5wt%Ni coatings based on the annealed gas atomized Ni powder had a more homogenous microstructure, thicker and denser coatings, lower porosity and crack density, larger carbide grain size, and a higher plasticity index. These properties led to the best slurry abrasive wear resistance.

Chapter 7

Future work

This research was largely focused on the type of cold spray coatings fabricated from WC-5wt%Ni blends made from two different manufacturing processes and thereafter assessing the abrasive wear properties. The following recommendations are therefore made;

- Annealing of WC-5wt. %Ni blend so as to investigate the effects of annealing the complete feedstock powder.
- Annealing of the cold sprayed coatings for comparison with coatings deposited by the High velocity oxy-fuel (HVOF) process and other thermal spraying processes. Currently, there is no literature for annealed cold sprayed coatings.
- Varying of milling parameters of the feedstock powder so as to have a broader understanding of different feedstock powder qualities at different milling parameters.
- Preheating of the substrate material using the spray gun carrier gas so as to understand the effects of conditioning the substrate before feedstock powder deposition.
- Transmission electron microscopy (TEM) analysis on annealed and un-annealed Ni powders to study the behavior and characteristics of these Ni powders at the nanoscale.

References

[1] Machio CN, Akdogan G, Witcomb MJ, Luyckx S. Performance of WC-VC-Co thermal spray coatings in abrasion and slurry erosion tests. Wear 2005;258:434–42.

[2] Karimi A, Verdon C, Barbezat G. Microstructure and hydroabrasive wear behaviour of high velocity oxy-fuel thermally sprayed WCCo(Cr) coatings. Surf Coatings Technol 1993;57:81–9.

[3] Magagula NBS, Sacks N, Botef I. Slurry abrasion of WC-4wt % Ni cold-sprayed coatings in synthetic minewater 2016;116:333–7.

[4] Sapate SG, Chopde AD, Nimbalkar PM, Chandrakar DK. Materials & Design Effect of microstructure on slurry abrasion response of En-31 steel. Mater Des 2008;29:613–21.

[5] Melendez NM, Mcdonald AG. Surface & Coatings Technology Development of WC-based metal matrix composite coatings using low-pressure cold gas dynamic spraying. Surf Coat Technol 2013;214:101–9.

[6] Moridi A, Hassani-Gangaraj SM, Guagliano M, Dao M. Cold spray coating: review of material systems and future perspectives. Surf Eng 2014;30:369–95.

[7] Siao A, Ang M, Berndt CC, Cheang P. Surface & Coatings Technology Deposition effects of WC particle size on cold sprayed WC – Co coatings. Surf Coat Technol 2011;205:3260–7.

[8] Cavaliere P, Perrone A, Silvello A. Processing Conditions Affecting Grain Size and Mechanical Properties in Nanocomposites Produced via Cold Spray. J Therm Spray Technol 2014;23:1089–96.

[9] Melendez NM, Narulkar V V, Fisher GA, Mcdonald AG. Effect of reinforcing particles on the wear rate of low-pressure cold-sprayed WC-based MMC coatings. Wear 2013;306:185–95.

[10] Lioma D, Sacks N, Botef I. Cold gas dynamic spraying of WC–Ni cemented carbide coatings. Int J Refract Met Hard Mater 2015;49:365–73.

[11] Nunthavarawong P, Sacks N, Botef I. Effect of powder feed rate on the

mechanical properties of WC-5 wt % Ni coatings deposited using low pressure cold spray. Int J Refract Met Hard Mater 2016;61:230–7.

[12] Sacks N. Low pressure cold gas dynamic spraying of tungsten carbide-nickel coatings. Met Powder Rep 2016;0:8–10.

[13] Luo X, Li Y, Li C. A comparison of cold spray deposition behavior between gas atomized and dendritic porous electrolytic Ni powders under the same spray conditions. Mater Lett 2016;163:58–60.

[14] Fauchais P, Vardelle A. Thermal Sprayed Coatings Used Against Corrosion and Corrosive Wear. n.d.

[15] Winnicki M, Ma A, Rutkowska-gorczyca M, Soko P, Ambroziak A, Paw L. Surface & Coatings Technology Characterization of cermet coatings deposited by low-pressure cold spraying. Surf Coat Technol 2015;268:108–14.

[16] Papyrin. A, Kosarev. V, Klinkov.S, Alkimov.A F. Cold Spray Technology 1995:1200. http://store.elsevier.com/Cold-Spray-Technology/Anatolii-Papyrin/isbn-9780080451558/ (accessed March 12, 2016).

[17] Champagne VK. The cold spray materials deposition process Fundamentals and applications. Cambridge : Boca Raton: Woodhead ; CRC Press; 2007.

[18] Centerline - CenterLine (Windsor) Ltd - Supersonic Spray Technologies (SST) Division 2015. http://www2.cntrline.com/en/about_full?page=CE25000&rp=7 (accessed May 24, 2016).

[19] Dizdar S. Fe-Based Powder Alloys Deposited by HVOF and HVAF for Applications Exposed to Solid Particle Erosion. Int Therm Spray Conf 2015:1013–9.

[20] Wang Q, Spencer K, Birbilis N, Zhang MX. The influence of ceramic particles on bond strength of cold spray composite coatings on AZ91 alloy substrate. Surf Coatings Technol 2010;205:50–6. doi:10.1016/j.surfcoat.2010.06.008.

[21] Singh H, Sidhu TS, Kalsi SB. Cold spray technology: future of coating deposition processes. Frat Ed Integrita Strutt 2012;22:69–84.

[22] Villafuerte, J. Wang J. Thermal Spray & of WC Research at WC-Co. Low Press Cold Spray Tungsten Carbide Compos Coatings 2009;4:1–3.

[23] Pawlowski L. The science and engineering of thermal spray coatings. vol. 34. 1995.

[24] Oladijo OP, Sacks N, Cornish LA, Venter AM. Effect of substrate on the 3 body abrasion wear of HVOF WC-17 wt.% Co coatings. Int J Refract Met Hard Mater 2012;35:288–94.

[25] Chen H, Hutchings IM. Abrasive wear resistance of plasma-sprayed tungsten carbide-cobalt coatings. Surf Coatings Technol 1998;107:106–14.

[26] Wang Q, Chen ZH, Ding ZX, Liu ZL. Performance study of abrasive wear and erosive wear of WC-12Co coatings sprayed by HVOF. 2008 2nd IEEE Int Nanoelectron Conf INEC 2008 2008;42:340–4.

[27] Nunthavarawong P, Sacks N, Botef I. Effect of Substrate Type on the Material Properties of WC-5wt % Ni Cold Sprayed Coatings. Conf. World PM2016 Congr. ProceedingsAt Hamburg, Ger. by Eur. Powder Metall. Assoc., 2016, p. 1–6.

[28] F.S. da Silvaa b, N. Cincab, S. Dostab, I.G. Canob, M. Coutob, J.M. Guilemanyb, et al. Corrosion behavior of WC-Co coatings deposited by cold gas soray onto AA 7075-T6. Corros Sci 2018:231–43.

[29] Lee YTR, Ashrafizadeh H, Fisher G, McDonald A. Effect of type of reinforcing particles on the deposition efficiency and wear resistance of low-pressure cold-sprayed metal matrix composite coatings. Surf Coatings Technol 2017;324:190–200. doi:10.1016/j.surfcoat.2017.05.057.

[30] Alidokht SA, Manimunda P, Vo P, Yue S, Chromik RR. Cold spray deposition of Ni-WC composite coating and its dry sliding wear behavior 2016;308:424–34. doi:10.1016/j.surfcoat.2016.09.089.

[31] Ji GC, Wang HT, Chen X, Bai XB, Dong ZX, Yang FG. Characterization of cold-sprayed multimodal WC-12Co coating. Surf Coatings Technol 2013;235:536–43.

[32] Wang HT, Chen X, Bai XB, Ji GC, Dong ZX, Yi DL. Microstructure and properties of cold sprayed multimodal WC-17Co deposits. Int J Refract Met Hard Mater 2014;45:196–203. doi:10.1016/j.ijrmhm.2014.04.018.

[33] Kim J, Kim S, Kim JH. Coating Properties of WC-Ni Cold Spray Coating for the Application in Secondary Piping System of Nuclear Power Plants. Trans Korean Nucl Soc Autumn Meet 2015.

[34] Yin S, Ekoi EJ, Lupton TL, Dowling DP, Lupoi R. Cold spraying of WC-Co-Ni coatings using porous WC-17Co powders: Formation mechanism, microstructure characterization and tribological performance. Mater Des 2017;126:305–13. doi:10.1016/j.matdes.2017.04.040.

[35] Professor Jukka Koskinen Instructors Merja Hakaste-Härmä S, Ahlfors H-M. Degree Programme of Chemical Technology Ville Roitto SLURRY FLOWS IN METALLURGICAL PROCESS ENGINEERING - DEVELOPMENT OF TOOLS AND GUIDELINES 2014.

[36] Hutchings LM. Triblology: Friction and wear of engineering materials. CRC Press London 1992:273.

[37] Stachowiak GW. Wear - Materials, Mechanisms and Practice 2005. doi:10.1002/9780470017029.

[38] Kovaříková I, Szewczyková B, Blaškovitš P, Hodúlová E, Lechovič E. Study and Characteristic of Abrasive Wear Mechanisms. Mater Sci Technol 2009;1:1–8.

[39] Williams J. Engineering Tribology. 1st ed. New York: Oxford University Press; 2005.

[40] Sapate SG, Selokar A, Garg N. Experimental investigation of hardfaced martensitic steel under slurry abrasion conditions. Mater Des 2010;31:4001–6.

[41] Liao H, Normand B, Coddet C. Influence of coating microstructure on the abrasive wear resistance of WC/Co cermet coatings. Surf Coatings Technol 2000;124:235–42.

[42] Kumari K, Anand K, Bellacci M, Giannozzi M. Effect of microstructure on abrasive wear behavior of thermally sprayed WC-10Co-4Cr coatings. Wear 2010;268:1309–19. doi:10.1016/j.wear.2010.02.001.

[43] Bearing G. Heat Treatment 2013.

[44] Assadi H, Kreye H, Gärtner F, Klassen T. Cold spraying - A materials

perspective. Acta Mater 2016. doi:10.1016/j.actamat.2016.06.034.

[45] Banhart J. Manufacture , characterisation and application of cellular metals and metal foams 2001;46:559–632.

[46] Huang, C.J., Yan, X.C., Li WY. Post-spray modification of cold-sprayed Ni-Ti coatings by high-temperature vacuum annealing and friction stir processing n.d.

[47] Vashishtha N, Sapate SG, Bagde P, Rathod AB. Effect of heat treatment on friction and abrasive wear behaviour of WC-12Co and Cr3C2-25NiCr coatings. Tribol Int 2018;118:381–99. doi:10.1016/j.triboint.2017.10.017.

[48] Stewart DA, Shipway PH, Mccartney DG. Influence of heat treatment on the abrasive wear behaviour of HVOF sprayed WC–Co coatings1. Surf Coatings Technol 1998;105:13–24.

[49] Janka L, Norpoth J, Trache R, Berger L-M. Influence of heat treatment on the abrasive wear resistance of a Cr 3 C 2 \\NiCr coating deposited by an ethene-fuelled HVOF spray process. Surf Coat Technol 2016;291:444–51. doi:10.1016/j.surfcoat.2016.02.066.

[50] Wang Q, Li L, Yang G, Zhao X, Ding Z. Influence of heat treatment on the microstructure and performance of high-velocity oxy-fuel sprayed WC–12Co coatings. Surf Coat Technol 2012;206:4000–10. doi:10.1016/j.surfcoat.2012.03.080.

[51] Picas JA, Punset M, Menargues S, Martín E, Baile MT. Microstructural and tribological studies of as-sprayed and heat-treated HVOF Cr 3 C 2 – CoNiCrAlY coatings with a CoNiCrAlY bond coat 2015. doi:10.1016/j.surfcoat.2014.10.039.

[52] ASTM C1327 - Standard Test Method for Vickers Indentation Hardness of Advanced Ceramics | Engineering360 n.d. http://standards.globalspec.com/std/9905618/astm-c1327 (accessed February 2, 2017).

[53] Upadhyaya GS (India. I of T. Cemented Tungsten Carbides, Production, Properties and Testing. Kanpur: William Andrew Publishing/Noyes; 1998.

[54] Nakamura T, Qian G, Berndt CC. Effects of Pores on Mechanical Properties of Plasma-Sprayed Ceramic Coatings. J Am Ceram Soc 2000;83:578–84.

[55] Beshish GK, Florey CW, Worzala FJ, Lenling WJ. Fracture Toughness of Thermal Spray Ceramic Coatings Determined by the Indentation Technique 1993;2:35–8.

[56] Conshohocken W. Standard Test Method for Plane-Strain Fracture Toughness of Metallic Materials 1 2003;3.

[57] Mod Y. a b n.d.

[58] Luo JK, Flewitt AJ, Spearing SM, Fleck NA, Milne WI. Young ' s modulus of electroplated Ni thin film for MEMS applications 2004;58:2306–9. doi:10.1016/j.matlet.2004.02.044.

[59] Zhang Y, Greer AL. Correlations for predicting plasticity or brittleness of metallic glasses. J Alloys Compd 2007;434–435:2–5. doi:10.1016/j.jallcom.2006.08.094.

[60] Molar Volume for all the elements in the Periodic Table 2019. http://periodictable.com/Properties/A/MolarVolume.html (accessed March 17, 2019).

[61] De Los Santos Valladares L, Ionescu A, Holmes S, Barnes CHW, Bustamante Domínguez A, Avalos Quispe O, et al. Characterization of Ni thin films following thermal oxidation in air. J Vac Sci Technol B, Nanotechnol Microelectron Mater Process Meas Phenom 2014;32:51808.

[62] ASTM E384 Standard Test Method for Knoop and Vickers Hardness of Materials. ASTM Int 2016. www.astm.org, West Conshohocken (accessed July 9, 2016).

[63] Zhang L, Chen X, Li D, Chen C, Qu X, He X, et al. A comparative investigation on MIM418 superalloy fabricated using gas- and water-atomized powders. Powder Technol 2015;286:798–806. doi:10.1016/j.powtec.2015.09.023.

[64] Scientific C, Engineering M. Mechanical property characterization of thin films using spherical tipped indenters 2006;253:204–11.

[65] Marple BR, Moreau C. Thermal Spray 2003 Advancing the Science and Applying the Technology. 2003.

[66] Prisco U. Size-dependent distributions of particle velocity and temperature at impact in the cold-gas dynamic-spray process. J Mater Process Technol 2015;216:302–14. doi:10.1016/j.jmatprotec.2014.09.013.

[67] Schmidt T, Gartner F, Assadi H, Kreye H. Development of a generalized parameter window for cold spray deposition. Acta Mater 2006;54:729–42. doi:10.1016/j.actamat.2005.10.005.

[68] Findik F. Investigation of explosive welding parameters and their effects on microhardness and shear strength 2017;3069. doi:10.1016/S0261-3069.

[69] Koivuluoto H. cold spraying – Overview of coating properties 2013.

[70] Lagutkin S, Achelis L, Sheikhaliev S, Uhlenwinkel V, Srivastava V. Atomization process for metal powder. Mater Sci Eng A 2004;383:1–6. doi:10.1016/j.msea.2004.02.059.

[71] Koivuluoto H, Lagerbom J, Kylmälahti M, Vuoristo P. Microstructure and mechanical properties of low-pressure cold-sprayed (LPCS) coatings. J Therm Spray Technol 2008;17:721–7. doi:10.1007/s11666-008-9245-6.

[72] Koivuluoto H. Microstructural Characteristics and Corrosion Properties of Cold-Sprayed Coatings. Tampere University of Technology, 2010.

[73] Ajdelsztajn L, Jodoin B, Schoenung JM. Synthesis and mechanical properties of nanocrystalline Ni coatings produced by cold gas dynamic spraying. Surf Coatings Technol 2006;201:1166–72. doi:10.1016/j.surfcoat.2006.01.037.

[74] Assadi H, G??rtner F, Stoltenhoff T, Kreye H. Bonding mechanism in cold gas spraying. Acta Mater 2003;51:4379–94. doi:10.1016/S1359-6454(03)00274-X.

[75] Leyman PF, Champagne VK. Cold Spray Process Development for the Reclamation of the Apache Helicopter Mast Support. Arl-Tr-4922 2009.

[76] Rourke RO. Cast Iron : A Solid Choice for Reducing Gear Noise. Gear Technol 1999.

[77] Mellor, B G.The Institute of Materials M& M. Surface coatings for protection against wear. Boston: Woodhead and Maney Publishing; 2006.

[78] Eksploatacji P. The influence of nanostructure coatings deposition on cavitation resistance of x6crniti 18-10 stainless steel 2007:167–74.

APPENDIX A

CROSS-SECTIONAL VIEWS FOR WEAR SURFACES

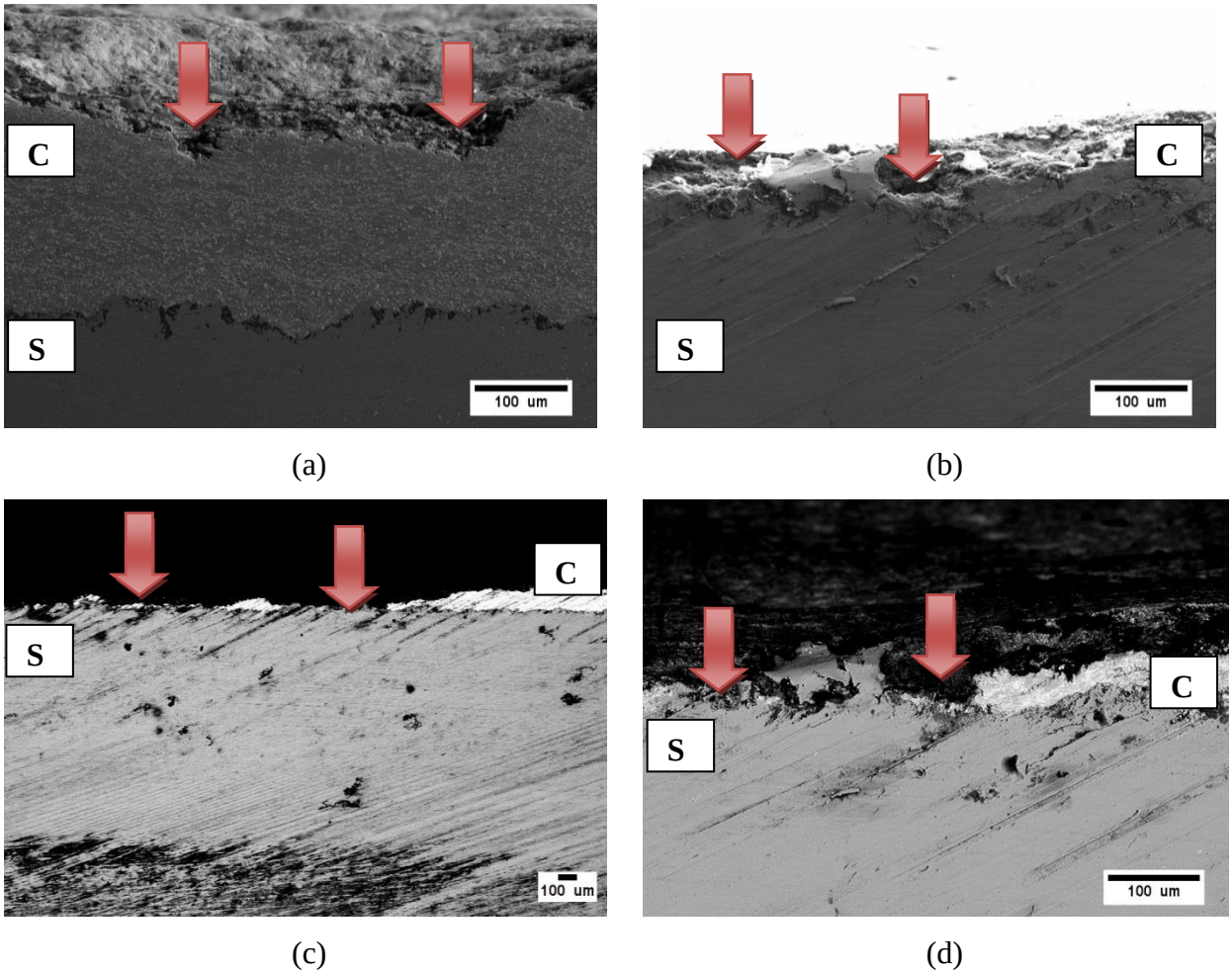


Figure A 1: Cross-sectional views showing the severity of the slurry abrasive medium (a & b) 5 ° tilted views and (c & d) level views. S = substrate and C = coating. Red arrows show regions of severe abrasion.

APPENDIX B

SLURRY ABRASION TESTS RAW DATA

Table B 1: Slurry Abrasion Tests Raw Data (in descending order) for WC-5wt%Ni coatings based on annealed (a) water atomized Ni powder (b) gas atomized Ni powder and as received (c) water atomized Ni powder and (d) gas atomized Ni powder

Time/min	Sample 1	Sample 2	Sample 3	Sample 4	Sample 1	Sample 2	Sample 3	Sample 4	Average mass loss at each interval/(mg/min)
0	11114	10979	10976	11487	0	0	0	0	0
5	11114	10975	10968	11486	0	4	6	1	2.75
10	11111	10972	10964	11485	3	3	4	1	2.75
15	11111	10969	10960	11485	0	3	4	0	2.333333
20	11108	10968	10956	11484	3	1	4	1	2.25
25	11108	10964	10953	11484	0	4	3	0	2.333333
30	11108	10960	10951	11481	0	4	2	0	1.5

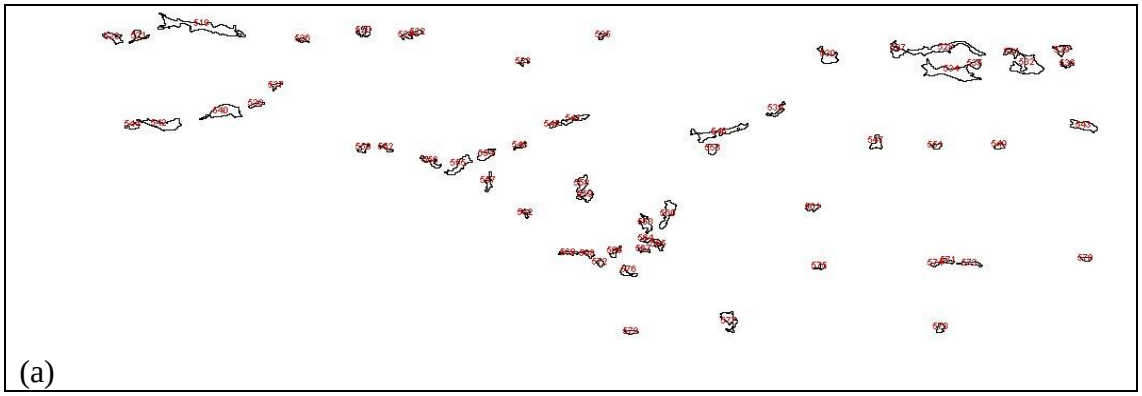
Time/min	Sample 1	Sample 2	Sample 3	Sample 4	Sample 1	Sample 2	Sample 3	Sample 4	Average mass loss at each interval	
0	11626	11700	11853	12553	0	0	0	0	0	0
60	11579	11687	11841	12513	47	13	12	40	25	18.12917
120	11526	11677	11839	12490	53	10	2	23	22	22.40536
180	11511	11670	11837	12460	15	7	2	30	13.5	12.23383
240	11496	11649	11836	12445	15	21	1	15	13	8.485281
300	11482	11637	11830	12438	14	12	6	7	9.75	3.86221
360	11473	11618	11828	12429	9	19	2	9	9.75	6.994045

Time/min	Sample 1	Sample 2	Sample 3	Sample 4	Sample 1	Sample 2	Sample 3	Sample 4	Average mass loss at each interval/(mg/min)
0	11.592	11.91	11.212	11.618	0	0	0	0	0
5	11.573	11.892	11.191	11.608	19	18	21	10	17
10	11.554	11.872	11.169	11.589	20	20	22	19	20.25
15	11.534	11.852	11.148	11.571	22	20	21	18	20.25
20	11.512	11.827	11.119	11.552	24	25	29	19	24.25
25	11.488	11.81	11.092	11.541	18	17	27	11	18.25
30	11.467	11.791	11.066	11.534	21	19	26	7	18.25

Time/min	Sample 1	Sample 2	Sample 3	Sample 4	Sample 1	Sample 2	Sample 3	Sample 4	Average mass loss at each interval/(mg/min)
0	11.654	11.477	11.814	11.34	0	0	0	0	0
5	11.638	11.464	11.799	11.325	16	13	15	15	14.75
10	11.623	11.443	11.782	11.31	15	21	17	15	17
15	11.606	11.429	11.76	11.301	17	14	22	9	16
20	11.586	11.41	11.746	11.29	20	19	14	11	16
25	11.573	11.397	11.735	11.273	13	13	11	17	13.5
30	11.558	11.377	11.721	11.258	15	20	14	15	16

APPENDIX C

PORE ANALYSIS IMAGES



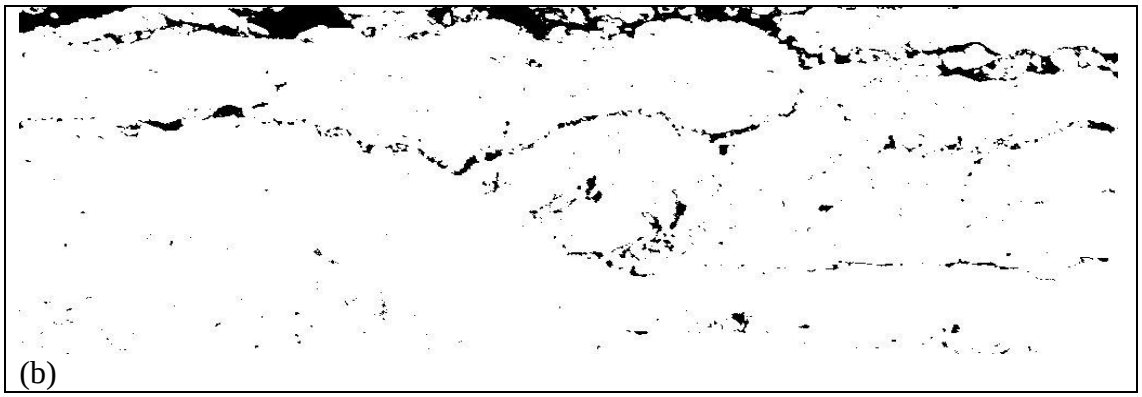
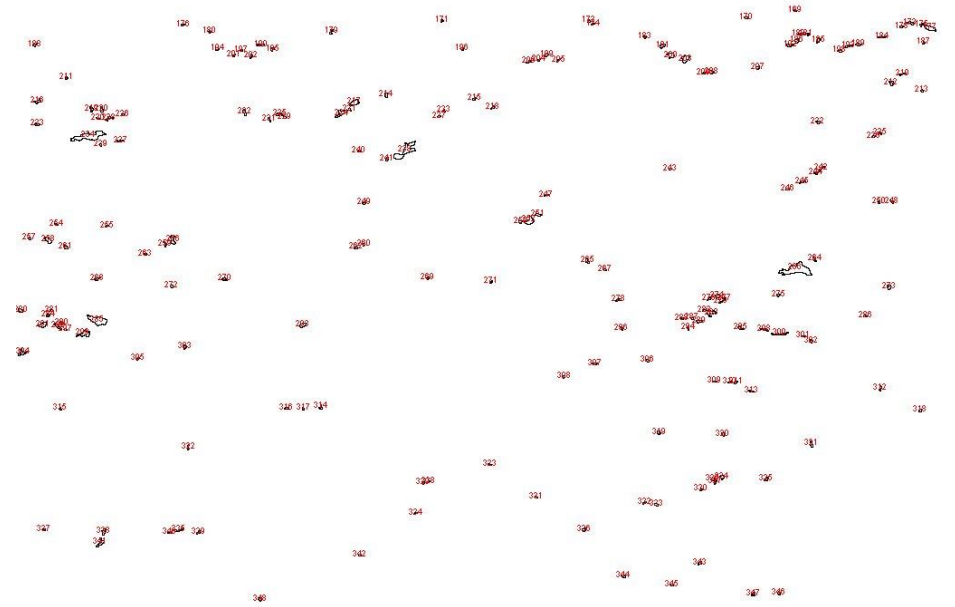
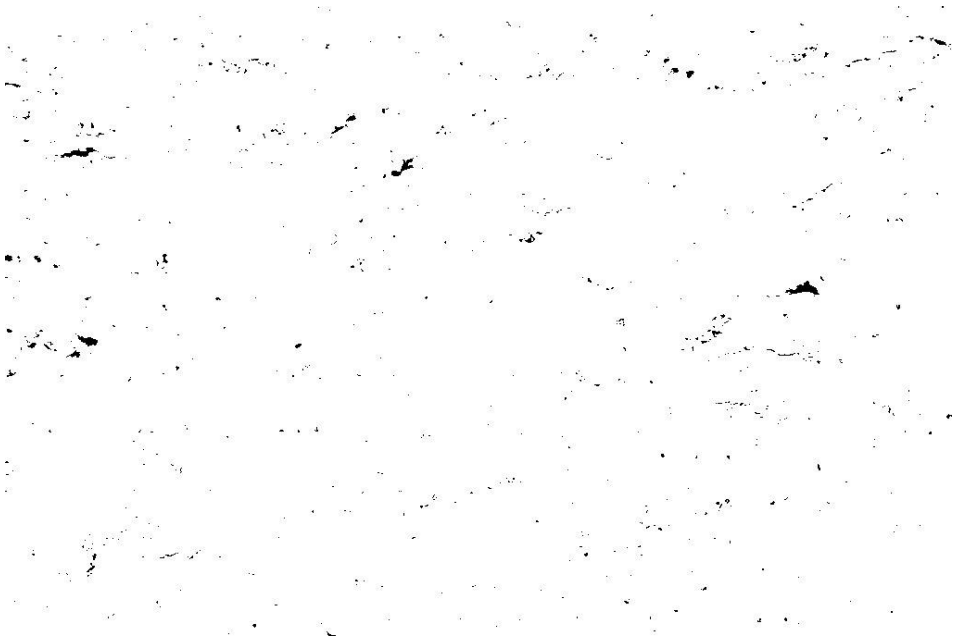


Figure C 1: Pore analysis for coatings based on annealed water atomized Ni powder (a) pore count & (b) pore identification.



(a)



(b)

Figure C 2: Pore analysis for coatings based on annealed gas atomized Ni powder (a) pore count & (b) pore identification.

APPENDIX D

PROBABILITY AND CUMULATIVE CURVES

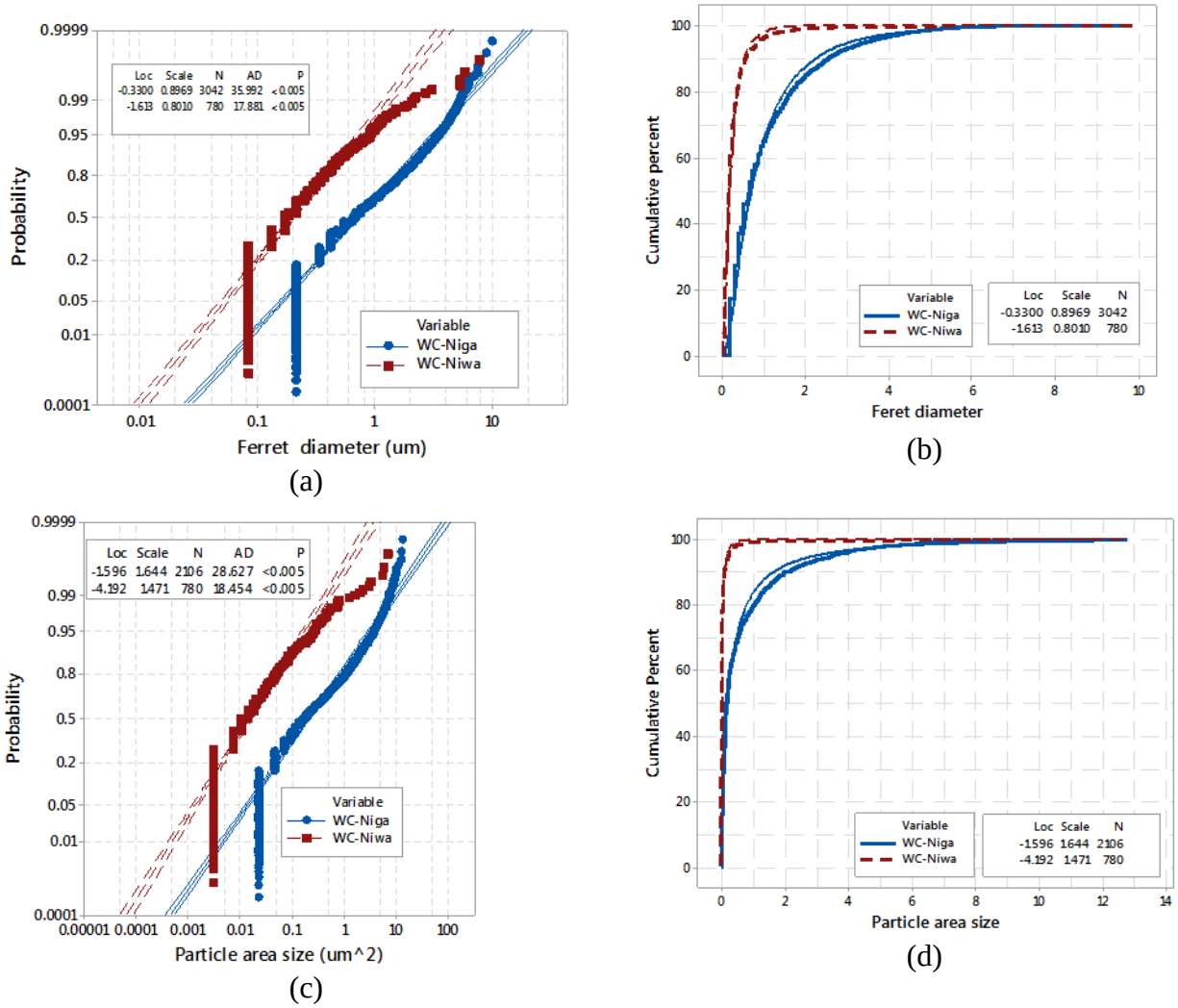


Figure D 1: Probability and cumulative curves for the CS coatings (a & b) for the carbide grain size and (c & d) for the particle area size of the carbide grains. Red = WC-Niwa and blue = WC-Niga coating.

APPENDIX E

PARTICLE SIZE DISTRIBUTION OF ANNEALED NI POWDERS

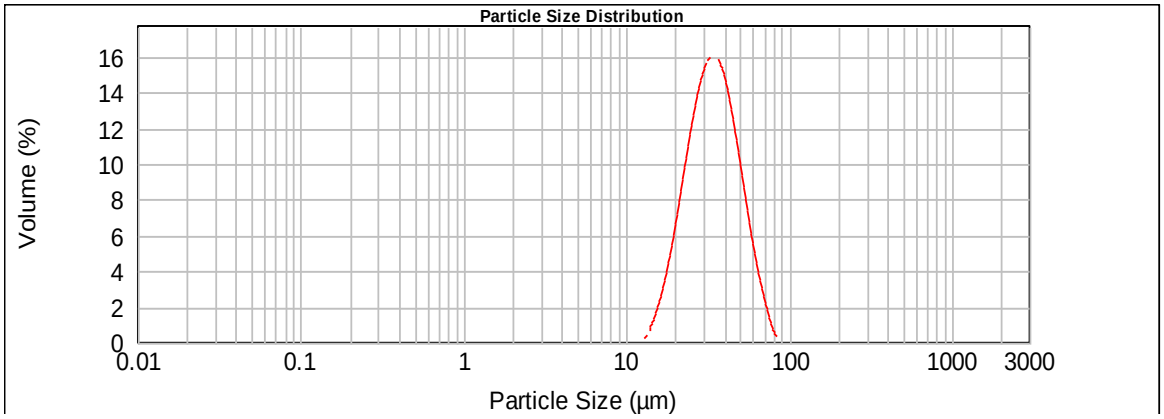


Figure E 1: Particle size of annealed gas atomized Ni powder

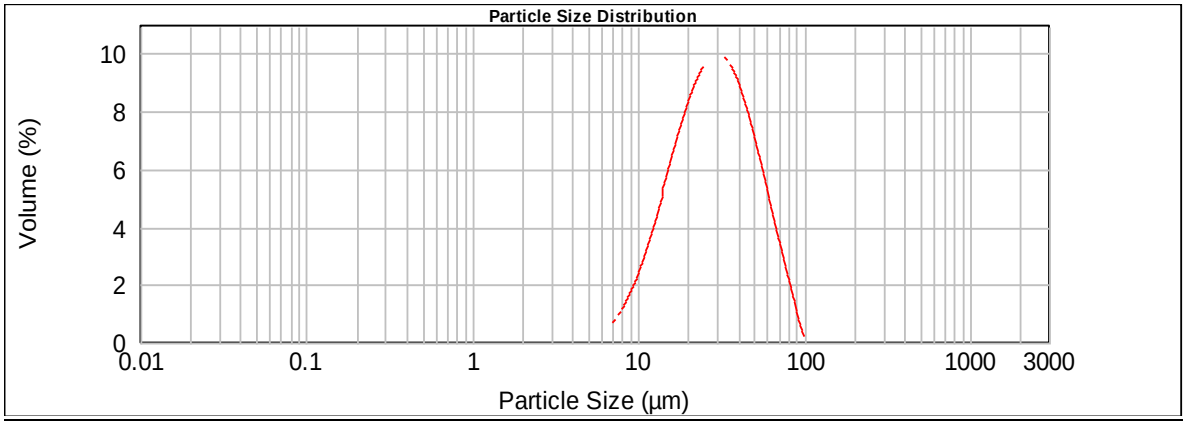


Figure E 2: Particle size of annealed water atomized Ni powder

APPENDIX F

ANNEALED NI POWDERS EDS RAW DATA

Table F 1: Raw data for EDS analysis on gas atomized Ni powder

Post-annealed water atomized Ni powder							Pre-annealed water atomized Ni powder			
Spot 1	**Element**	**Weight %**	**Atomic %**				**Spot 1**	**Element**	**Weight %**	**Atomic %**
	C K	23.99	58.5					O K	2.87	9.72
	O K	2.5	4.57					Si K	0.55	1.05
	Si K	0.44	0.46					Ni K	96.59	89.22
	Ni K	73.08	36.46				Totals		100	
Totals		100								
Spot 2	**Element**	**Weight %**	**Atomic %**				**Spot 1**	**Element**	**Weight %**	**Atomic %**
	C K	23.54	57.95					O K	2.58	2.82
	O K	2.45	4.53					Si K	0.51	0.99
	Si K	0.45	0.47					Ni K	96.91	90.19
	Ni K	73.57	37.06				Totals		100	
Totals		100								
Spot 3	**Element**	**Weight %**	**Atomic %**				**Spot 1**	**Element**	**Weight %**	**Atomic %**
	C K	24.02	58.65					O K	2.83	9.59
	O K	2.41	4.41					Si K	0.58	1.12
	Si K	0.36	0.38					Ni K	96.59	89.29
	Ni K	73.21	36.57				Totals		100	
Totals		100								

Table F 2: Raw data for EDS analysis on water atomized Ni powder

Post-annealed gas atomized Ni powder							Pre-annealed gas atomized Ni powder			
Spot 1	**Element**	**Weight %**	**Atomic %**				**Spot 1**	**Element**	**Weight %**	**Atomic %**
	C K	17.14	47.2					O K	0.81	2.93
	O K	4.08	8.43					Ni K	99.19	97.07
	Ni K	78.78	44.37				Totals		100	
Total		100								
							Spot 2	**Element**	**Weight %**	**Atomic %**
								O K	0.81	2.89
Spot 1	**Element**	**Weight %**	**Atomic %**					Ni K	99.19	97.11
	C K	18.92	50.23				Totals		100	
	O K	3.96	7.89							
	Ni K	77.12	41.88				**Spot 3**	**Element**	**Weight %**	**Atomic %**
Total		100						O K	0.74	2.68
								Ni K	99.26	97.32
							Totals		100	
Spot 1	**Element**	**Weight %**	**Atomic %**							
	C K	15.03	43.62							
	O K	3.76	8.18							
	Ni K	81.21	48.2							
Total		100								

APPENDIX G

PRESENTATIONS AND CONFERENCES

1. Microscopy Society of Southern Africa (MSSA), December 5^{th} – 9^{th} 2016, Port Elizabeth, South Africa.
2. The 16th Frontiers of Electron Microscopy in Materials Science (FEMMS) International Conference, September 10-15, Johannesburg, South Africa 2017.
3. The International Conference on Surfaces, Coatings and Interfaces (SurfCoat Korea 2018) March 28 - 30,2018 | Incheon, Seoul, Korea